2011

Analysis of static lateral load test of battered pile group at I-10 Twin Span Bridge

Binay Pathak
Louisiana State University and Agricultural and Mechanical College, bpatha2@lsu.edu

ANALYSIS OF STATIC LATERAL LOAD TEST OF BATTERED PILE GROUP AT I-10 TWIN SPAN BRIDGE

A Thesis

Submitted to the Graduate School of the
Louisiana State University and
Agriculture and Mechanical College
in partial fulfillment of the
requirements for the degree of
Mater of Science in Civil Engineering

in

The Department of Civil and Environment Engineering

By
Binay Pathak
B.Tech., National Institute of Technology, Rourkela, India (2004)
May, 2011

DEDICATION

To my family, friends and LTRC

ACKNOWLEDGEMENTS

I would like to express my very special thanks to my advisor Dr. Murad Abu-Farsakh for giving me an opportunity to pursue this unique research work and for the financial support during my MS study. I appreciate all his brilliant ideas, guidance and helps. The privilege of study under him will always remain a memorable part of my education. I would also like to express my deepest thanks to my co-advisor Dr. Khalid A. Alshibli for the endless support and guidance throughout this study. It is with pleasure to express my gratefulness to Dr. Guoping Zhang for being in my advisory committee; his cooperation and guidance have been valuable.

I would like to express my deepest gratitude to my family for their blessings and showing faith, love and support. I would also like to thank staff members at Louisiana Transportation Research Center, LTRC. A specially thank you goes to Dr. Ximbao Yu for his valuable suggestion. Without his support, this research work would not have been possible.

Special thanks goes to Dr. Quiming Chen, Rohit Raj Pant, Alok Dhungel, Vivek Laldas, Sanjay Dhakal and Yida Zhang for their endless support during thesis writing.

Finally, I would like to thank all my friends and faculty at Louisiana State University who have helped me to accomplish my goals.

TABLE OF CONTENTS

LIST OF TABLES

LIST OF FIGURES

ABSTRACT

In offshore structures, battered piles have been used as an alternative to vertical piles because of their capability in resisting higher lateral loads. The foundations of the newly built I-10 Twin Span Bridge over Lake Pontchartrain, LA, mostly consist of battered piles group. Understanding the behavior of these batter pile group foundations under lateral loading is very important to the design of highway bridge foundations. This study focuses on the evaluation of the lateral responses of battered pile group subjected to lateral loading and assessment of the current design methodology used for the design of I-10 Twin Span Bridge over Lake Ponchartrain.

A full-scale lateral load test was conducted at the M19 eastbound pier of the bridge, which consist of 24 prestressed concrete battered (slope = 1:6) piles with spacing of 4.33B, where B is the pile width. The lateral responses of piles measured by Micro Electro Mechanical Sensor (MEMS) In-place inclinometers (IPI), were interpreted using a high order polynomial method in deduce the profile of lateral deformation, moments, soil resistance. The p-y curves for the given soil condition were then back-calcutaed.

The M19 pier was also analyzed using the finite element program, FB-MultiPier program. The FB-MultiPier analysis, in general, over-predicted the lateral deformation behavior of the M19 eastbound pier as compared to IPI derived values. However, it verified the axial force calculated form strain gauges, which showed that the piles near the loading zone developed tensile forces whereas the piles located farther developed compressive forces.

In addition, a statnamic lateral load testing that conducted on a separately located single vertical pile was analysed. The static load-deflection response was developed by deriving the static load from the statnamic loading and compared with the results of FB-MultiPier program as well as the LPILE program. The non-linear analyses using these programs over-predicted the measured lateral measured response; whereas the results of linear analysis results were very close to the measured values.

CHAPTER 1
INTRODUCTION

1.1 Pile Foundation

Pile foundation is often used in bridges and other structures to support the applied axial and lateral loads. It is considered a cost effective approach to utilize the stronger bearing capacity of deep layer soil where either the top layer of soil is not strong enough to bear the structure's load or the water level is higher than the ground level.

Pile are classified into different types depending on the kind of material used in the construction such as timber, concrete, steel pile etc., the shape of pile such as square, circular and tapered; and the alignment of pile such as vertical and batter pile which furthermore classifies as positive and negative batter pile depending on the loading direction. Battered piles are usually used in offshore foundations and bridges to resist the lateral impact caused by wind and waves. The boundary constraints at the top of the pile can be further classified piles into fixed head and free head piles. For fixed end piles, the rotation is restricted by the presence of rigid pile cap at the top or the presence of rigid soil having high modulus of elasticity at the bottom. If the rotation or displacement is allowed at the bottom of the pile, due to the presence of soft soil then it is called floating pile. In addition, piles are also classified into precast piles; casted in the field such as drilled piers, drilled shafts and drilled cassions, and driven piles: precasted piles driven into the ground using a hammer. The piles described here can be used in single or in group to increase the soil resistance. The piles in a group behave differently than a single pile due to group interaction effect (will be discussed later), which depends on center-to-center spacing between piles and pile type.

Piles are usually slender, having high length to width ratio, and are mainly designed to resist axial loads. However, some structures such as high rise buildings, offshore structure (Quay, harbors), earth retaining walls are also subjected to horizontal or lateral pressure caused by wind force, wave force, traffic movement, water pressure and earth quake. For instance, in the bridge abutment, foundations can be subjected to lateral load induced by water waves and ship impact. Hence, the pile in a single or in a group as part of deep foundation of a structure has to resist both axial load and lateral load induced by the super-structure.

The lateral load induced on the pile foundation generates deflections, rotations, bending moments or translations depending upon the geometry and boundary condition of the pile as shown in the Figure 1.1a; whereas the lateral load on pile group causes lateral movements, vertical movement rotations of piles and also rotation of the pile cap as presented in the Figure 1.1b. If the rotation of the pile cap is not significant, then the piles can be assumed to move only in the horizontal direction.

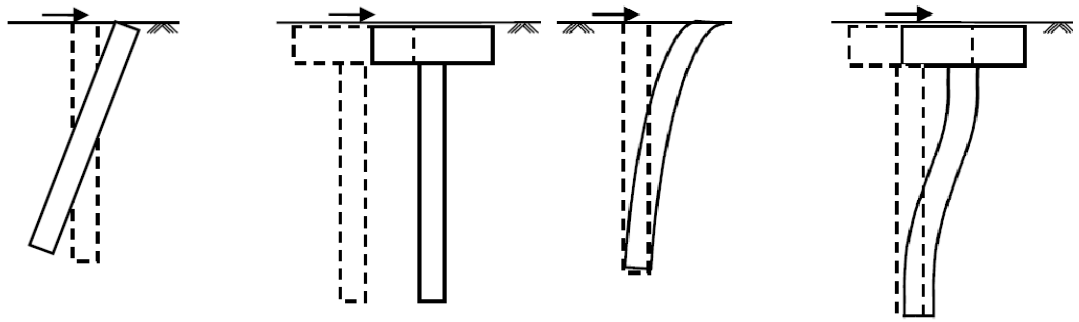

Figure 1.1 a: Response of a single pile under lateral load (Salgado, 2008)

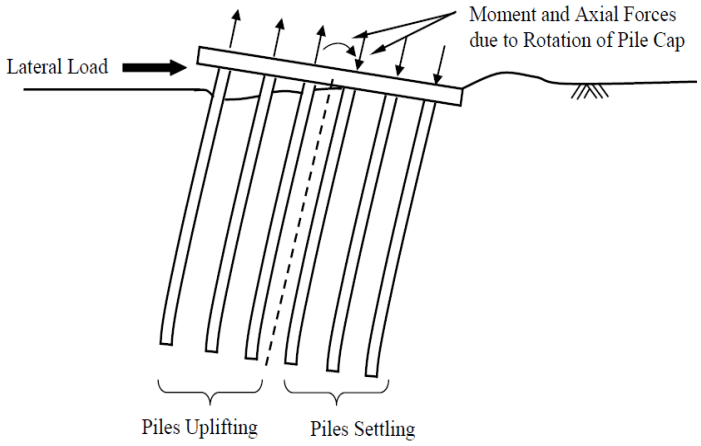

Figure 1.1b: Response of pile group under lateral load (Salgado, 2008)

The displacement of the pile caused by the applied lateral load displaces the soil in front of the pile in the loading direction. This displacement generates compressive stresses, shear stresses and strains in the soil that resist the pile movement as shown in the Figure 1.2a. This is known as lateral resistance of pile or soil reaction. The displacement of the pile and the corresponding soil

reaction caused by the lateral load is graphically represented by the p-y curve. The design of laterally loaded individual and group of piles usually utilizes the concept of p-y curves where piles are treated as beams and soils are represented with discrete spring elements at different depths. The stiffness of these springs is defined by the soil unit resistance, p, and the lateral soil displacement, y. The p-y relationship depends on many factors including soil type and properties, pile type, soil-pile interactions, and groundwater level. Hence, there may be several types of p-y curves along the depth of length depending upon the type and strength of different soil layers. Figure 1.2b illustrates the p-y curves for each layer of the soil along a vertical pile.

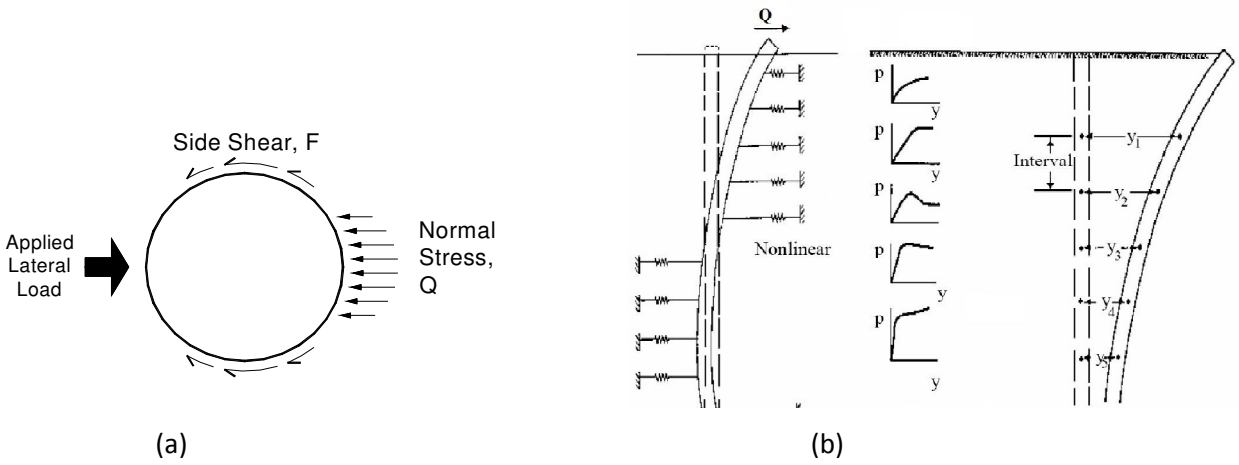

Figure 1.2: a) Soil reaction over cross section of pile, b) P-Y curve model

In comparison to vertical pile, the batter pile expected to have different p-y curve since the lateral resistance increases due to the effect of pile inclination. The pile inclination influences the ultimate soil resistance transferring some lateral to axial load and consequently modifies the p-y curve of vertical pile. Several p-y curves have been developed for the different soil conditions and pile geometries such as p-y curves for clay (e.g, Matlock, 1970) and p-y curve for sand, (Reese et al., 1974, O'Neill et al., 1984). The development of p-y curves will be covered in detail in the literature review Chapter 2.

The p-y curves for a pile within a group pile can be different than an isolated single pile due to the soil-pile-soil or group interaction effect, which substantially influences the lateral resistance. The application of lateral load on the closely spaced pile groups forms a gap behind each pile

and the failure zones or displacement field for individual piles overlaps with the adjacent files. The overlapping with the front pile is termed the shadowing effect and overlapping with the edge pile is called edge effect as shown in the Figure 1.3.

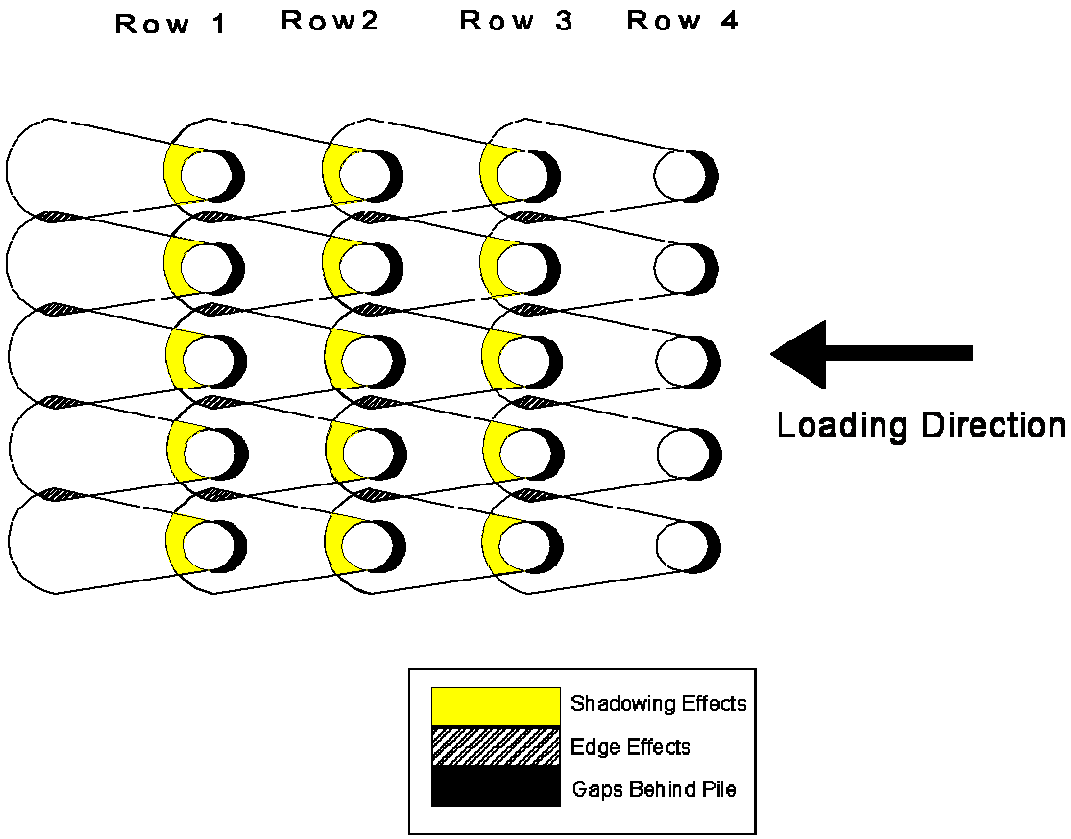

Figure 1.3: Effect of lateral load on pile groups

All these effects contribute to reducing the lateral resistance of last rows (trailing rows) piles, and hence the pile group will undergo a little different displacement and bending moment than the single isolated pile for the same given average load per pile. Although piles in the front (leading row pile) of a group may have a load versus deflection curve similar to that for a single pile, piles in trailing rows will experience smaller load versus displacement curves. Researchers introduced the reduction factor or constant multiplier "P-mulitipliers (P_m)" concept to deduce the p-y curve for a group pile. Several researches performed either full-scale testing or centrifugal testing (e.g, Brown et al., 1988, McVay et al., 1998, Ruesta and Townsend, 1997) to determine the p-multiplier values for group pile, and they all agree that the value of p-multiplier depends on the

soil properties and pile spacing, i.e. the increment of center-to-center pile spacing increases the value of p-multiplier. The traditional p-y curve for a single vertical pile, batter pile and group pile is presented in Figure 1.4.

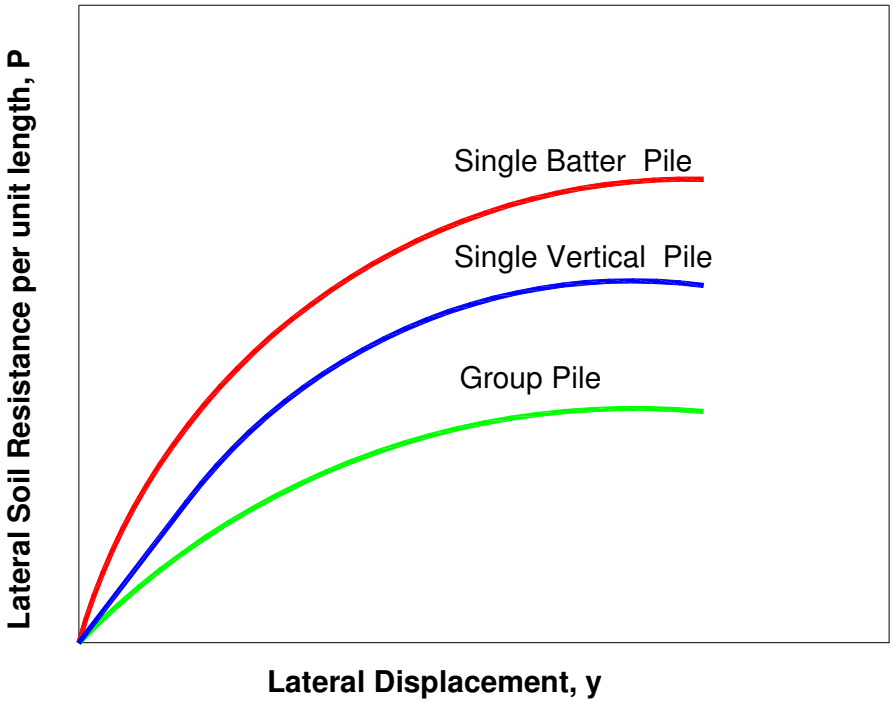

Figure 1.4: Typical p-y curve of single and group pile

1.2 Objectives of This Research

The current methods for analyzing lateral load behavior of piles are mainly focused on the vertical single or group of piles. The objective of this study is to analyze the lateral load test that was conducted at M19 eastbound pier to evaluate the lateral performance of batter pile group foundation. The M19 eastbound pier consists of 24 batter piles (batter 1:6) with 36 in diameter PPC piles. The data collected during the test using the In-place Inclinometer (IPI) and strain gauges will be used to derive the lateral deformation profile, moment distribution profile, soil resistance profile, and shear profile; and to back calculate p-y curves. This study will also verify the reliability of the FB-MultiPier computer program, which is being used by the LADOTD for

the entire design of the I-10 Twin Span Bridge to predict the performance of batter pile group under lateral loading.

The objectives of this research are:

1) To verify or develop a model to predict the lateral deformation of batter pile group,
2) To deduce the bending moment, shear force and soil reaction profiles,
3) To back-calculate the p-y curves for the given soil condition,
4) To analyze the lateral load test at M19 eastbound pier using FB-MultiPier program and to compare its result with the measured values.

1.3 Scope of the Work

The study involved in this research mainly consists of two parts: (1) Analyze the full-scale lateral load field testing of M19 eastbound pier and theoretically back-calculating the p-y curves of batter pile groups for the given soil condition using high order polynomial curve fitting. An evaluation of existing methods will be carried out to identify the most suitable analytical method for predicting the lateral deformation of battered pile group and back-calculating p-y curves by using the recorded data obtained from the fully instrumented piles. (2) The FB-MultiPier program developed by the University of Florida will also be used to analyze the behavior of the M19 eastbound pier foundation under lateral loading, and the results will be compared with the measured values as well as values calculated from high order polynomial curve fitting of rotation data.

A literature review on the design and analysis methods of laterally loaded piles in soil is performed. The collected literature review on existing analytical method for analyzing lateral load tests with IPI and strain gauge instrument, and back-calculating p-y curves will be reviewed and examined. The most suitable method will be used and recommended for calculating the profile of moments, shear, and soil reaction, and for deriving the p-y curves for the soil conditions similar to M19 subsurface soil condition.

1.4 Thesis Outline

Chapter 2 presents the literature review on several full-scale lateral load tests carried out on single or group piles and their results. The method of deriving p-y curves and existing p-y curves

for different soil condition are reviewed. Also, methods for interpreting data from inclinometers and strain gauges are also reviewed.

Chapter 3 presents a brief description of the M19 eastbound Pier of the I-10 Twin Span Bridge, subsurface soil condition and pile instruments. The chapter will also cover procedure of the unique full-scale lateral load test and its result.

Chapter 4 presents the method of analysis applied for the lateral load tests analysis by interpreting inclinometer and strain gauges readings.

Chapter 5 presents the results of analysis of lateral load test using high order polynomial curve fitting

Chapter 6 presents FB-MultiPier analysis and its comparison with the measured results.

Chapter 7 presents summaries, conclusions and recommendations.

CHAPTER 2
LITERATURE REVIEW

2.1 Review of Previous Lateral Load Tests

The tests conducted so far for understanding the lateral load behavior of pile/pile groups are generally categorized into full-scale test, centrifuge and model tests. Full-Scale tests are not easy to perform because of the associated high cost, technical difficulties and uncertainties, so only few full-scale tests have been performed since early nineteenth century, whereas comparatively more centrifugal tests that can simulate the actual field condition have been conducted. The important findings of researches corresponding to these tests are briefly reviewed in this Chapter.

2.1.1 Full-Scale Lateral Load Tests

Full-Scale tests are considered to be the best method for understanding the behavior of laterally loaded piles. However, only few full-scale tests have been conducted so far on pile/pile groups due to the high cost, uncertainty, and difficulties associated with it. The literature review revealed no record of the full-scale test before Fealing (1937) who conducted a field test on laterally loaded timber and concrete piles. After that countable researchers such as Kim et al. (1976, 1979), Matlock et al. (1980), Meimon et al. (1986), Brown et al. (1987, 1988), Rollins et al. (1998), and Ruesta and Townsend (1997) had performed full-scale tests on pile/pile group under different soil conditions. Their findings showed agreement in that average soil resistance per pile decreased in pile group due to group interaction effect which increases with larger deflection and decreases with the increment of center-to-center spacing. Also the average load per pile for the group is lower than a single isolated pile at the same deflection. Matlock (1970) conducted lateral-load tests on steel pipe pile of 12.75 in diameter for both static and cyclic loading, and developed a p-y curves by assuming the pile remain linear. Kim et al (1976) conducted full-scale test in pile group consisting of battered piles and noted that battered piles provide more lateral resistance with less bending stress. The analysis of lateral load was revolutionized by Brown et al. (1987, 1988) who conducted full-scale test on vertical pile groups on steel piles and generated p-y curves based on Winkler-type soil model with polynomial curve fitting to the bending moment data. Furthermore, Brown et al. (1988) introduced the p-multiplier

concept to analyze the reduced resistance of the group pile and produced a modified p-y curves for pile group. Their findings also showed that the depth of the maximum bending moment increased from front row to back row, and was greater and occurred at greater depths for the piles in the group than the single pile. The p-multiplier concept was adopted by the Ruesta and Townsend (1997) through conducting full-scale tests on reinforced concrete pile and also noted that the outer piles took more load than inner pile of same row due to greater influence of shadowing effect at inner piles. Rollins et al. (1998) suggested more p-multiplier value after conducting a full-scale test on vertical pile group in clay. The other observations made by Rollin et al. (1988) are: a) the displacement of pile group is 2-2.5 times higher than the single pile for the same average pile load, b) the load distribution in pile group is not uniform but is a function of the row position, c) there is no consistent trends in the load distribution among piles in the same row which agrees with the previous results of Brown et al. (1987, 1988), and d) The back row (trailing) carried somewhat higher loads than middle row, completely conflicted with Brown et al. (1988) conclusion that the back rows resist lowest load. The explanation given by Rollins et al. (1988) for this conflicting result is due to possibly negative pressure developed behind the back row that would increase resistance in back row.

In the early 21st century, Huang et al (2001) conducted a full-scale test on bored and driven precast pile groups to investigate the influences of installation procedure of piles in lateral soil resistance. The conclusion was that driven pile installation increased the group interaction by causing the soil to move laterally and hence become denser; while bored pile installation loosens the soil and decrease group interaction. Rollins et al. (2003a, 2003b and 2005) conducted several full-scale lateral load tests of piles in clayey soil as well as sandy soil at different pile spacings. Some important findings of Rollins et al. (2003, 2005) are: 1) The middle pile of the same row carried the smallest load in the row at a given displacement, while the left and right piles carried 20–40% higher loads in the sandy soil, which agrees with most pile group tests in sands (Ruesta and Townsend, 1997 and McVay et al., 1998). However, this observation conflicts with some previous full-scale pile group load tests in clays (Brown et al., 1987; Rollins et al., 1998; and Rollins and Sparks, 2002). For verification, Rollins et al. (2005) explained that the increment of friction angle increases the width of the passive wedge which forms in soil in front of a laterally loaded pile; and as sands generally have a higher friction angle than clays, there is more pile-

soil-pile interaction, thereby more interaction in middle pile in a row with the adjacent piles, so carrying less loads than the outer piles. 2) The group effect becomes negligible when spacing between rows increased to more than 6B, where B is the pile width. 3) In both clay and sand soils, group pile has significantly higher bending moments than those in isolated single pile for a given load. The maximum bending moments in the back (trailing) row tended to be higher and at a lower depth due to group effects causing reduced soil resistance close to the surface which shows agreement with Brown et al. (1987) findings. However, for a given deflection, the maximum bending moments in the front (lead) row were higher than the back (trail) row, which can be attributed to the lower loads carried by the back rows for a given deflection level. 4) The passive resistances on the pile cap can significantly increase the lateral load capacity provided by the pile group. They suggested that for the mobilization of full passive resistance in the dense compacted sandy gravel, nearly 6% of the pile cap height wall movement is necessary. Nip et al. (2005) conducted a full-scale test on 1.5 m diameter single vertical bored piles and successfully used the fourth order polynomial equation for the soil reaction profile to deduce the shear force profile, bending moment profile and to back calculate the p-y curves.

2.1.2. Centrifuge and Model Load Test

In contrast to full-scale tests, centrifuge and model tests are inexpensive and easier to understand the lateral load behavior of piles. Cox et al (1984) conducted centrifuge testing using sand and suggested that the elastic theory does not account for the non-linearity behavior in pile group interaction, and also the total load carried by each pile within the group was not evenly distributed. According to McVay et al. (1994, 1998), soil density influences the average load resistance which increases with the increase in soil density; however, the increment was not significant unlike pile spacing. Also, in larger pile group, the load resistance continues to decrease until about the fourth row, after which it stabilizes. McVay et al. (1998) also agreed with the p-multiplier concept of Brown et al. (1988) and suggested to use different p-multiplier at different pile spacing. Moss et al. (1998) conducted model tests on cyclic loading and found that the soil resistance was more dependent upon the pile stiffness, instead of the p-y curves since the cyclic loading compress the soil and form the gap in-front of the pile. Llyas et al. (2004) performed centrifuge tests on piles group in clay and noted that the reduction in pile group efficiency is less for piles installed in overconsolidated soils than those installed in normally

consolidated soils, and the group interaction effect becomes insignificant when center-to-center spacing reaches a value of 5D. Llyas et al. (2004) also concluded that for the middle row, center piles often carried much less load and bending moment than those of the outer piles in the same row.

2.2. Analysis Methods of Laterally Loaded Pile

From the findings of full-scale tests, centrifuge and model tests and analytical analysis, researchers recommended several analytical methods for analyzing the lateral load behavior of piles. Based on the assumption applied for modeling the pile and soil behavior, the existing analysis methods can be classified into six methods: 1) Hansen (1961) and Broms (1964 a, b) developed an analytical model based on the lateral earth pressure theory to analyze the lateral load behavior on short pile foundation. 2) For relating the load-displacement behavior of pile, Winkler (1867) correlated the subgrade resistance with the linear characteristic of spring representing the soil reistance behavior. The pile was assumed as a transversely loaded beam. 3) Based on an elastic continuum approach which assumes both the soil and pile as elastic materials, Poulos (1971) developed a model to analyze lateral load behavior using the finite difference technique. 4) The finite element method where the soil-pile interaction can be modeled easily is also used for the analysis of lateral load tests. Several computer programs were developed based on finite difference method and finite element technique; these programs will be discussed in section 2.4. 5) The method which is the most popular and widely used in research is the p-y curves method. In this method, Matlock (1970) and Reese (1974) modified the Winkler approach by representing the soil as a non- linear characteristic material. 6) Norris (1986) developed a strain wedge model, later updated by Ashour et al. (1998), which analyzed the behavior of laterally loaded piles by considering the pile properties such as pile shape, bending stiffness, and head condition.

Since the model developed by Hansen and Broms (1964) is applicable to only short pile foundation, and that the finite element method and finite difference method require long process, so these models will not be covered in detail. The p-y curves method is found to be the most reliable method, so the Winkler approach, on which the p-y curves is based, and the method of development of p-y curves are presented in this Chapter. The summaries of all five models proposed by different researchers are presented in Table 2.1.

Table 2.1: Features of Methods for Analysis of Laterally Loaded Piles

Analysis type	Features
Hansen (1961)	Developed for short pile with free or fixed head condition. It can be applied to clay, sand or layered soil. The ultimate soil resistance at any depth is calculated by $P_u = \sigma_v K_q + cK_c$
Broms (1964 a, b)	Similar to Hansen model, developed based on the lateral earth pressure theory. Soil is assumed to be purely cohesionless or cohesive soil. It's simple to use and useful for small foundation such as electric poles etc; however this model is difficult to use in complicated soil condition.
Winkler Model (Winkler, 1867)	Soil is modeled as horizontal elastic springs. Nonlinearity of soil is not considered
Elastic continuum Method (Poulos, 1971)	Considered soil as continuum, homogenous, isotropic and soil modulus is linearly increased. This model is difficult to use in layered soils. Poulos implemented this method for his model using finite difference technique.
Finite element Method (Rajashree , 2001)	Non homogeneity, non-linearity of soil, and soil-pile interaction is considered. However, it is very complicated constitutive equation and interface modeling
P-y curves Method (Matlock, 1970)	Based on Winkler foundation model. Soil is modeled as non-linear elastic springs. This model is widely used because of its versatility and simplicity.
Strain Wedge method. (Norris, 1986; Ashour 1998)	SW model evaluates the passive wedge soil developed in front of pile by employing stress-strength behavior. Simply, it is a theoretical approach which can predict the p-y curves at any point considering the influences of pile properties, soil properties and the effect of a change in the neighboring soil. The model relates the horizontal soil strain of passive wedge to the deflection of pile, lateral stress change to the soil-pile reaction (p) and the nonlinear variation of subgrade reaction to the group interaction effect.

2.2.1 Winkler Approach

Winkler (1867) proposed that the resistance of a subgrade against external forces can be assumed to be proportional to the ground deflection where soil is modeled as a set of elastic springs, so that the elastic deflection of the spring represent the displacement of beam under the applied load. The spring coefficient represents the material properties or soil is known as the coefficient of subgrade reaction (k).

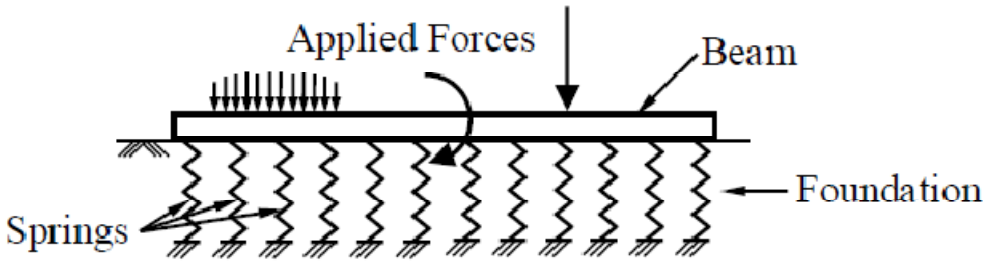

Figure 2.1: Winkler concept of beam lying on elastic soil (after Winkler, 1867)

As illustrated in Figure 2.1, the force induced on the spring is,

$$F = k\,y \qquad (2.1)$$

where, F = force,

k = spring stiffness coefficient and

y = spring displacement or ground displacement.

Terzagi (1955) related the spring coefficient to the modulus of subgrade reaction of a soil mass. If P (F/L^2) is the pressure applied at the interface of soil and beam due to the applied load and y is the deflection then

$$P = k_h\,y \qquad (2.2)$$

where, k_h = modulus of subgrade reaction = P/y (F/L^3), hence spring coefficient $k = k_h / y$

If P(F/L) is soil resistance force per unit length ,

$$P = K_s\,y \qquad (2.3)$$

Where, K_s = subgrade modulus = $k_h\,z$

z = depth below the ground level.

Since, the value of subgrade reaction (k_h) may represent the exponential function of the depth and pile deflection as illustrated in Figure 2.2. (Palerm and Brown, 1954; Shinohora and Kubo, 1961) the subgrade modulus ($K_s = k_h z$) is ought to be a non-linear function of depth z and the pile deflection y; i.e $K_s = f(z,y)$.

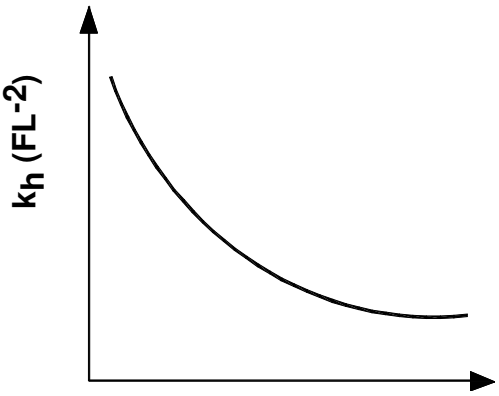

Figure 2.2: Exhibiting kh as non-linear function of z and y (Prakash et al.,1996)

Other researchers (e.g., Davisson, 1970; Francis, 1964; Broms, 1964a, b; Matlock and Reese, 1960; and Reese and Matlock, 1956) applied the Winkler concept on laterally loaded piles by considering the pile as a beam against lateral (transverse) loading. Winkler assumption was that the behavior of soil is elastic linear; however there is complexity in the behavior of soil under the lateral load due to the non-linearity behavior of the soil.

2.2.2 P-y Curves

The p-y curves is the relationship between the soil resistance (P) and the displacement of the soil (y), where the soil resistance (force per unit length) is the product of spring constant and the soil displacement. Several approaches have been made to develop or to derive the p-y curves from field load tests or laboratory tests. Smith and Slyh (1986) explained that when the lateral load is applied on the pile, the produced lateral soil response, (P) is predominantly a result of two components: frictional resistance, (F) produced by tangential interface stresses, and frontal resistance, (Q) produced by stresses normal to the pile cross section as shown in the Figure 2.3. The trends of developing the p-y curves for analyzing the lateral load behavior of piles began in

the mid 20th century when McClelland and Focht's (1958) correlate the p-y curves with stress-strain curve obtained from the laboratory test. The correlation given for ultimate lateral soil resistance, P_u is $P_u = 5.5B\sigma_{\Delta}$, where σ_{Δ} = deviator stress in triaxial test with confining pressure close to the actual overburden pressure in psi and for displacement, y is $y=1/2B\varepsilon$, where B is pile diameter or frontal size in inches, and ε = average normal strain in the direction of pile movement.

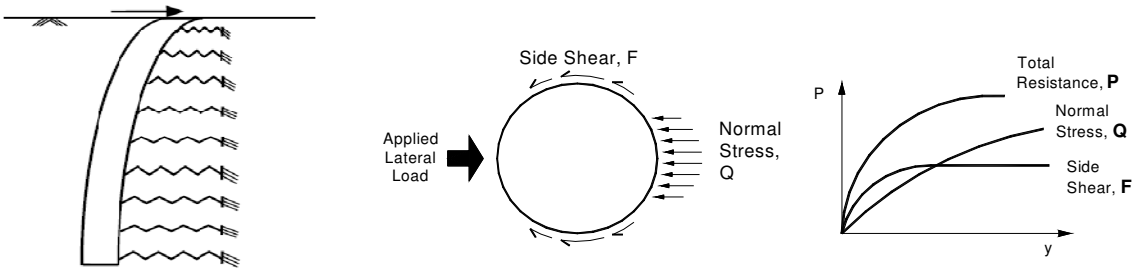

Figure 2.3: Mechanism that generates the total soil resistance force (P) (Smith and Slyh, 1986)

In contrast to McClelland and Focht's (1958) assumption that the soil in front of the pile fails in horizontal plane only, Reese (1958) argued that the soil near the ground surface fails by moving upward in the form of a wedge and the behavior of a laterally loaded pile is greatly influenced by wedge formed soil. Reese also developed the p-y curves by simulating the stress-strain curves assuming parabolas shape. As discussed earlier, horizontal subgrade reaction (k_h) is a non-linear function of displacement or strain in soil around the pile and the secant modulus of p-y curves represents the subgrade modulus, so p-y curves function should be non-linear. Matlock and Reese (1970) incorporated non-linearity behavior of soil in the model developed by modifying Winkler's approach, assuming pile as a flexible beam and the soil continuum as a set of independent non-linear springs. The varying characteristics of these springs reflect the non-linearity behavior of soil. Several researchers suggested that the non-linearity behavior in the p-y curves can be represented by different mathematical functions such as power, exponential and hyperbolic. The suggested p-y curves is typically comprised of three segments; straight line, parabola and straight line. The initial straight portion of the p-y curves represents the elastic behavior of soil and the slope is the constant of horizontal subgrade reaction, whereas the middle

parts reflect the non-linear portion of the in-situ stress strain curve. Many studies were performed to predict the middle portion of a p-y curve; however, there is no widely accepted analytical procedure for the standard shape of the middle portion. The third segment is again a straight horizontal line which represents the plastic behavior of soil. The typical p-y curve of a single pile is presented in the Figure 2.4.

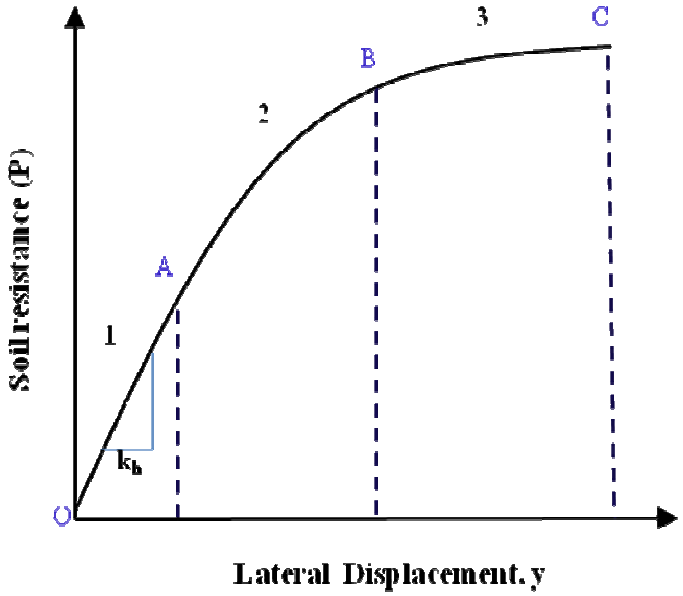

Figure 2.4: Typical p-y curve shape

Since the p-y curves depend on the soil, and that the soil through which pile is embedded comprised of different layers with varying properties such as variation in classification, undrained shear strength, these varying properties of soil influence the shape of p-y curves. Many researchers including Matlock (1970), Resese and Welch (1975), Reese (1997), and O'Neil (1984) had developed different shape of p-y curves for different soil conditions, which will be discussed in details in next Section.

2.2.2.1 P-y Curves for Soft Clay Soil

Matlock (1970) produced a p-y curve for soft clay in the presence of water for static load as shown in Figure 2.5, where the water level was above the ground surface. The getoechnial parameters necessary for the develpement of p-y curves are the undrained shear strength (S_u) and

axial strain at 50% of failure load (ε_{50}). The initial slope of the p-y curves can be established by using k_h.

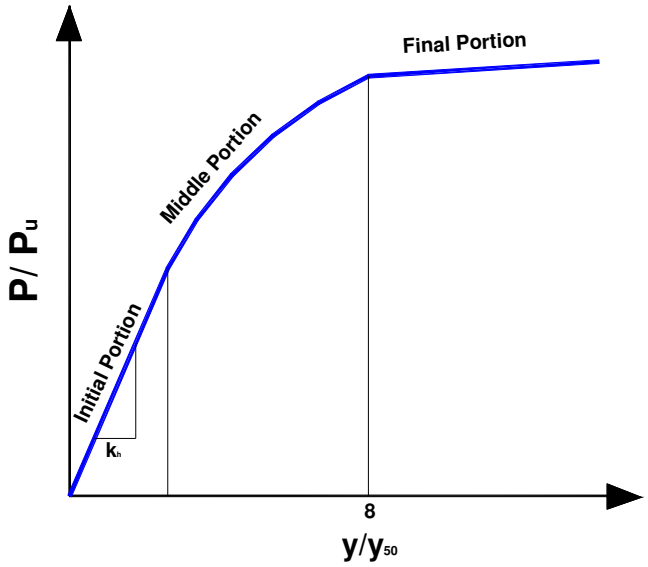

Figure 2.5: Characteristics shape of P-y curves for soft clay (after Matlock, 1970)

The equation for the middle poriton of curve is given by

$$\frac{p}{Pu} = (\frac{y}{y50})^{1/3} \qquad (2.4)$$

where,

P = lateral soil resistance per unit length,

P_u = ultimate lateral soil resistance per unit length,

y = lateral displacement,

y_{50} = lateral displacement corresponding to one half of the ultimate lateral soil resistance.

The ultimate soil resistance per unit length of pile is computed using Equations 2.5 and 2.6 and the smaller value is used for the p-y curve.

$$P_u = S_u * B(3 + \frac{\gamma'}{S_u} + {}^{je}/_{B} * z) \qquad (2.5)$$

$$P_u = 9\, S_u B \qquad (2.6)$$

where,

γ' = average effective unit weight from ground surface to p-y curves,

z = depth from ground surface to p-y curves,

B = pile width or diameter of pile,

j_e = experimentally derived unit parameter normally has a value between 0.25- 0.8.

According to Matlock (1970), the value of J_e is 0.5 for soft clay and about 0.25 for medium clay. The value of 0.5 is frequently used for J_e. The value of P_u is computed at each depth where a p-y curve is desired based on the undrained shear strength at that depth.

The lateral displacement y_{50} corresponding to one half of the ultimate soil resistance is computed as $y_{50} = 2.5\ B\varepsilon_{50}$, where the value of ε_{50} can be obtained from the stress-strain curve or taken from Table 2.2 in the absence of stress strain curve. Then p-y curves can be developed using Equation 2.4 and the value of P remains constant beyond $y/y_{50} = 8$ as shown in the Figure 2.5

Table 2.2: Matlock (1970) recommended values of ε_{50} based on the consistency of clay

Consitency of Clay	Undraiend shear strength(kPa)	ε_{50}
Very soft	<12	0.02
Soft	12-24	0.02
Medium	24-48	0.01
Stiff	48-96	0.006
Very stiff	96-192	0.005
Hard	>192	0.004

2.2.2.2 P-y Curves for Stiff Clay

Reese et al (1975) generated a p-y curve by conducting lateral load tests on overconsolidated stiff clay as described in Figure 2.6. The initial straight portion of the line is evaluated from the equation $P = (k_h z)y$, where the value of k_h is proportional to the undraiend shear strength. The reasonable suggestion is made that the initial slope of the p-y curves be established using k_h from Table 2.3.

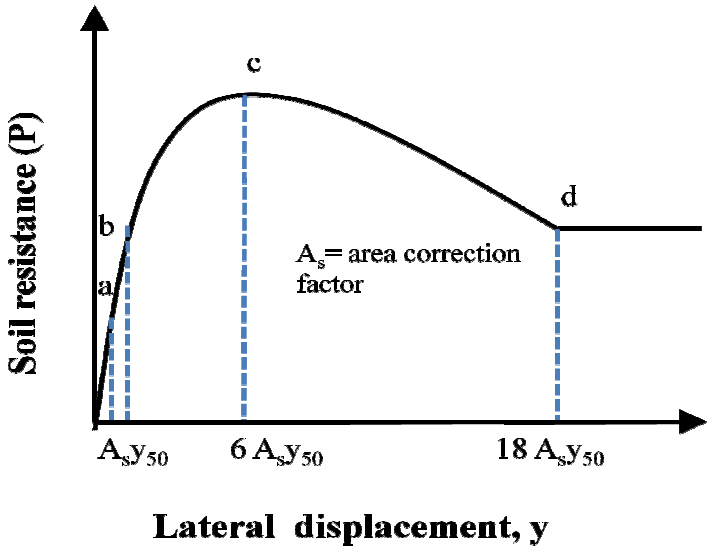

Figure 2.6: Characteristics shape of P-y curves for stiff clay (Reese 1975)

Table 2.3 Value of k_h corresponding to the undrained shear strength

Undrained Shear Strength (kPa)	50-100	200-300	300-400
k_h (MN/m^3)	135	270	540

The ultimate soil resistance per unit length (P_u) is computed according to the following equations and the lesser value is used in developing the p-y curves.

(2.7)

(2.8)

The value of y_{50} is computed from $y_{50} = \varepsilon_{50} B$ and the first parabolic portion (a-b) can be obtained according to the following equation.

— (2.9)

Similarly, the second parabolic portion (b-c) is given as:

— - — (2.10)

The third inclined straight line is obtained from the following Equation:

- ——— (2.11)

The final straight line is developed by the following Equation

$$P = p_u(1.225A_s^{0.5} - 0.75A_s - 0.411) \quad (2.12)$$

where,

S_u = average undrained shear strenght over depth,

A_s = area correction factor given in Figure 2.7.

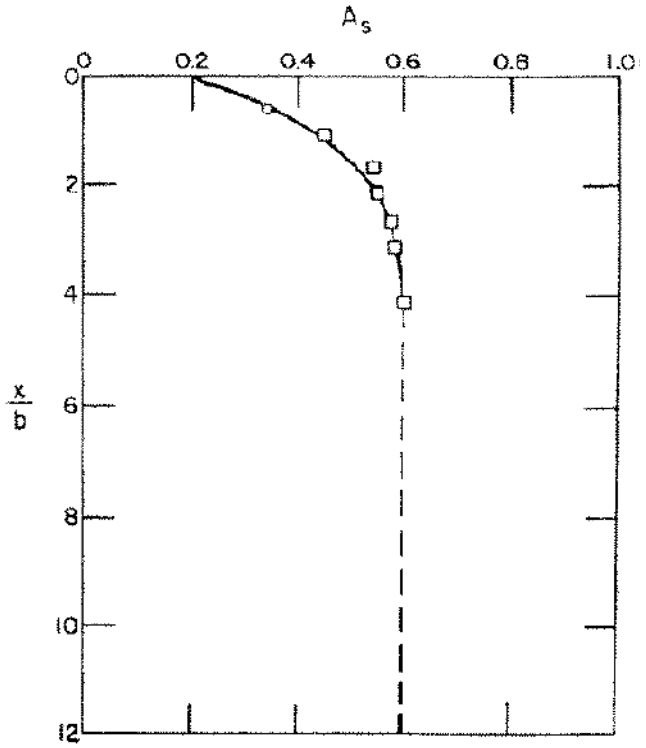

Figure 2.7: Vlaue of parameter As (Reese et al 2006)

2.2.2.3 P-y Curves for Sand

- **Reese Model**

The ultimate resistance per unit length (P_u) for Reese et al. (2006) is computed from Equations 2.13 and 2.14 and the lesser value is used in developing the p-y curves as shown in Figure 2.8.

$$P_u = \gamma\, z[\frac{K_o.tan\phi.tan\beta}{\tan(\beta-\phi).\cos\left(\frac{\phi}{2}\right)} + \frac{tan\beta}{\tan(\beta-\phi)} * \left(B + z\ tan\beta \tan\left(\frac{\phi}{2}\right)\right) + K_o\ z\ tan\beta\ \left(tan\phi sin\beta - \tan\left(\frac{\phi}{2}\right)\right) - K_a B] \quad (2.13)$$

or

$$P_u = K_a B\ \gamma\ z\left[\tan\beta^8 - 1\right) + K_o B\ \gamma\ z\ tan\phi.tan\beta^4 \quad (2.14)$$

where,

K_a = Rankine active earth pressure coefficient=(1-sinϕ)/(1+sinϕ),

K_o = Rankine coefficient of earth pressure at rest=1-sinϕ.

ϕ =angle of internal friction.

β=ground surface slope angle =45^0+ϕ/2,

B=Pile width or diameter.

The ultimate resistance is modified with a constant A'$_s$, $P = P_{ut}\ A'_s$, where the area correction factor A'_s can be estimated from Figure 2.9a. Then using $P_m = B_s\ P_u$ to calculate the value of P_m in Figure 2.8, where the value B_s is obtained Figure 2.9b. The parabolic section (k-m) of the curve can be obtained from $C'y^{1/n}$, where the value of n can be found from $n = \frac{P_m}{my_m}$ and the value $C' = \frac{P_m}{y_m^{1/n}}$. The slope of linear line between u and m section is $m = \frac{P_u - P_m}{y_u - y_m}$. The initial straight line is P = (k_hz)y, where k_h is proportional to the relative density of sand and can be obtained from Table 2.4. The point y_k is calculated as $y_k = \frac{C\prime}{K_{py}z}$.

Table 2.4: The value of k_h (MN/m^3)

Relative Density	Loose	Normal	Dense
Unsubmerged	6.8	24.4	61
Submerged	5.4	16.3	34

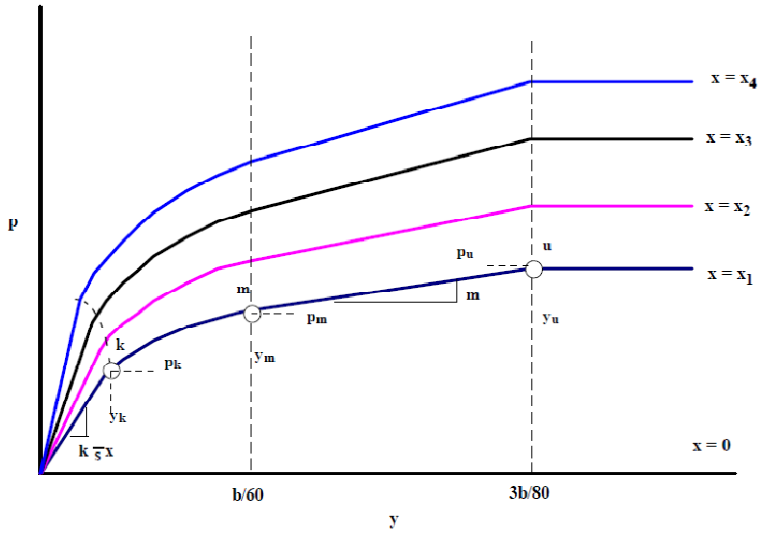

Figure 2.8: P-y curvess for sand (Reese et al., 1974)

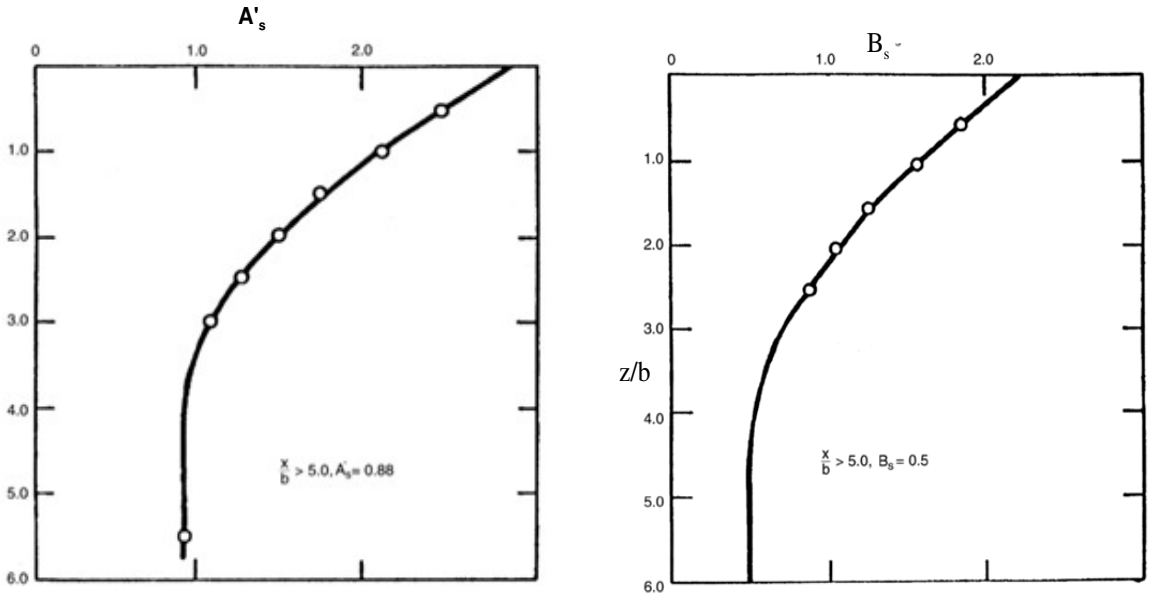

(a) Value of A'_s (b)Value of B_s

Figure 2.9: Vlaue of parameter (Reese et al., 2006)

- **O'Neill Model**

In O'Neil (1984), the ultimate soil resistance P_u is determined as the lesser value of Equations 2.15 and 2.16.

$$P_u = \gamma z[D((K_p - K_a) + zK_p tan\phi\ tan\beta) \qquad (2.15)$$

$$P_u = \gamma Dz(K_p^3 + 2K_o K_p^2 tan\phi + tan\phi - K_a) \qquad (2.16)$$

where, K_p= Ranking passive earth pressure coefficient; $(^1/_{K_a})$

The soil resistance per unit length (P) is calculated using Equation 2.17 The p-y curve shape obtained from this equation is presented in Figure 2.11 and the comparison of O'Neil (1984) and Reese (2006) p-y curve is shown in Figure 2.12.

$$P = \eta\, A\, P_u tanh[\left(\frac{k_h z}{A\, \eta\, P_u}\right) y] \qquad (2.17)$$

where, η = a factor used to describe pile shape generally taken as 1.0 for circular piles;

A = 0.9 for cyclic loading, and 3-0.8z/D≥0.9 for static loading,

The value of ϕ is obtained from the SPT as shown in Figure 2.10a and the value of the k_h is obtained from the ϕ as shown in Figure 2.10b.

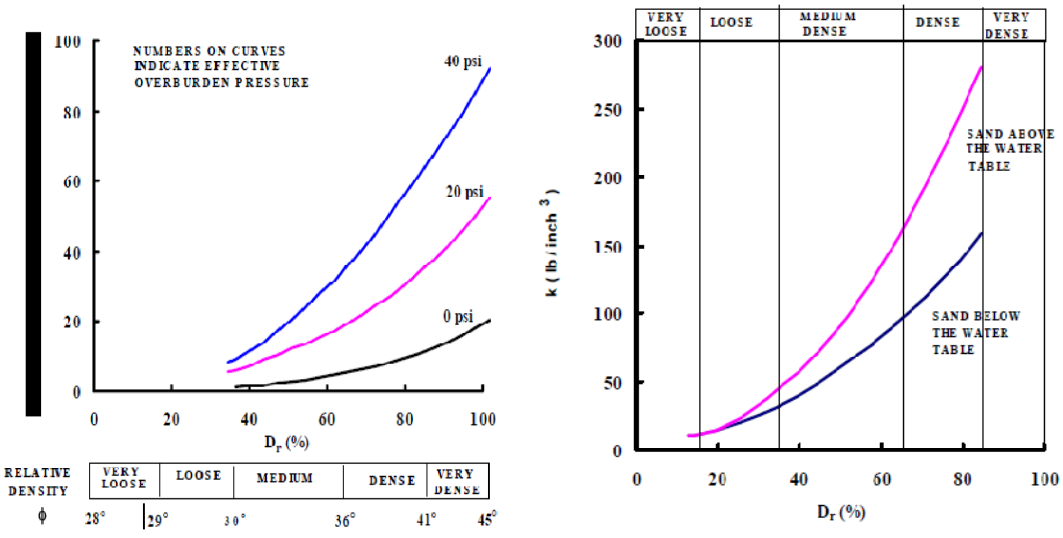

(a) (b)

Figure 2.10: a) SPT blow count versus ϕ and relative density, Dr b) kh versus Dr

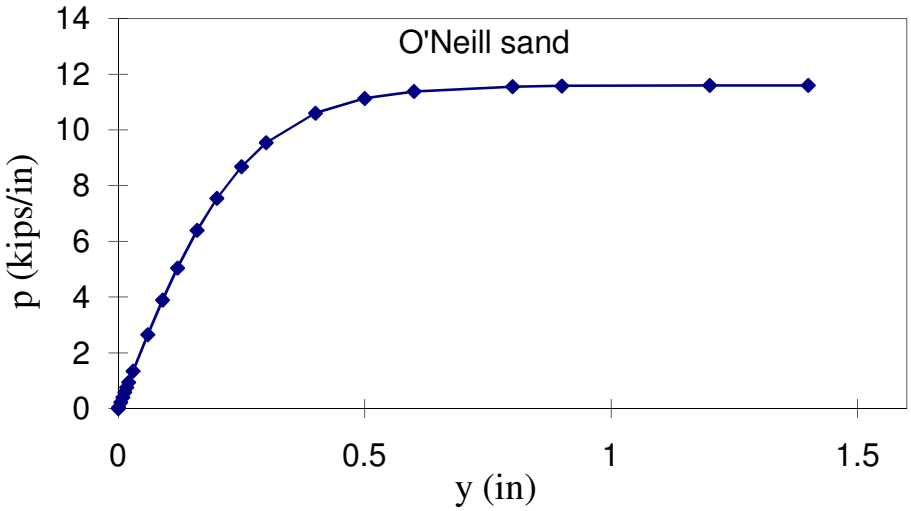

Figure 2.11: P-y curve according to O'Neill Method (O'Neill, 1984)

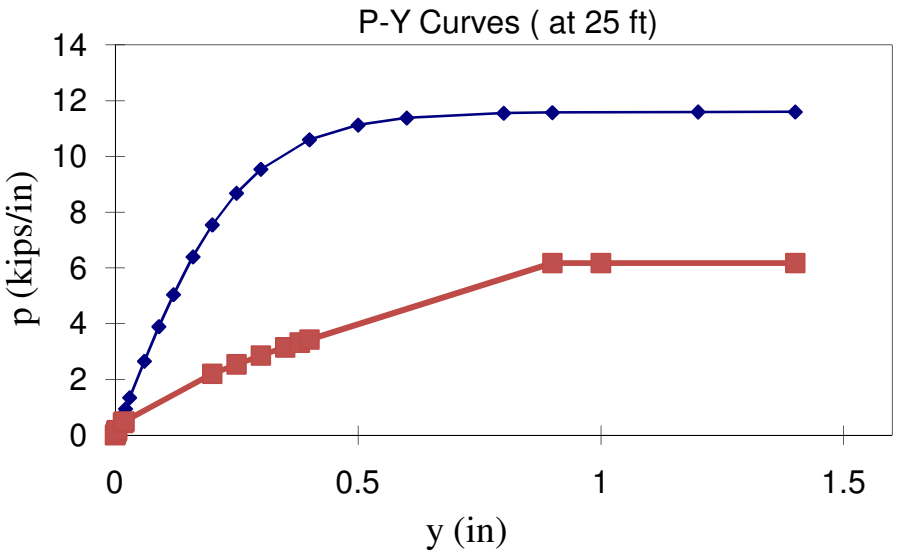

Figure 2.12: Comparison Chart of p-y curves of Reese (2006) and O'Neill (1984) Methods

2.2.2.4. P-y Curve for Pile Group

The application of the lateral load causes piles to move in the loading direction. For the pile group, the soil in front of the leading row resists the lateral movement of pile, whereas, the piles in the trailing rows push the soil which in turn pushed on the piles in front of them, eventually

reducing the lateral resistive force for trailing rows (Prakash and Sharma, 1990; Salgado, 2008; Ilyas et al., 2004; and Ashour et al. 2004). The soil-pile-soil or group interaction effect reduces with the increasing of center-to-center spacing between the piles. Brown (1988) introduced the concept of p-multipliers, and the value of p-multipliers represents the intensity of group interaction. The p-y curves for group pile are developed by multiplying the p-multiplier value to p-y curves of single pile as show in the Figure 2.13. Similarly, Ruesta and Townsend (1997) evaluated the behavior of laterally load pile group at Roosevelt Bridge and observed similar value of p-multipliers suggested by Brown (1988) for prestressed pile in both free and fixed head conditions in the soil profile consisted of loose sand (Figure 2.14). McVay et al (1998) found that p- multipleers are indepnedent of soil densities and only a funciotn of the pile group geometery. However, Ashour and Norris, (2000) assumed that the mobilizaotn of p-multipliers appear to be a functions of soil types, soil densities, pile spacing, pile location with respect to loading direction and pile head connections. Mokwa (1999) recommended that the piles in a group be modeled as an equivalent single pile with a flexural stiffness equal to the number of pile in the group multiplied by the flexural stiffness of a single pile within the group. The summary of p-multiplier observed form the several researchers in literature are presented in Table 2.5

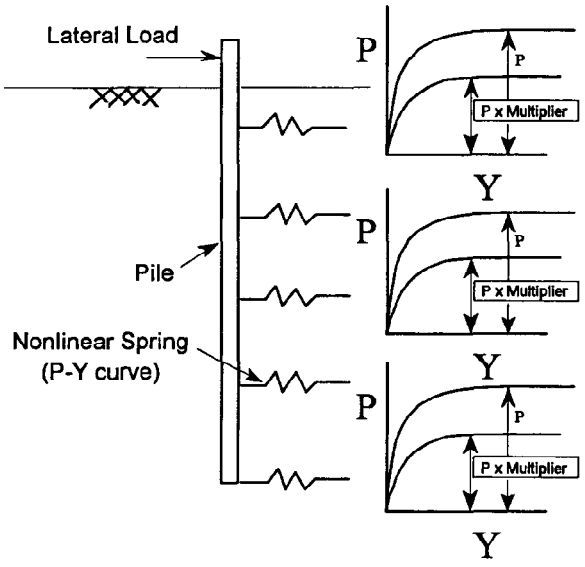

Figure 2.13: P-Y curves of piles in group pile using p-multiplier approach (Brown et al., 1988)

Table 2.5 Recommended values of p-multipliers

Reference	Test type	Pile			Values of p-multiplier						
		pattern	spacing	head fixity	Row1	Row 2	Row 3	Row 4	Row 5	Row 6	Row 7
Brown et al. (1988)	Full scale	3x3	3D	Pinned	0.8	0.4	0.3				
Brown et al. (1987)	Full scale		3D	Pinned	0.7	0.5-0.6	0.4-0.5				
McVay et al. (1995)	Centrifuge	3x3	3D	Pinned	0.8	0.4	0.3				
	Centrifuge	3x3	3D	Pinned	0.65	0.45	0.35				
	Centrifuge	3x3	5D	Pinned	1	0.85	0.7				
Ruesta and Townsend (1997)	Full scale	4x4	3D	Fixed	0.8	0.7	0.3	0.3			
McVay et al. (1998)	Centrifuge	3x3	3D		0.8	0.4	0.3				
	Centrifuge	3x4	3D		0.8	0.40	0.3	0.3			
	Centrifuge	3x5	3D		0.8	0.40	0.3	0.2	0.3		
	Centrifuge	3x6	3D		0.8	0.40	0.3	0.2	0.2	0.3	
	Centrifuge	3x7	3D		0.8	0.40	0.3	0.2	0.2	0.2	0.3
Rollies et al. (1998)	Full scale		3D	Pinned	0.6	0.4	0.4				
Rollines et al. (2003a)			2.8D		0.6	0.38	0.43				
			5.65D	-	0.98	0.95	0.88				
Rollines et al. 2003b		3x3	3D		0.82	0.61		0.45			
		3x5	3.3		0.82	0.61	0.45	0.45	0.46		
		3x4	4.3		0.90	0.81	0.69	0.73			
		3x3	5.6		0.94	0.88	0.77				

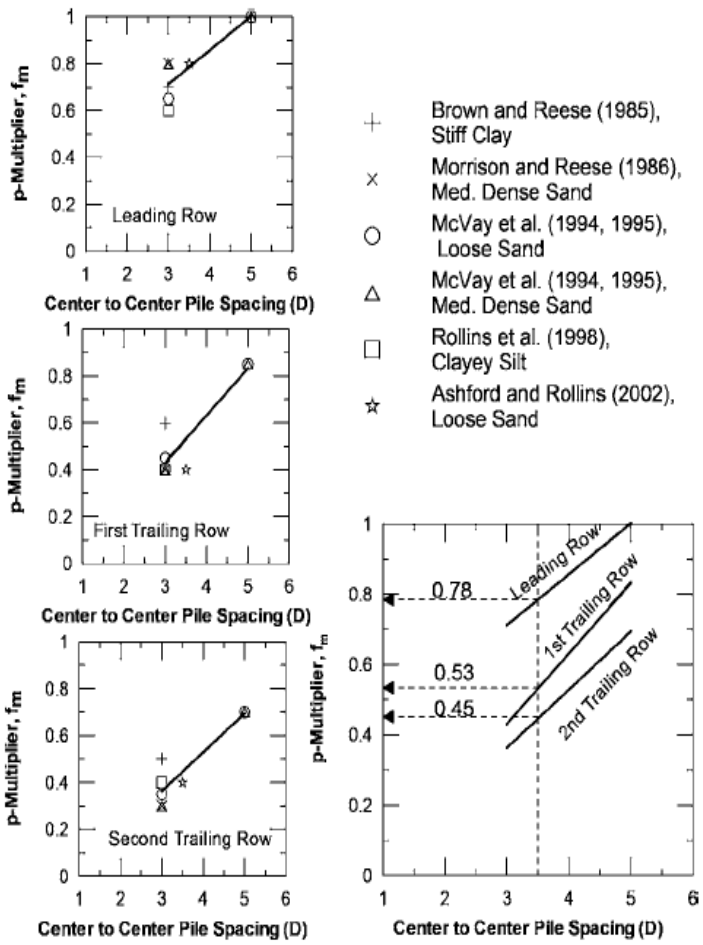

Figure 2.14: Relationship between the p-multiplier and the pile spacing for each row in the Group (Mokwa, 1999)

2.3 Research Review on Battered Pile

Batter pile or inclined pile generally classified into two types based on the loading direction;. the pile which is battered toward the loading direction is negative batter or reverse batter pile, whereas, the pile battered against the loading direction is positive or forward batter pile as shown in Figure 2.15. Batter piles are widely used in offshore structure due to their considerable resistance against lateral loading induced by ship impact, water wave, etc. The research on the laterally loaded battered piles began with Fealing (1937) who performed full-scale tests on battered timber pile followed by model tests performed by few researchers (e.g., Tschebotarioff

1953; Murthy 1964; and Prakash and Subramanyam,1965). Kim and Brungraber (1976) and Manoliu et al. (1977) also performed full-scale tests on battered piles. It was reported that negative batter piles offer more resistance than positive batter piles which was also agreed by Ranjan et al. (1980) based on their laboratory test result. Lu (1981) also supported the concept and explained that the soil reaction at ground level is zero for a positive batter pile and maximum for a negative batter pile, indicating that the upper layer soil support in a negative batter is enormous so the negative batter pile has larger lateral resistance.

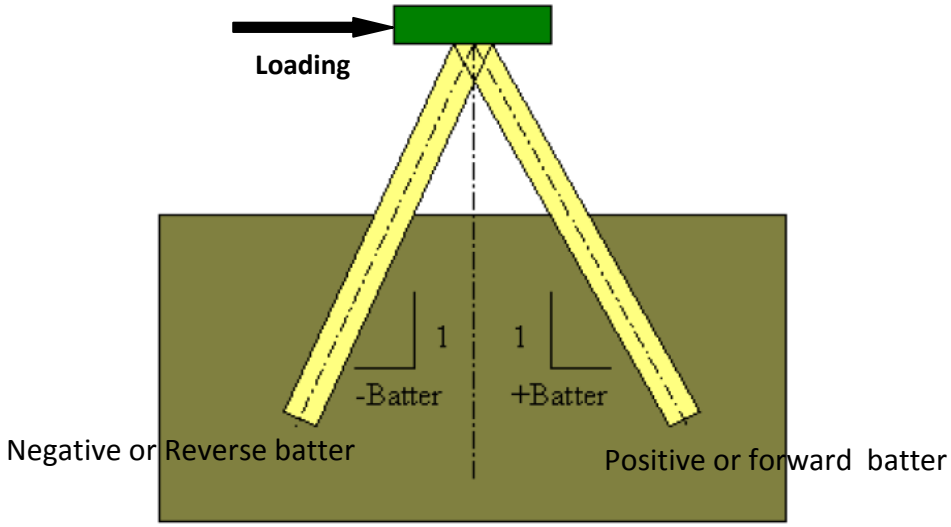

Figure 2.15: Battered pile categorized into positive and negative battered pile

Based on a centrifugal tests on laterally loaded single battered piles in sand with different relative density, Zhang et al. (1999) inferred that the effect of pile inclination on the lateral resistance is more effective in the dense sand and the lateral resistance of pile increases with the increment of the batterness of reversed or negative battered pile, whereas the lateral resistance decreases with the increment of batterness of forwarded or positive battered pile. Similarly, Rajashree and Sitharam (2001) performed a non-linear static analysis for both positive and negative batter piles at different angles (10°-30° inclination) and observed that the lateral deflection predicted at the ground line for a pile in positive batter is more than for vertical pile and less than for a negative batter pile, which agrees with Lu (1981) observation that there is zero lateral resistance for positive battered pile and maximum for negative battered pile at the ground line. Zhang et al. (2002) explained that the lateral resistance of the individual battered

piles in a given soil is influenced by the pile inclination and loading direction, and the application of vertical loading also influences the lateral behavior of battered pile.

As illustrated in Figure 2.16, at zero vertical load, when the lateral load is applied with no vertical load, the horizontal movement of the negative battered pile will cause a positive $\Delta\sigma_0$ in the soil in front of pile so the lateral resistance for the negative battered pile will be greater than the vertical pile.

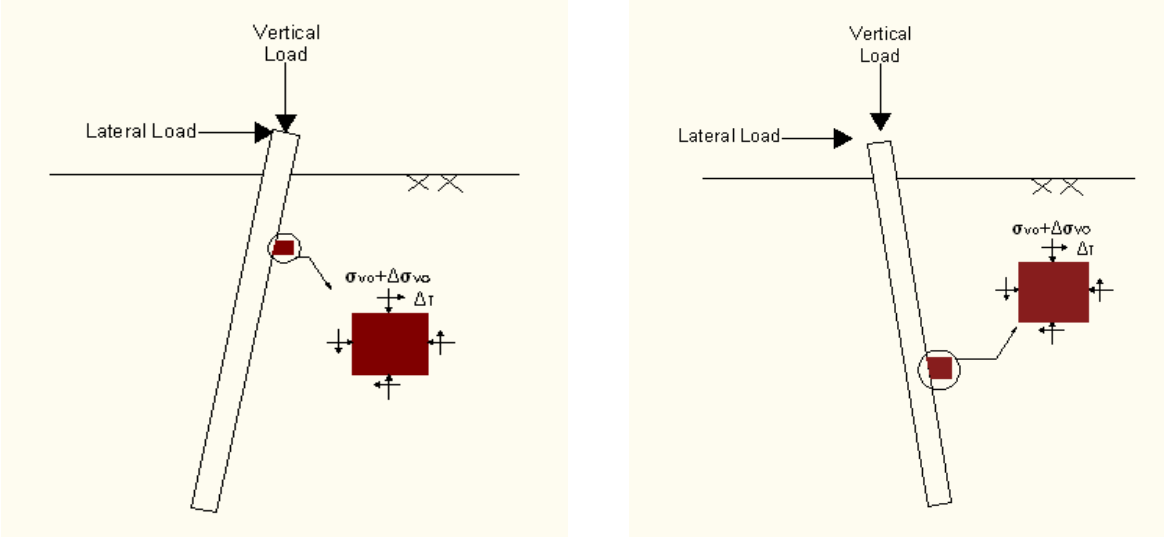

(a) For negative battered pile (b) For positive battered pile

Figure 2.16: Movement of soil around battered pile (after Zhang et al., 1999)

To the contrary, the lateral movement of the positive battered pile will cause an upward movement of soil which will reduce the vertical stress and hence the lateral resistance of the positive battered pile will be smaller than the vertical load. In comparison, the lateral resistance of negative battered pile will have a higher lateral resistance, followed by the vertical pile and positive battered pile will have the least lateral resistance. However, when the vertical load is applied, the lateral resistance of the negative battered pile reduced because of the bending moment by the vertical load component causes an additional lateral defection, whereas the lateral resistance of the positive battered pile since the bending moment caused by the vertical load negates the effect of the lateral load component.

Pinto et al. (1997) conducted centrifuge tests on battered pile groups and concluded that the group effects for 5B spacing and fixed-head conditions appear to be minimal and suggested the p-multipliers values of 1.0, 0.85, and 0.7 for rows 1, 2 and 3 of 3x3 pile configuration. Recently, Sheikhbahaei and Vafaeian (2009) conducted dynamic response of concrete batter pile group under seismic excitation through finite element modeling and concluded that the increment of either batterness or center-to-center spacing reduces pile displacement, bending moment and shear force.

2.3.1 P-y Curves of Battered Piles

The effect of pile inclination on the p-y curves was investigated by Kubo (1965), Awoshika (1971) and Zhang et al. (1999). Their findings indicated that the shape of the p-y curves for battered piles and vertical piles are similar, but the batterness of pile influences the ultimate soil resistance (P_u), and the subgrade modulus (K_s). The variation of two important parameters: subrgade modulus which defines the initial slope of p-y curve, and the ultimate resistance, which governs the pile response at large deflections are controlled by the unit weight and angle of internal friction leads to modification of p-y curves of vertical pile in order to generate p-y curves of batter piles. Zhang et al. (1999) suggested that changes in subgrade modulus (K_s) and the soil's ultimate resistance for battered piles (P_{ub}) are proportional to the ratio of passive earth pressure coefficient for battered pile to passive earth pressure coefficient for vertical pile as shown in Equations 2.18 through 2.20.

$$P_{ub} = \Psi P_u \tag{2.18}$$

$$\text{where , } \Psi = \lambda * \frac{K_{pb}}{K_p} \tag{2.19}$$

$$K_p = \frac{sin^2(\theta-\phi)}{sin^2\theta \ sin(\theta+\delta)[\,1-\sqrt{\frac{sin(\phi+\delta)sin(\phi+\beta)}{sin(\theta+\delta)sin(\theta+\beta)}}\,]^2} \tag{2.20}$$

where, λ = coefficient that accounts for the size of the sand's passive soil wedge,

K_p = passive earth pressure coefficient for vertical pile,

K_{pb} = passive earth pressure coefficient for battered pile,

θ = wall inclination,

ϕ = internal frictional angel of the soil,

δ = soil-pile interface friction angle,

β = the ground slope angle.

Similarly, the initial subgrade modulus for the battered piles, K_{sb} is obtained by multiplying the vertical pile subgrade modulus, K_s, with the same factor, Ψ (i.e., $K_{sb} = \Psi^* K_s$) . The value of Ψ factor for the modification can be estimated from Figures 2.17 and 2.18. The soil-pile interface friction angel δ has a considerable influence on the lateral resistance of battered piles. According to Sherif et al. (1982), the magnitude of δ depends not only on the soil properties but also on the amount and direction of the soil movement. Jardine and Chow (1996) found that the value of δ is independent of the relative density and tends to decline with particle size. It is noted that the soil-pile interface friction angel δ has a significant effect on the p-y curves. Specifically, the larger the δ value, the larger the K_b and P_{ub} values for the positive battered piles and the smaller the K_b and P_{ub} values for the negative battered piles versus vertical pile values. Figure 2.19 depicts the modified p-y curve for battered pile.

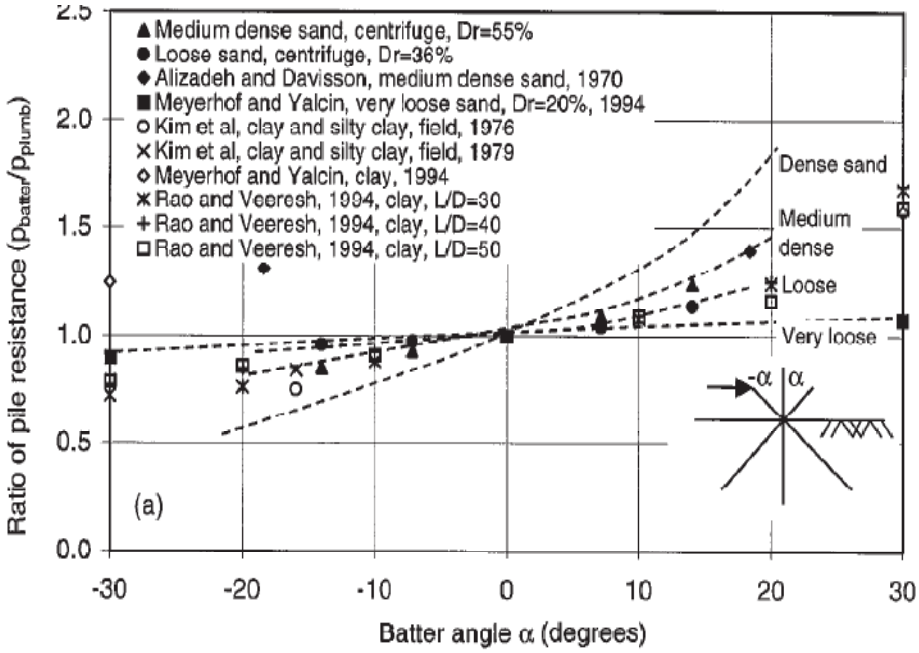

Figure 2.17: Influence of pile batter on pile resistance (Zhang et al. 1999)

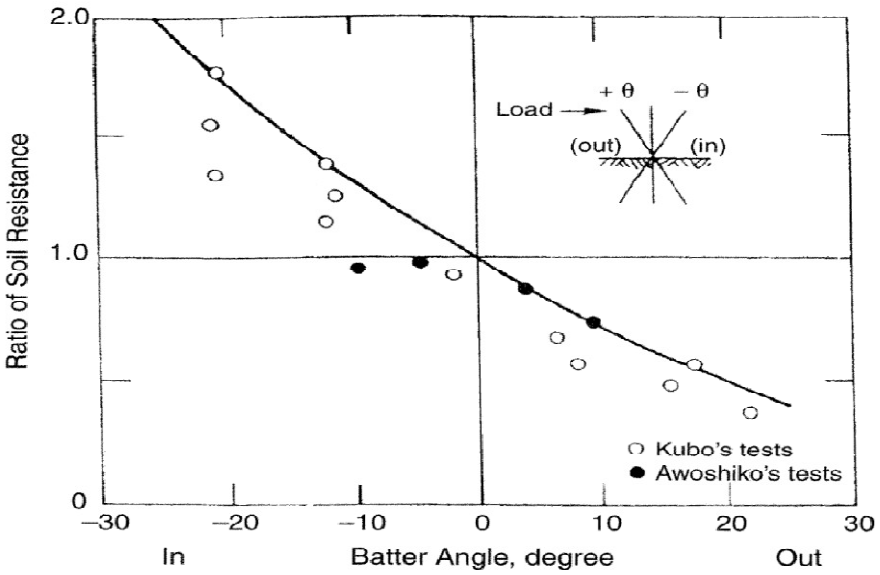

Figure 2.18: Influence of pile batter on pile resistance (Kubo, 1964)

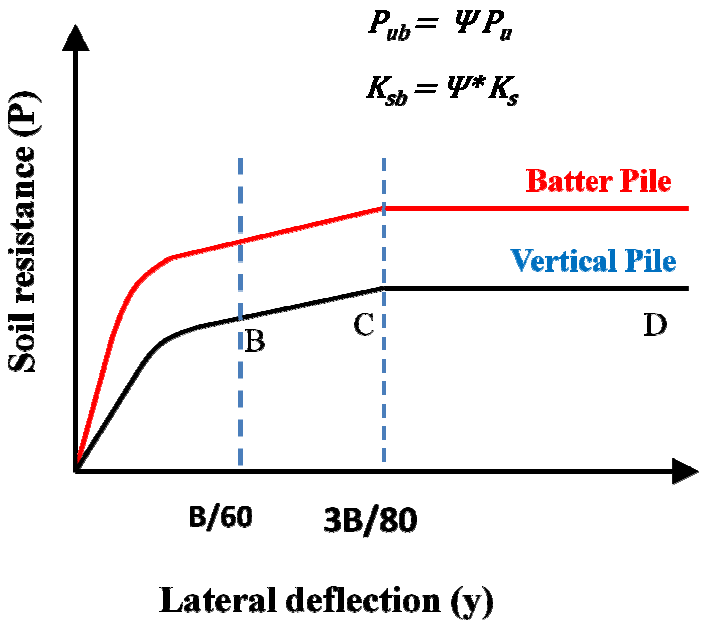

Figure 2.19: Modified P-y curves for battered pile in sand (Zhang et al., 1999)

2.4 Numerical Simulation Using Computer Programs

With the development of finite difference and finite element techniques, several computer programs such as COM624P/ GROUP (Wang and Reese, 1993), LPILE (Reese et al., 1997), FLPIER (McVay et al., 1996), FB-MultiPier (University of Florida, 2000) were developed. The applicability and structures of these programs are discussed in details in the following sub-sections.

2.4.1 Finite Difference Method Based Programs

COM624P and LPILE program uses the finite difference method to analyze the response of single pile subjected to lateral loading by incorporating several p-y curves. LPILE models the pile as a beam with lateral stiffness based on the modulus of elasticity and moment of inertia of the pile and models the soil as a non-linear spring. The program can calculate the pile's stiffness as either linear or non-linear, depending on the user input. Typically, concrete pile stiffness is assumed non-linear whereas steel pile stiffness is assumed linear. To analyze or calculate the displacement, shear, and moment in the laterally loaded pile, LPILE requires information of structural properties, each soil layer properties including modulus of lateral subgrade reaction or lateral subgrade modulus, and *p–y* curve shapes. The analysis of pile group is more complicated than single pile because of pile-soil-pile interaction. The LPILE and COM624P are not capable of analyzing group pile. GROUP program, the advanced form of COM624P, has incorporated *p-y* multipliers to predict the effect of pile-soil interaction and have been used by many researchers (Walsh, 2005, and Rollins et al., 2008) for the analysis of pile group. However, this program is directed principally at the case in which the individual piles are so widely spaced that the piles do not influence each other. The GROUP and LPILE runs through same finite difference method based computational technology, the inputs are almost similar. Rollins et al. (1998, 2002) and White et al. (2008) used the LPILE program for the single pile analysis and GROUP program for pile group analysis.

2.4.2 Finite Element Programs

A non-linear finite-element program, FLPIER, developed at the University of Florida for analyzing bridge pier structures is a flexible program that can model different pile and pier

configurations, for example, battered piles, variable spacing between piles, and missing piles. FLPIER is coupled with a graphical preprocessor, PIERGEN, to define the structure configuration and a postprocessor, PIERPLOT, to plot the deflected shapes, internal stresses, and forces (Hoit et al., 1995; Ruesta and Townsend 1997; McVay et al., 1995). The finite element program divides each pile into 16 two-node, three-dimensional elements consisting of 10 degrees of freedom, 3 degrees of translation, and 2 rotations at each node. At each node of the pile, lateral pile-soil interaction is modeled by nonlinear springs p-y curves. The incorporated p-y curves included O'Neill's p-y curves for cohesionless soil and cohesive soil, and default p-y curves similar to COM624P, and a user-defined p-y curves option for linear interpolation is also available. The intensity of group interaction effect is modeled using p-multiplier values. The advancement of this program took place by incorporating cracking effects of reinforced and prestressed pile to consider the non-linearity behavior of pile, because not considering cracking effects generally overestimates the stiffness of a pile subjected to relatively high loadings. Charles at al. (2001) investigated the behavior of large-diameter bored pile groups and studies the design parameters for modeling the non-linear response of soil and bored piles using FLPIER. Similarly, Zhang et al. (1999) simulated several centrifugal test models in FLPIER program in order to validate and improve it. They concluded that this finite element program is a reliable and powerful tool for laterally loaded pile group analysis. With the success of FLPIER, the Florida department of transportation advances this software by making some changes in interface and features that generates more powerful tool called FB-MultiPier, the newest development of the FB-Pier program.

Similar to FLPIER, the FB-MultiPier program couples the non-linear structural finite element analysis with non-linear static soil models for axial, lateral and torsional soil behavior to provide a robust system of analysis for coupled bridge pier structures and foundation systems. FB-MultiPier performs the generation of the finite element model internally given the geometric definition of the structure and foundation system as input graphically by the designer. This allows the engineer to work directly with the design parameters and lessens the bookkeeping necessary to create and interpret a mode. Poissel (2008) modeled the response of full-scale tests in FB-MultiPier and found that the model produced results within 10% error of the measured results for the desired 1.5 in pile deflection. Similarly, McVay et al. (2009) performed numerical

analysis using FB-MultiPier for time-domain analysis of soil- structure interaction from a full-scale vessel impact loading of a bridge pier.

2.5 Interpretation of Data for Deriving p-y Curves

Load-deflection responses of laterally loaded piles depend on many factors, such as pile geometry, structure material properties, adjacent soil conditions, soil-structure interaction, and loadings. The governing differential equations derived by Hetenyi (1946) for the lateral loaded pile derive are given in equation 2.21 and the typical profiles of displacement, bending moment, shear force and lateral soil resistance force per unit length are presented in Figure 2.20.

$$\theta = \frac{dy}{dz} \qquad M = EI\frac{d^2y}{dz^2}, \qquad V = EI\frac{d^3y}{dz^3} \quad P = EI\frac{d^4y}{dz^4} \qquad (2.21)$$

where,

θ = slope or rotation

y = lateral displacement

z = depth below

M = bending Moment

E = youngs modulus of concrete

I = moment of inertia

V = shear force

P = lateral soil resistance per unit length

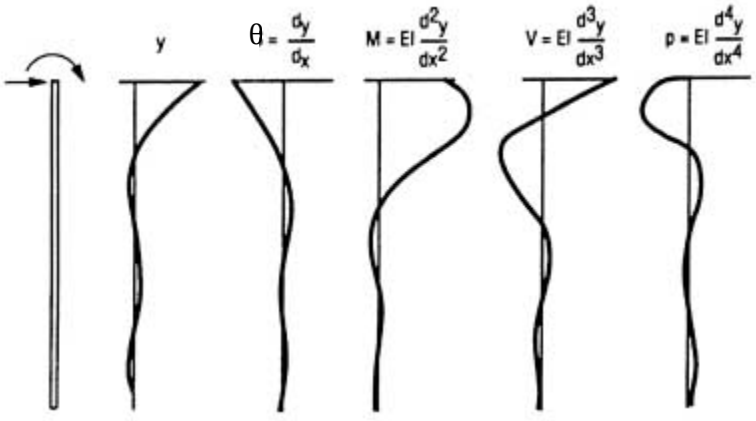

Figure 2.20: Typical profiles of y, θ, M, V and P

The equation for soil reaction (P) is commonly solved by numerical methods such as finite difference method or finite element method or modeling the soil reaction using p-y curvess. In general, the raw data in the form of horizontal displacement or angular displacement obtained from the instruments such as inclinometer and strain gauge can be utilized to analyze the lateral responses of laterally loaded piles. Problems faced in such analysis are the difficulties during data interpretation obtained from inclinometer. It is essential to find a reliable method of data interpretation for deducing bending moment, shear force profile and back-calculating p-y curvess from the measured strain and deflection data.

The deflection from the inclinometer and strain gauges can be obtained by the following equations

$y = \iint \phi dz$……..from stain gauges (2.22)

$y = \int \theta dz$……..from inclinometer (2.23)

where θ is slope or rotation measured from the inclinometer, ϕ is the curvature (compression strain-tension strain) measured from strain gauges. The integration of discrete data such as rotation, curvature measurements provides fairly reliable results due to minimization of error during process, but deducing bending moments and soil reaction from rotation measurements amplify error values. So far, several methods have been proposed to fit the data obtained by double differentiating to evaluate the p-y curves. Herein these methods are briefly reviewed:

A) High order global polynomial curve fitting (Reese and Welch, 1975)

B) Piecewise polynomial curve fitting (Matlock and Ripperger, 1956)

C) Weighted residual method (Wilson, 1998)

D) Brown least square error method (Brown, 1994)

E) Energy Method (Lao and Jen, 2003)

F) Cubic Spline (Dou and Byrne, 1996)

2.5.1 High Order Global Polynomial Curve Fitting Method

Broms (1964) assumed that the reaction profile could be described by a polynomial, which is generally true for long piles. King (1994) said that fitting simple polynomial to the discrete data points and differentiating the polynomial might not be realstic and smooth, hence a high order polynomial becomes essential. Many researchers have interpolated discrete measurements of moment or curvature of a pile and double differntiated their interpolating fucntions to calculate the lateral resistances along the pile (Matlock and Ripperger, 1956; Dou and Byrne, 1996). Ruesta et al. (1997) used third order polynomial to fit bending moments profiles. Wilson, (1998) applied three mehtods: cubic splines, polynomial functions and finite element techniques to fit the data obtained from the strain gauges. In polynomial technique, Wilson (1998) fitted 5^{th} and 6^{th} order polynomial equation to the discrete bending moment data using the least square method.

$$M = a + bz + cz^2 + dz^3 + ez^4 + fz^5 \quad (2.24a)$$

$$M = a + bz + dz^3 + ez^4 + fz^5 \quad (2.24b)$$

$$M = a + bz + cz^{2.5} + dz^3 + ez^4 + fz^5 \quad (2.24c)$$

Equation 2.24a has five lowest order integer terms was used to fit seven recoreded moment points along the pile, whereas Equation 2.24b includes five fitting terms but assume the lateral resistance is zero at the surafce of the soil leaving out the quardratic term. Equation 2.24c contains non interger fitting terms by assuming zero lateral resistance at gound surface. Furthermore, Wilson (1998) used these equations and concluded that Equation 2.24b is clearly inconsistent with the other methods, wheras Equation 2.24a is the most reasonable approximation. Similay, Illyas et al. (2003) analyzed the bending moment profile using a 7^{th} order polynomial curve fitting method.

All polynomal Equations are used for the discrete moment data obtained directly from the strain gauge measurements using $M = EI\frac{d^2y}{dz^2}$. The moment from strain gague data can be easily calculated from strian gauge measurement, whereas neither integration nor differentiation is necessary. However, the data obtained from the inclinometer need to be integrated and differentiated to deduce deflection and bending moment profiles. Nip et al. (2005) introduced the

4^{th} order polynomial to interpret inclinometer data in which non-liner flexural concerete behavior is also considered . The fourth order polynomial was chosen on the basis of three known boundary conditions and one reasonably assumed boundary condition at the pile head. By introducing the 4^{th} order polynomial, Nip et al. (2005) calculated the shape of a soil reaction profile and by back-analysis the p-y curves were generated. The 4^{th} order polynomial function for the soil reaction (P_z) is given as:

$$P = az^4 + bz^3 + cz^2 + dz \quad (2.25)$$

$$V = \frac{az^5}{5} + \frac{bz^4}{4} + \frac{cz^3}{3} + \frac{dz^2}{2} + F_0 \quad (2.26)$$

$$M = \frac{az^6}{30} + \frac{bz^5}{20} + \frac{cz^4}{12} + \frac{dz^3}{6} + F_0 z + M_0 \quad (2.27)$$

$$\theta = \sum_{z_{i=z_0}}^{z} \left(\frac{az^6}{30} + \frac{bz^5}{20} + \frac{cz^4}{12} + \frac{dz^3}{6} + F_0 z + M_0\right) * dz/EI \quad (2.28)$$

At the pile head rotation, the shear force (V_o) is known and bending moment (M_o) is calculated by multiplying the measured lateral force with the eccentricity of the force above the pile head for a free head pile. It is also assumed that bending moment, shear force and soil reaction are assumed to become zero at the same particular depth z_o, to provide the three necessary constraints. In the pile load test, z_o lies approximately between 1.5 to 3.5 m, which equal to 1-2 times the pile diameter below the depth of zero rotation. By assuming zero depth, the coefficient values a, b, c, d can be easily calculated from Equation 2.28 and then the moment, hence the rotation value is also analyzed. This technique allows the evaluation of the coefficient of the horizontal subgrade reaction (k) and p-y curves. This method assumes a shape of soil reaction profile instead of a shape of p-y curves. Since the shape of p-y curves in complex soils, such as silty soil or clayey soil with sand lenses are difficult to obtain, this method appeared good for such soils.

2.5.2 Piecewise Cubic Polynomial Function

Yang et al. (2006) evaluated four methods: global fifth-order polynomial curve fitting, piecewise cubic polynomial curve fitting, weighted residuals and smoothed weighted residuals method, and recommended the use of piecewise cubic polynomial curve fitting method (See Figure 2.21) for deriving p-y curves from instrumented lateral load tests, recommended piece wise cubic

polynomial curve fitting method for deriving p-y curves . Matlock and Ripperger (1956) and Dunnavant (1986) employed similar method to moment discrete data. In this method every five successive moment data points along the pile length are fitted to one cubic polynomial curve. This method requires at least five points of strain gages deployed at five different depths in the shaft. The double differentiation of the local fitted polynomial curve with respect to middle point yields p at that point.

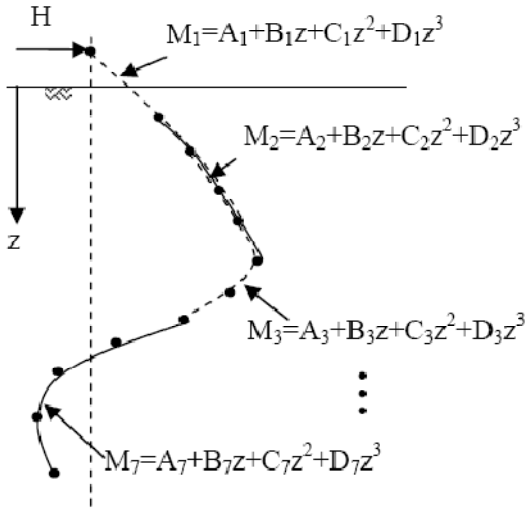

Figure 2.21: Procedure for reducing moment data to p using piecewise polynomial. (Dunnavant, 1986)

2.5.3 Weighted Residual Method

Wilson (1998) developed this finite element approximation method based on the minimizing weighted residuals to deduce the soil resistance from strain gauges. The residual function R(x) is considered zero in average as shown in Equation 2.29.

$$\int_0^L R(x)\Psi(x)dx = 0 \qquad (2.29)$$

Where, Ψ(x) is an arbitrary weighting function.

The pile is assumed as a discretized finite elements with nodes at each bending moment gauge location. Wilson (1998) invoked this weighted residual method in his dissertation and compared it with the polynomial method and cubic spline method. He found that weighted residual method appeared to be the most reliable one. Janoyana et al. (2001) examined cubic spline method, polynomial and weighted residual method for fitting smooth curves through profile data and concludes that weighted residual method provides the most satisfactory results.

2.5.4 Brown Method

Brown (1994) proposed an analytical method to derive the p-y curves from simple inclinometer data using the least squares regression technique. The variations in the shape of the p-y curves and the variations with depth are defined using several variables which are the subject of the fitting process, the variables are input soil strength and stiffness parameters, undraiend shear strength (C_u) and strain corresponding to half ultimate stress (ε_{50}) for clays, angle of internal frictional (ϕ) and subgrade modulus (K_s) for sands. Other parameters could be used as the unknown fitted variables. The lateral deflection, (y) was computed from the soil parameters, using COM624 program by solving set of nonlinear equations. Also the deflections are known from the test. Then the value of soil parameters is estimated by using the least squares "inversion" technique similar to that used for interpreting geophysical data. Brown (1994) successfully used this technique and concluded that this analytical method is a rigorous and reliable method of interpreting lateral load test on piles or drilled shafts using inclinometer data.

2.5.5 Energy Method

Energy conservation concept has been used by some researchers (Liao and Lin 2003; Han and Frost, 2000), to derive the deflection function form the inclinometer data of laterally loaded piles. The total energy for a pile embedded in the soil is the sum of strain energy (U) and work (V). The strain energy is the function of the deflection, and the potential energy depends upon the soil pressure and the applied lateral load. Liao and Lin (2003) expressed the total energy as (Equation 2.30) and generated the deflection function as per the Rayleigh-Ritz method. Han and Frost (2000) derived an equation for the total energy considering the shearing deformation effect using Timoshenko Beam theory solutions for load-deflection responses

$$TE = 1/2 \int_0^L EI(y")^2 dz + 1/2 \int_0^L P(z) y dz - Hy(L) \qquad (2.30)$$

Where,

L = embedded length of pile

H = lateral forces applied at the pile head

Liao and Lin, (2003) verified this method by analyzing a data of a full-scale lateral load test conducted by Washington DOT, and lateral load test on H piles. The authors claimed that this method delivered a reasonable prediction of pile performance in both single piles and pile groups in comparison to Brown (1994) method and also simple spreadsheet is required for the iteration, wheras Brown method requires COM624 program.

2.5.6 Cubic Spline Method

Mezaziagh and Levacher (1998) employed cubic spline method to fit the discrete moment data points. It is considered as the simplest interpolation of discrete test data that can be double differentiated. However, it is more prone to any potential measurement error. Dou and Byrne (1996) used cubic splines to derive p-y relationships from dynamic hydraulic gradient model tests with good results.

CHPATER 3
DESIGN OF LATERAL LOAD TEST

The newly built I-10 Twin Span Bridge of 5.4-miles length replaced the old bridge that had suffered massive damages caused by Katrina, a category 3 hurricane that hit Louisiana in 2005. The old bridge with an elevation of 9 ft could not resist the storm surge generated in Lake Ponchartrain and consequently most part of bridge remain unusable. In order to resist the high storm surge, the new bridge was built with an elevation of 30 ft, which is 21 ft higher than the old bridge. Figures 3.1and 3.2 show the project site location and a photo of the newly built I-10 Twin Span Bridge, respectively.

Understanding the proper behavior of superstructure and substructure of the newly built bridge under induced axial and lateral load is essential to ensure proper performance of the bridge during service life. In order to understand the lateral load mechanism of the pile foundation at I-10 Twin Span Bridge, a full-scale lateral load test was designed and conducted at M19 eastbound pier. The M19 pier was selected as it is second pier from the marine traffic under pass and more susceptible to lateral load due to possible ship impact in addition to the wind and water waves. It consists of 24 battered pile group in which some selected piles were instrumented with advanced instruments prior to the full-scale lateral load test.

It is also understood that the performance of group pile differs from the performance of single pile because of pile-soil-pile interaction. In order to compare the performance of group pile with the single pile and to determine the group effects, a statnamic lateral load test was also performed on one single vertical instrumented pile. The measurements obtained from instrumentation can be used to evaluate the performance and behavior of a single pile, as well as battered pile group under lateral loading.

Figure 3.1: Location of I-10 Twin Span Bridge site

Figure 3.2: Newly constructed Twin Span Bridge

3.1: Full-Scale Lateral Load Test at M19 Pier

A unique full-scale lateral load test was conducted at M19 Pier in order to evaluate the performance of batter group pile under lateral loaded conditions. The test was conducted by pulling the M19 eastbound pier and westbound pier toward each other using high strength tendons. The foundation of both M19 east bound and west bound pier consist of 6 X 4 precast prestressed concrete battered pile group. The center-to-center spacing between piles located in parallel to the loading at the cap level is 13 ft or 4.33B, where B is pile width. This section presents a review of geotechnical site condition, instrumentation, design of lateral load tests, and result of the lateral load test on pile group for battered pile group.

3.1.1 Description of the Tested Pier's Foundation

The M19 pier supports 200 ft long steel girders in the north side and 135 ft long concrete girders in the south side. The M19 pier is the second pier south of the marine traffic underpass. The size of pile cap (or footing) of the M19 piers is 44 ft × 42.5 ft × 7 ft. The view of M19 east and west bound piers are depicted in Figure 3.3. The foundations of M19 piers consist of 24 precast presetressed concrete (PPC) piles in a 6 X 4 configuration, 4 rows piles in the direction of loading and 6 rows piles perpendicular to the direction of loading. The center-to-center spacing of piles in the direction of loading at the cap level was 13 ft or 4.33 B and 7.5 ft or 2.5 B in the direction of perpendicular to the loading. The plan view of pile configuration is presented in Figure 3.4. All 24 piles were 110 ft long with an outer dimension of 36 in including a circular void of 22.5 in with the exception of top 20 ft was solid section. The average embedded length of the piles was 87 ft. The pile were battered at 1:6 slope; the two row piles closer to the eastern side of pile cap (position of loading) were battered in the direction of loading and the two row piles closer to the western side of pile cap were battered against the loading. Each pile was reinforced with 36 number of 0.6 in. diameter strands with an initial tension of 43980 lbs. The piles were designed to have a minimum compressive strength of 6000 psi at 28 days and of 4500 psi at the time of transferring the prestressed force.

Figure 3.3: M19 east and west bound piers site

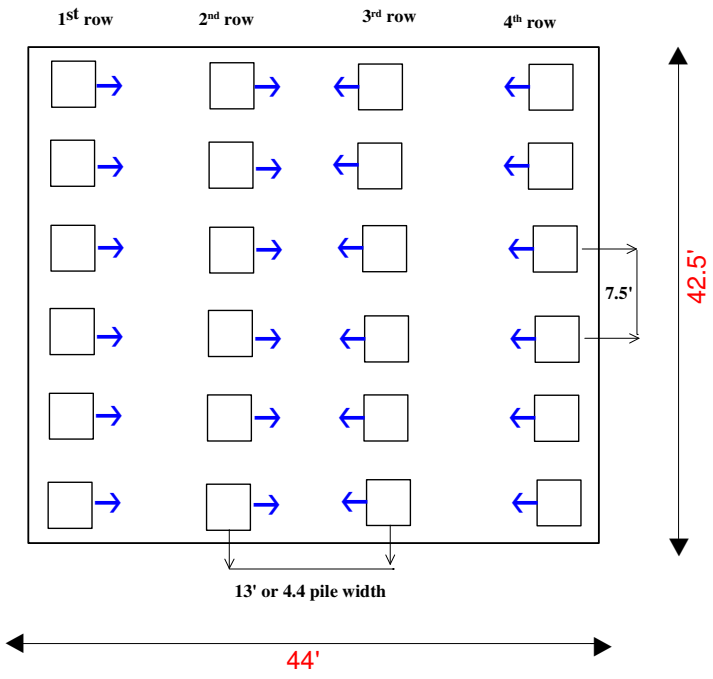

Figure 3.4: Plan view of pile layout

3.1.2 Geotechnical Site Conditions at M19 Pier

Several geotechnical tests including in-situ and laboratory tests were performed by Fugro Inc. for the site characterization. The generalized subsurface profile at I-10 Twin Span Bridge developed by Fugro Inc. is presented in Figure 3.5. As a full-scale lateral load test was designed to perform on M19 pier, five CPT tests and one soil boring test with several SPT tests were conducted in order to investigate subsurface soil properties and to determine the pile's tip elevation. Out of the five CPTs, four tests were conducted at distances 5 to 10 ft from the four corners and one at the center of foundation as shown in Figure 3.6. The depth of CPT test ranges from 160 ft to 185 ft. below mudline. The main purposes of performing CPT tests were to define soil profile, to observe any variation of soil properties across the foundation site, and to locate the depth of the bearing sand layer to support the piles. The approximate water depth measured nearby M19 Pier was nearly 11to 12 ft. The depth of bearing sand layer at the M19 pier was found to be at depths ranging from 100 ft. to 110 ft. below the water surface.

The CPT tests measured tip resistance (q_c), friction resistance (f_c), and pore pressure (u): the average q_c and f_c for top 20 ft depth below mudline were 1.23 tsf and 0.028 tsf, respectively. The undrained shear strength (S_u) were calculated and plotted using CPT soil classification software version 5 developed by Louisiana Transportation Research Center (Abu-Farsakh et al. (2008). The undraiend shear strength based on CPT was computed using the following Equation 3.1.

$$S_u = \frac{q_c - \sigma_{vo}}{N_{kt}} \qquad 3.1$$

where,

S_u=undrained shear strength, σ_{vo}=vertical overburden stress and N_{kt} is a bearing factor. The value of N_{kt} is chosen to be 15 based on current Louisiana practice.

CPT soil classification was determined based on probabilistic method (Zhang and Tumay, 1996), which gives probability of soil behavior as sandy, silty and clayey. The CPT result shows that the soil profile at the M19 pier foundation mostly consist of silty clay soil down to 45 ft depth underlain by cohesionless soil from 45 to 57 ft followed by clayey soil. Cohesionles soil below the depth of 100 ft has limited influence on the lateral resistance force. Only soil layer up to

depth of 5 B to 10 B below pile tip influences pile-soil interaction (Reese and VanImpe, 2001). The average undrained shear strength computed from CPT were,

- 162 psf for the top soil (12-20) ft depth,
- 800 psf for 20-25 ft depth,
- 1300 psf for 25-35 ft depth,
- 902 psf for 35-45 ft depth,
- 1500 psf for 45-110 ft depth.

The summary of CPT result and corresponding soil classification is presented in Figure 3.7

One soil boring close to the M19 pier was drilled down to 200 ft and SPT tests were performed in sandy soil layers. The soil samples were retrieved from the ground surface and/or mud line to the completion depth of the boring using Shelby tube samplers. Laboratory tests consist of moisture content, atterberg limits and unconsolidated undrained (UU) triaxial tests were conducted on the collected samples for soil classification and evaluation of properties such as the undrained shear strength and compressibility characteristics of the foundation soils. The summaries of borings, SPT and laboratory tests are also illustrated in Figure 3.7. Based on laboratory and in-situ tests results the subsurface soils of M19 foundation are classified as:

- 0 to 35 ft depth: medium to stiff gray and tan silty clay to clay soil with silt pockets. Laboratory testing indicates that the soils have undrained shear strength ranging from 140 to 1000 psf.
- 35 ft to 47 ft depth : soft to medium clay.
- 47 ft to 57 ft depth: medium to dense light gray sand. The SPT-N values ranged from 16 to 22.
- 57 ft to 85 ft depth: medium to stiff gray clay with sandy clay/silt pockets. The undraiend shear strength ranged between 1700 psf to 2000 psf.
- 85 to 98 ft depth: medium to very stiff clay having undrained shear strength of around 2000 to 2600 psf.
- 99 ft to 160 ft depth: medium dense to very dense sand with interlayers of silty sand, clayey sand and silty clay soil. The SPT-N values range from 3 for loose sand to 86 for the very dense sand.

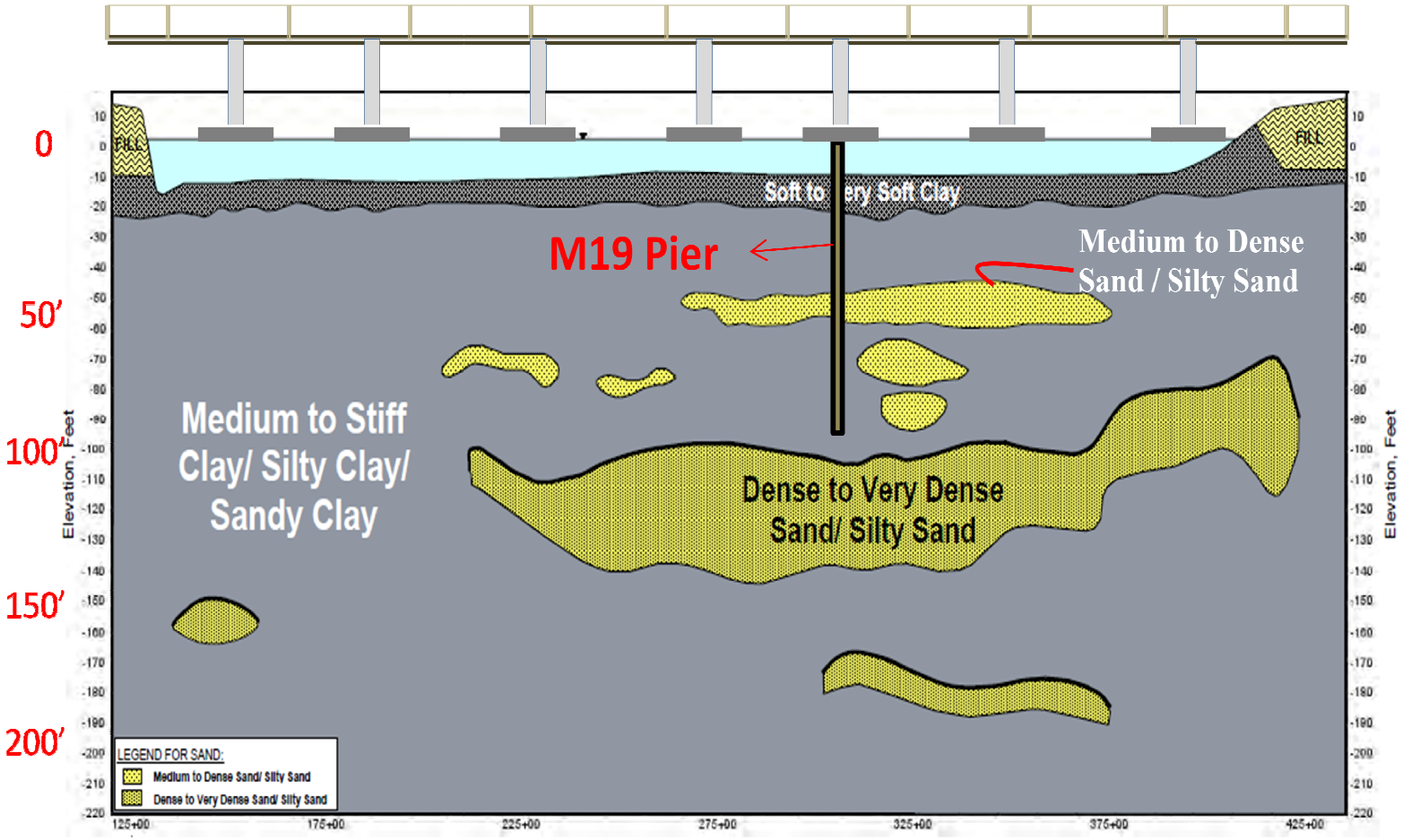

Figure 3.5: Generalized subsurface profile at twin span bridge

BENT M 19E

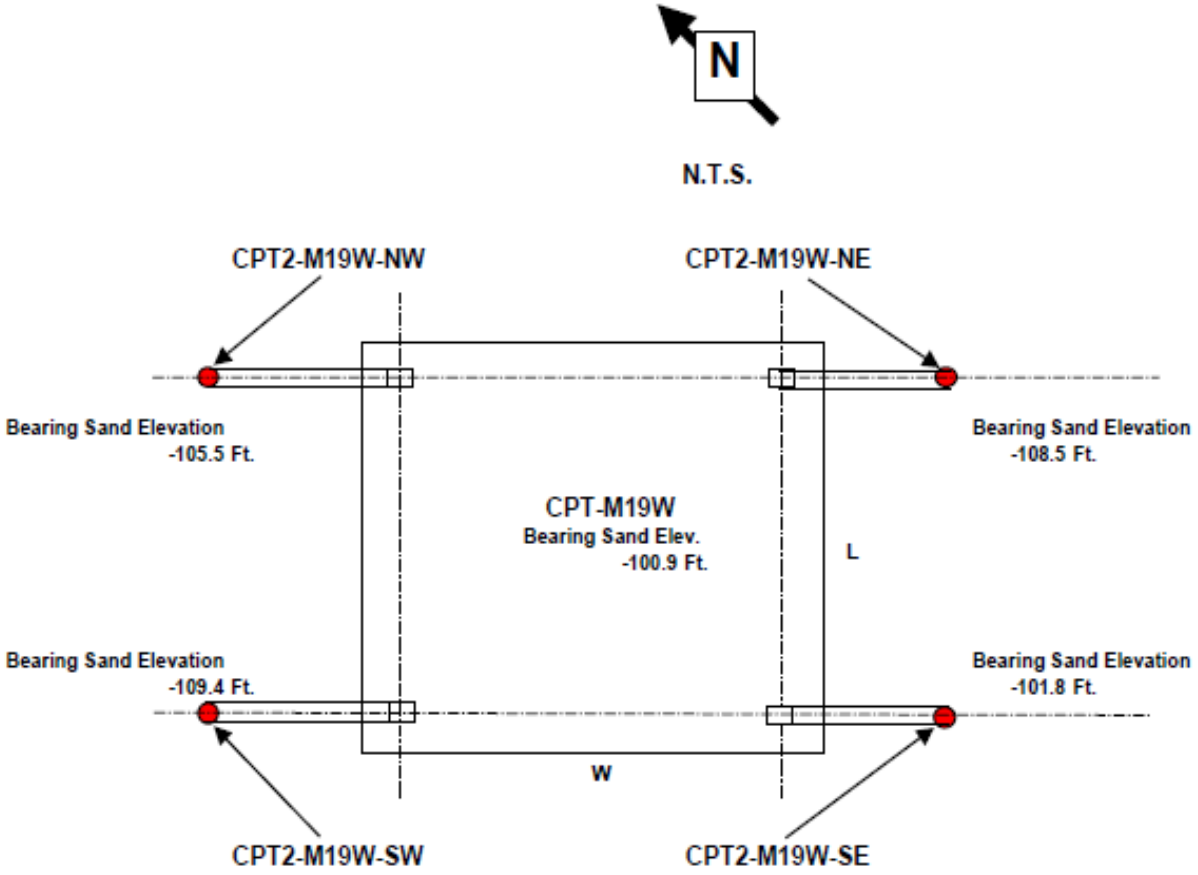

Figure 3.6: Location of CPT tests conducted at M19 Pier

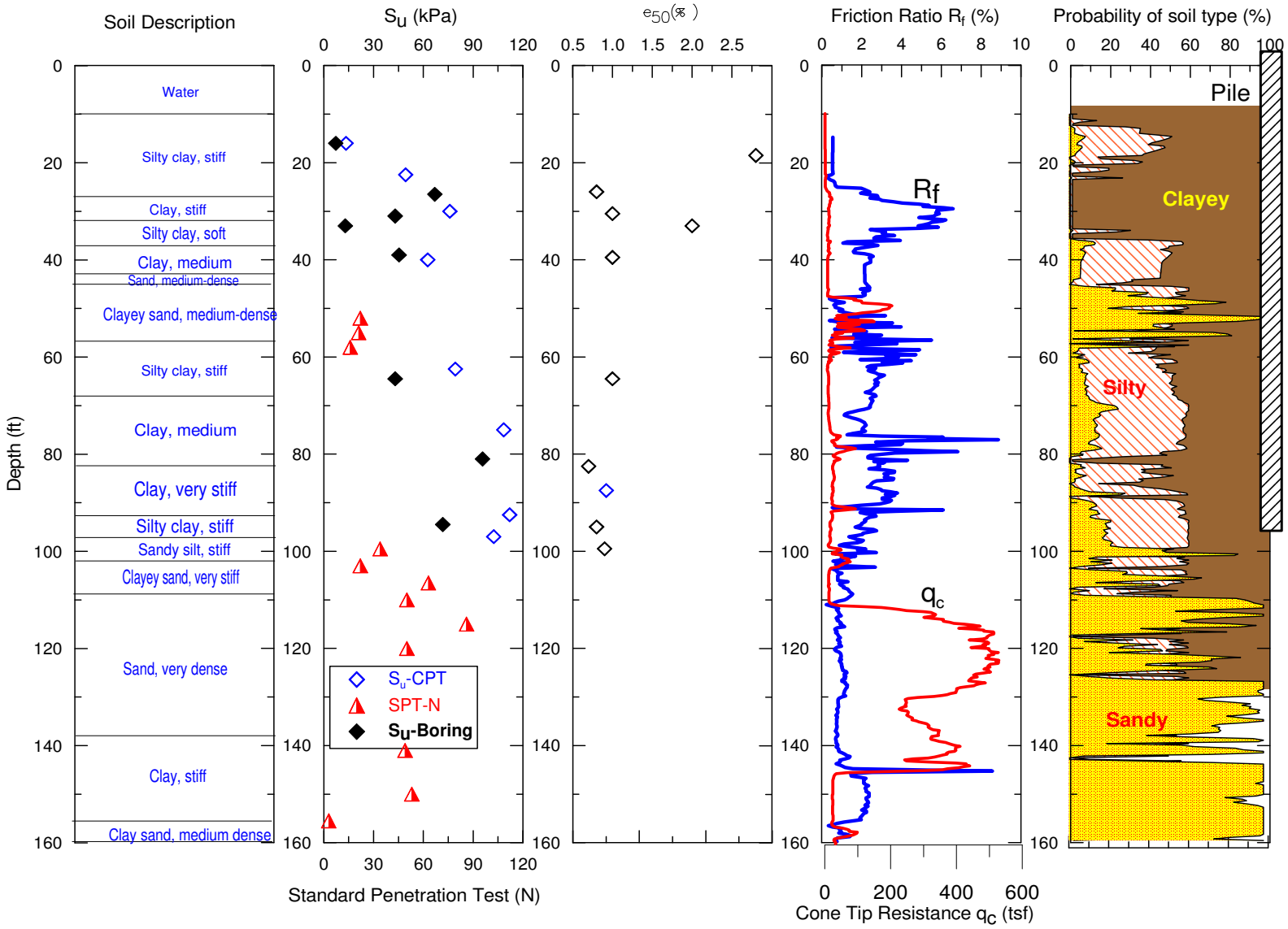

Figure 3.7: Summary of in-situ exploration and testing of site M19 pier

3.1.3. Pile Instrumentation

The selected piles of M19 pier were instrumented with MEMS In-place inclinometer (IPI) and strain gauges at different locations. The main purpose of installing inclinometers and strain gauges in selected piles was to measure the lateral deformation profiles with depth and to calculate the axial load and bending moments transferred to the piles. A plan view of M19 eastbound footing with layout of instrumented piles is presented in Figure 3.8.

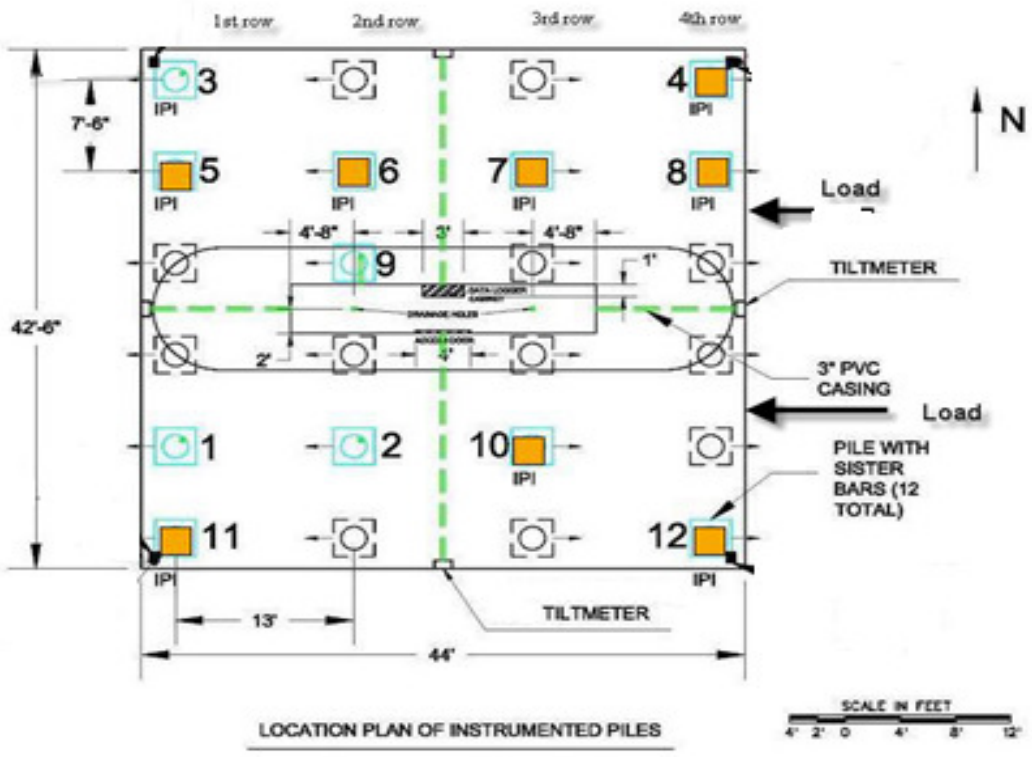

■ **IPI,** □ **Sister Bars**

Figure 3.8: Plan view of M19 pier footing with layout of substructure instrumentation

The In-placed inclinometers (IPIs) were installed in eight selected piles (piles number 4, 5, 6, 7, 8, 10, 11, and 12) after driving and cap casting. Each pile was instrumented with six inclinometer sensors located at elevations of -65, -45, -35, -25, -15, and -5 ft from the bottom level of the pile cap with the lowest one tied to an anchor point at the bottom of PVC casing at 85 ft. The inclinometer sense the position change (inclination) of access tube in two planes at

right angles to each other, and output from the probe is directly proportional to the sine of the angle of inclination of the long axis. The differences of subsequent readings with the initial base reading provide angular or lateral deformation on data logger at corresponding depth. The measurements from the six IPIs can provide a profile with depth of the lateral deformation of the pile for each load increment.

In addition, two pairs of resistance type strain gauges were installed at -16 ft and -21 ft from the pile top prior to concrete casting, taking into consideration the possibility of pile cutoff after driving. A total of twelve piles (piles number 1 through 12) were instrumented with strain gauges. The bending moment and axial loads moment developed at the piles can be easily calculated from the measured strains. The bending moments calculated from the strain gauges can be used to compare with the moments derived from the inclinometer data.

Also, in order to monitor the movements of laterally loaded M19 pile cap footing, four automated laser survey station prisms were installed at M19 eastbound and westbound, M17 eastbound, and M20 eastbound piers. The data obtained from the survey station prism were compared with the data obtained from the inclinometers. Figure 3.9 shows the photo of IPI sensor and survey prism. Figure 3.10 shows the position of instruments.

(a) (b)

Figure 3.9: (a) Inclinometer (b) Survey prism

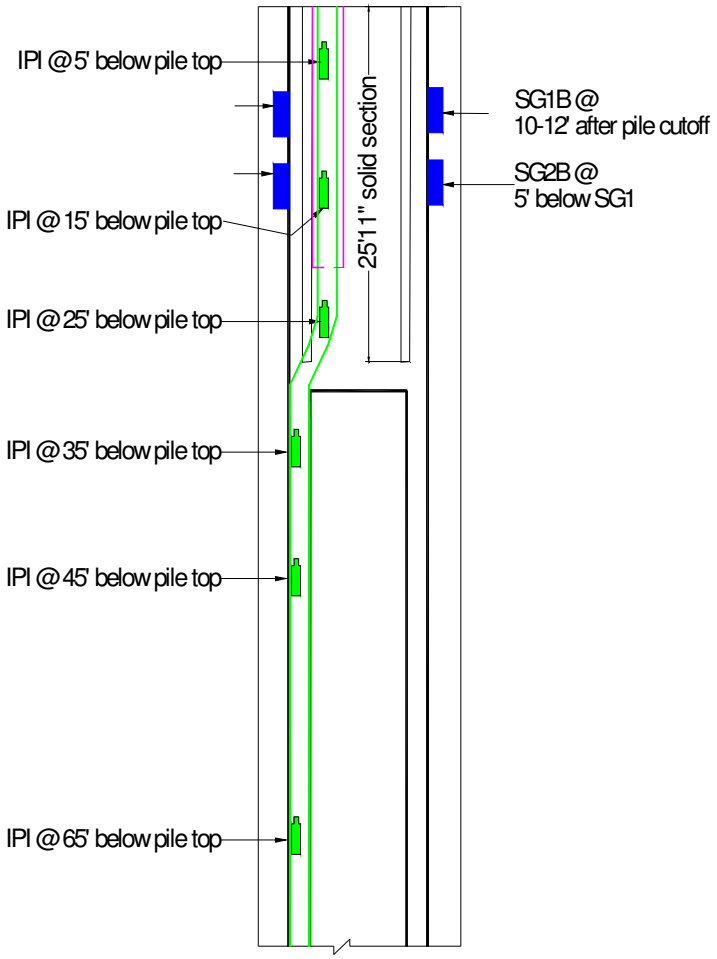

Figure 3.10: Location of inclinometer and strain gauges

3.1.4 Design of Lateral Load Test

A unique lateral load test was designed and conducted at M19 piers of the new I-10 Twin Span Bridge by Louisiana transportation geotechnical research team to evaluate the lateral response of battered piles group foundations and to verify the FB-MultiPier's analysis program which was used in the design of the bridge pile foundations. The test was conducted by pulling the eastbound and west bound toward each other using high strength steel tendons run through 4-in. PVC piles installed in both pile caps.

For setup of lateral load test, the M19 eastbound pier was designed as dead end and M19 west bound pier was designed as live end. The steel strands were first anchored at the dead-end side,

and then were threaded one-by-one through the two 4 in. PVC pipes from the dead-end at the eastbound pier toward hydraulic jack of the live-end at the westbound pier. Each steel tendon includes 19-0.62 in. diameter strands of low relaxation, high yield strength steel (E_s = 28,500 ksi). The lateral load was applied using 600-ton jacks with piston-end facings to pull the M19 eastbound and the west bound pier toward each other using the steel tendons.

The designed sequence of lateral load test includes preloading each tendon to 300 kips, then loading, unloading and reloading as presented in Table 3.1. The design maximum applied load was 2000 kips. However, the test was unloaded earlier at a maximum applied load of 1870 kips when the stroke in one of the 600-ton jacks reached its maximum limit. Figure 3.11 and Figure 3.12 depict the schematic diagram of the lateral load setup at M19 piers and the photos of M19 eastbound dead end and westbound piers live end design, respectively.

Table 3.1 Loading-Unloading-Reloading Table

No	**Lateral loads(kips) per cable**	**Total Lateral loads(kips)**	**Load Duration (min)**	**No**	**Lateral loads(kips) per cable**	**Total Lateral loads(kips)**	**Load Duration (min)**
Pre-Load	300	600	90	10	700	1400	15
1	350	700	5	12	800	1600	20
2	400	800	5	13	850	1700	20
3	450	900	5	14	900	1800	20
4	500	1000	15	15	935	1870	20
5	400	800	5	16	800	1600	10
6	300	600	5	17	550	110	10
7	400	800	5	18	300	600	10
8	500	1000	10	19	**Strands cut**		
9	600	1200	15				

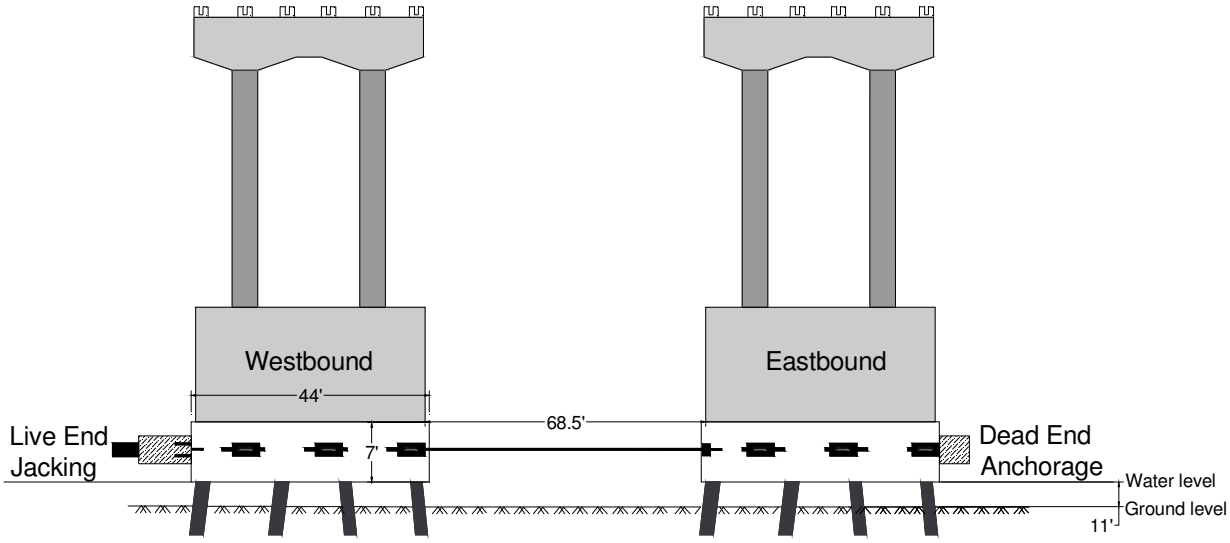

Figure 3.11: Schematic Diagram of Test Pile Cap Setup (Elevation View)

(a) Eastbound Pier with steel strands anchored at the dead end side

Figure 3.12: Setup of lateral load test

b) Jacking System at the Live-End of Westbound Pier

Figure 3.12: Setup of lateral load test (continued)

3.1.5 Result of Lateral Load Tests

The measurements obtained from the installed IPI sensors at selected piles (4, 6, 7, 8,10, 11, and 12) were recorded in the datalogger during the lateral load tests. Direct measurements from the six IPI sensors installed at -5, -15, -25, -35, -45 and -65 ft depth from the bottom of pile cap for each pile instrumented give the profile of rotation angles with depth. The displacements at corresponding depth for each pile were obtained using trigonometry method. For convenient visualization of pile deflections, lateral displacement profile over depth from pile cap to 65 ft depth below pile cap were calculated from IPI readings. Figures 3.13a through 3.13f present the deflection profiles obtained for the selected piles. The figures indicate that most of the lateral deformation occurred within the upper 50 ft of the piles' length. The maximum lateral deformation measured at 5 ft from the bottom level of the pile cap was ranged from 0.59 in to 0.67 in. This is in agreement with the measured lateral deformations of the pile cap using the automated laser survey, which were 0.58 in and 0.66 in for northwest and southwest corners of the M19 eastbound pier, respectively as shown in Figure 3.14.

The measured tension and compression strains at each load increment collected from the two pair of resistance type sister bar strain gauges installed at the selected piles 1 through 12 at 16 ft and 21 ft from the pile head before pile cutoff were also recorded. During test, some strain gauges were incapable of capturing the strain at the applied maximum load of 1870 kips. Also some stain gauges such as SG1 of pile 2 and SG2 of pile 7 were inactive, i.e, no data were recorded. Similarly, some measured data from SG1 of pile 8 and SG II of pile 1 were deemed unreliable as the difference of compression and tension strain found to be substantially high. Figures 3.15a through 3.15l present the measured strains obtained for the instrumented piles at two peak lateral loads, 600 and 1780 kips, respectively.

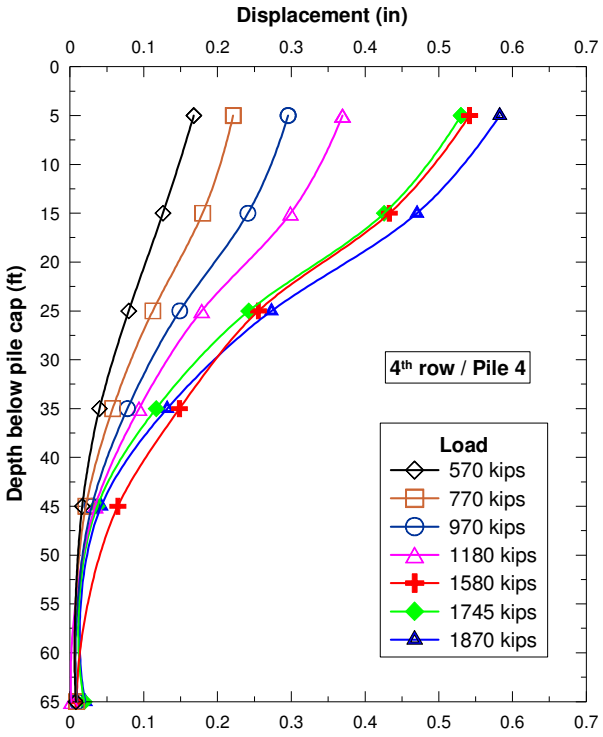

(a) Pile 4

Figure 3.13: Profile of lateral deformation of Piles with load increments

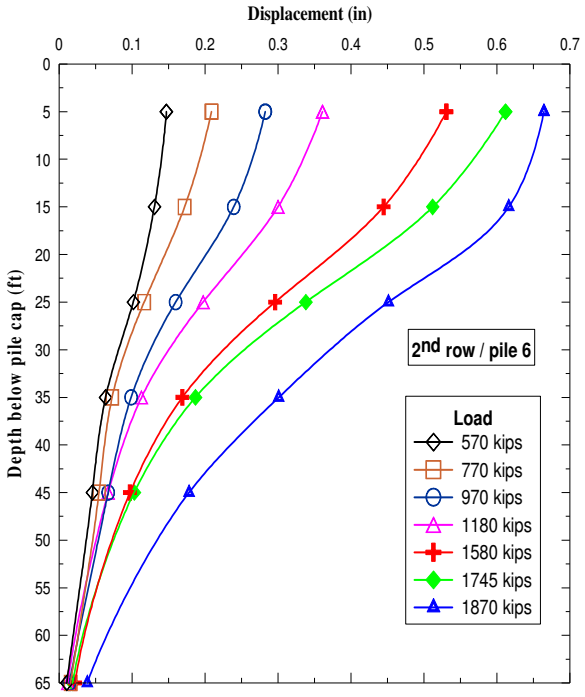

(a) Pile 6

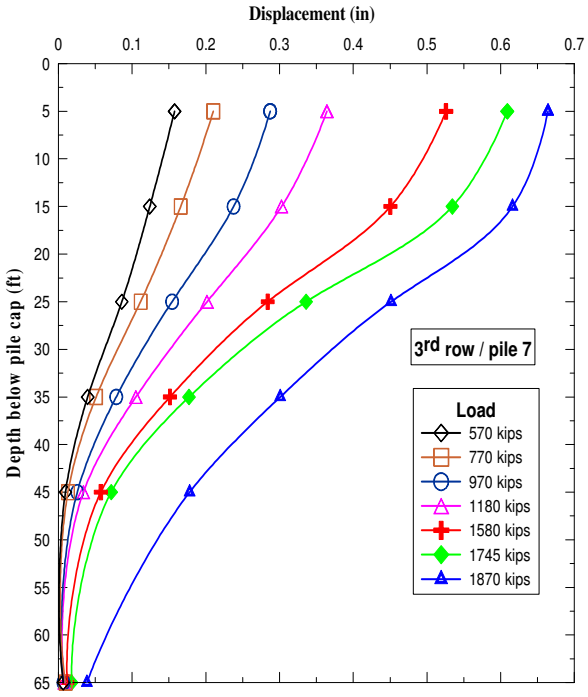

(c) Pile 7

Figure 3.13: (Continued)

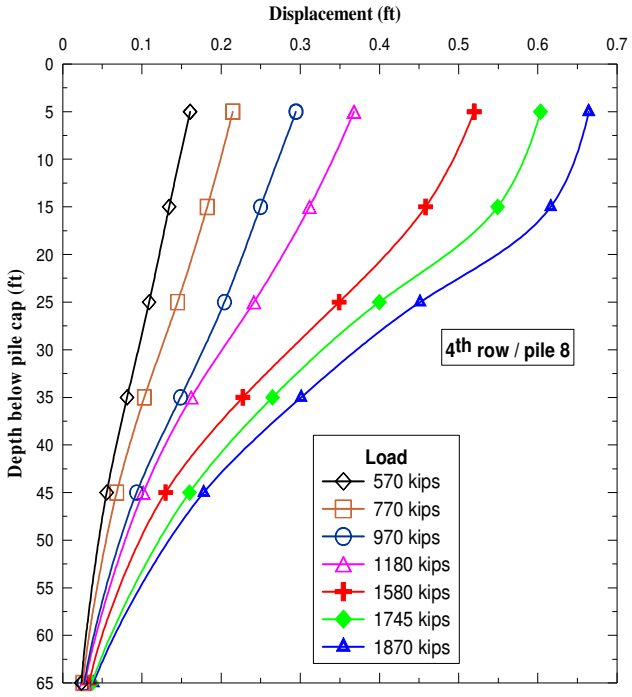

(d) Pile 8

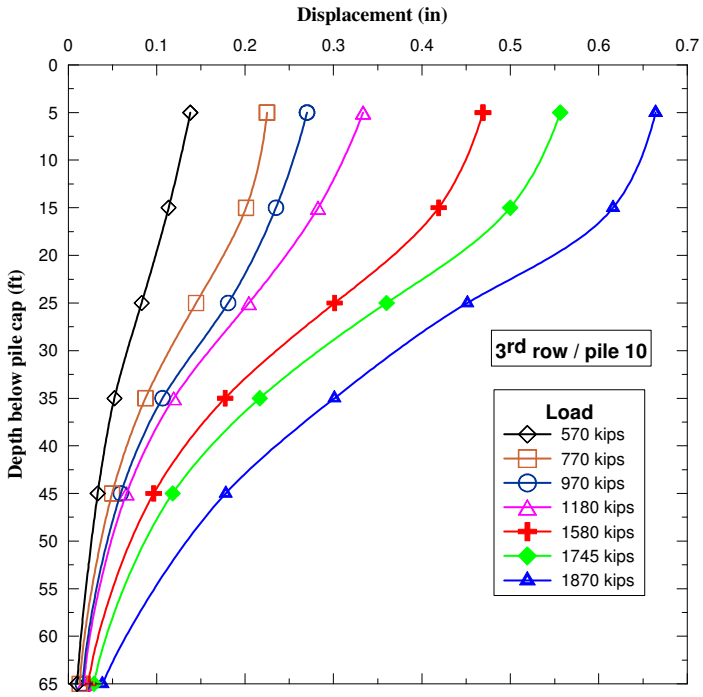

(e) Pile 10

Figure 3.13: (Continued)

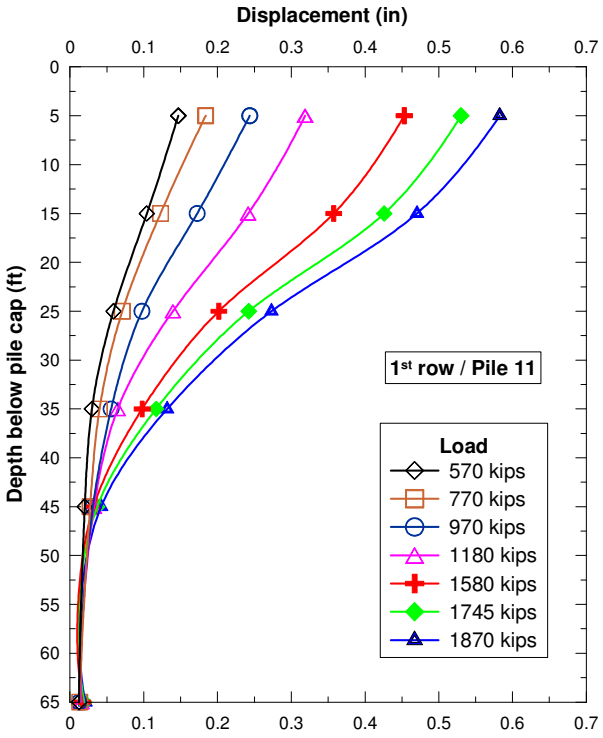

(f) Pile 11

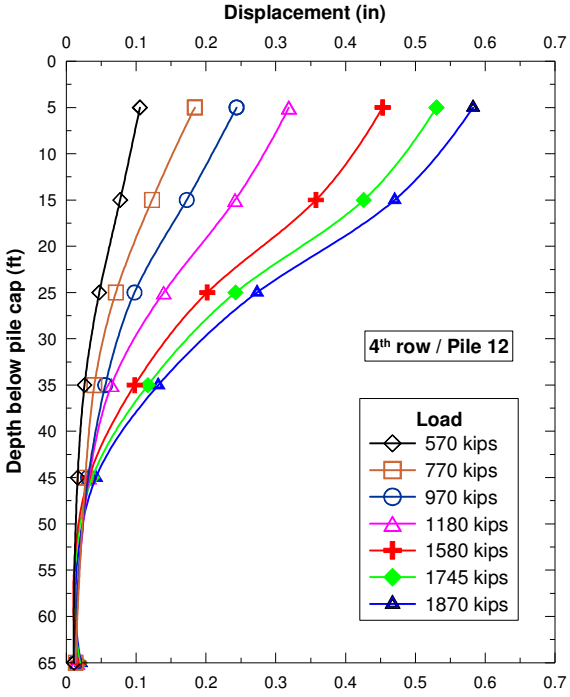

(g) Pile 12

Figure 3.13: (Continued)

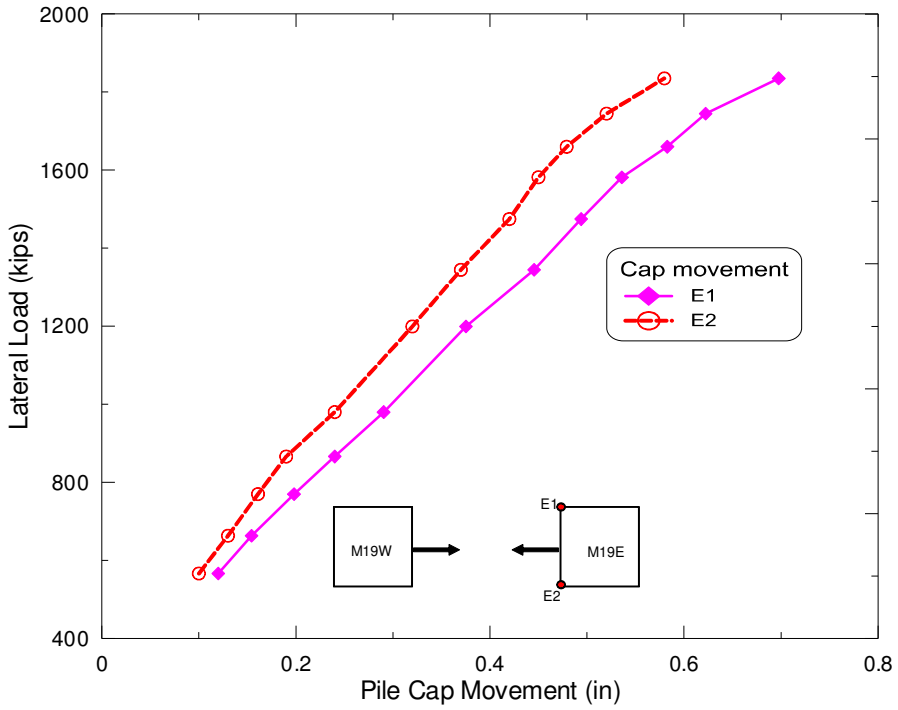

Figure 3.14: Profile of lateral deformation measured from survey prism

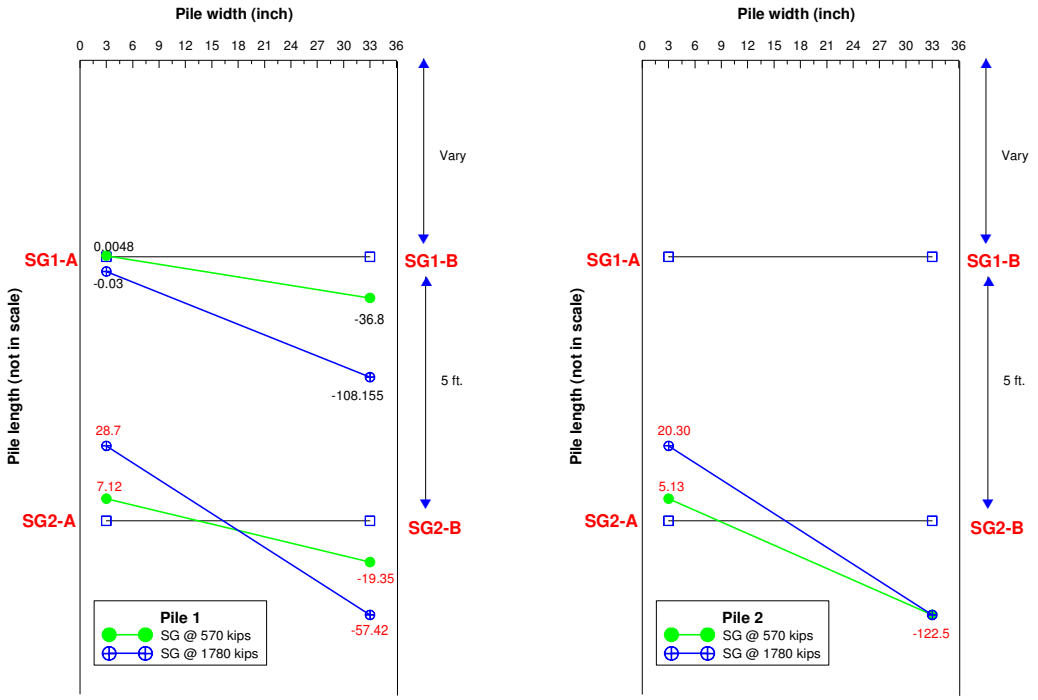

(a) Pile 1 (b) Pile 2

Figure 3.15: strain at two peak load obtained from strain gauge

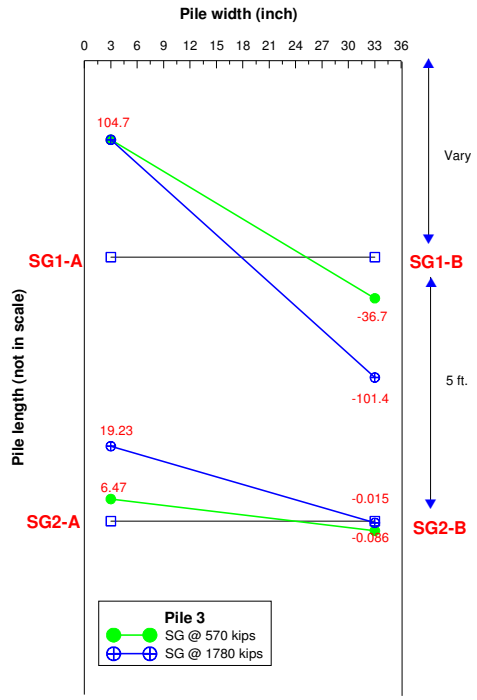

(c) Pile 3

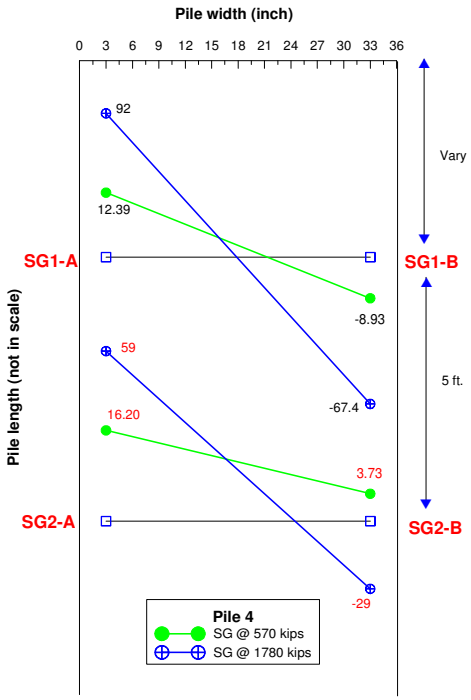

(d) Pile 4

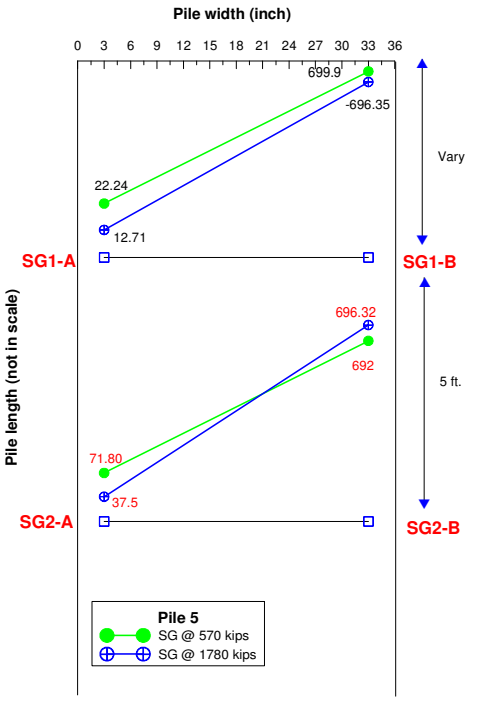

(e) Pile 5

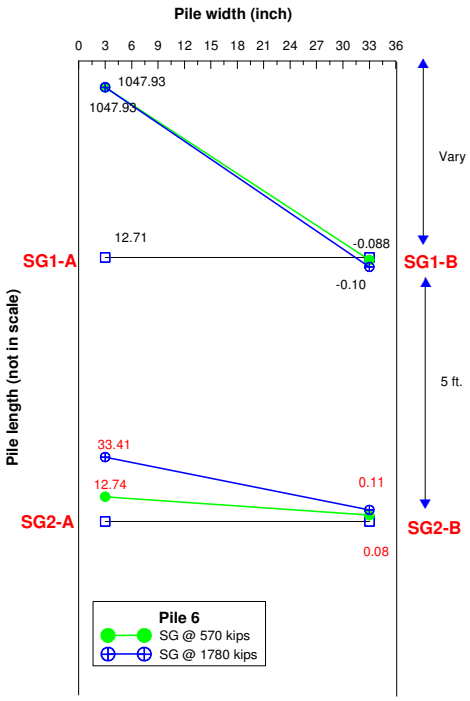

(f) Pile 6

Figure 3.15: (Continued)

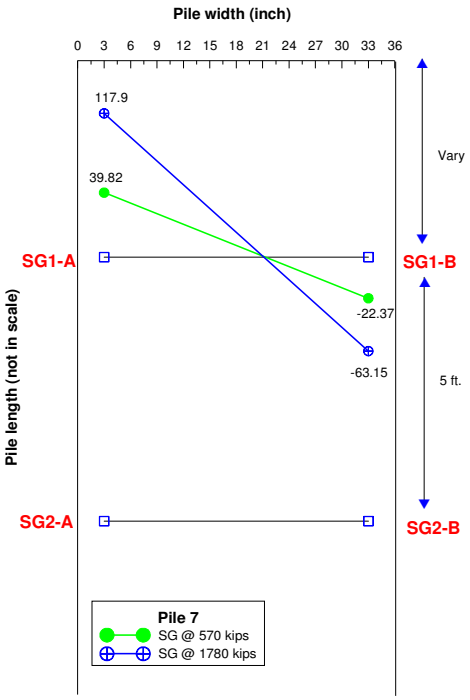

(g) Pile 7

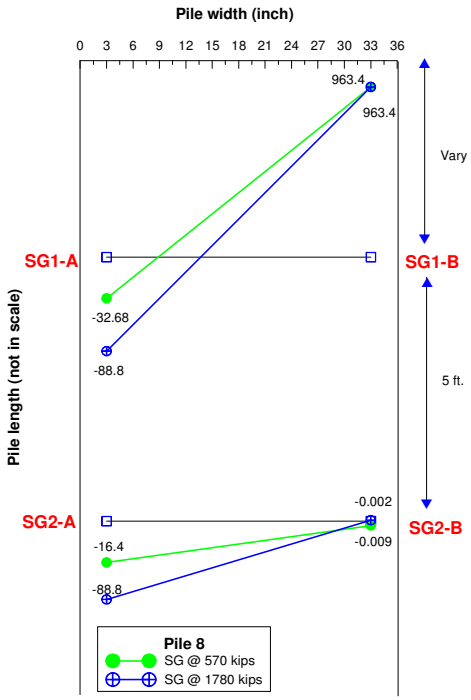

(h) Pile

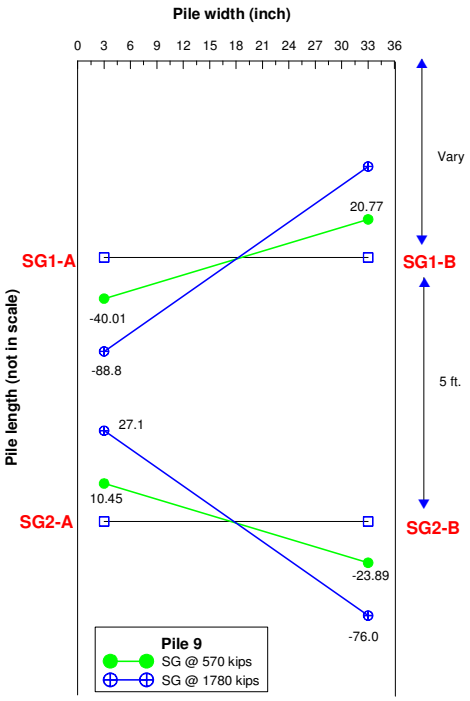

(i) Pile 9

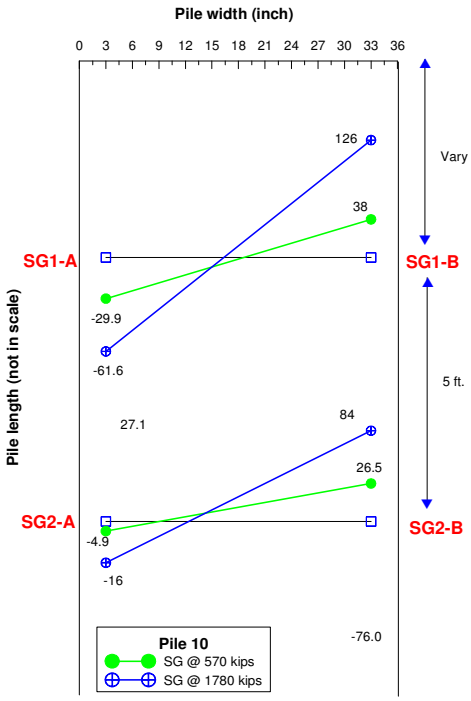

(j) Pile 10

Figure 3.15: (Continued)

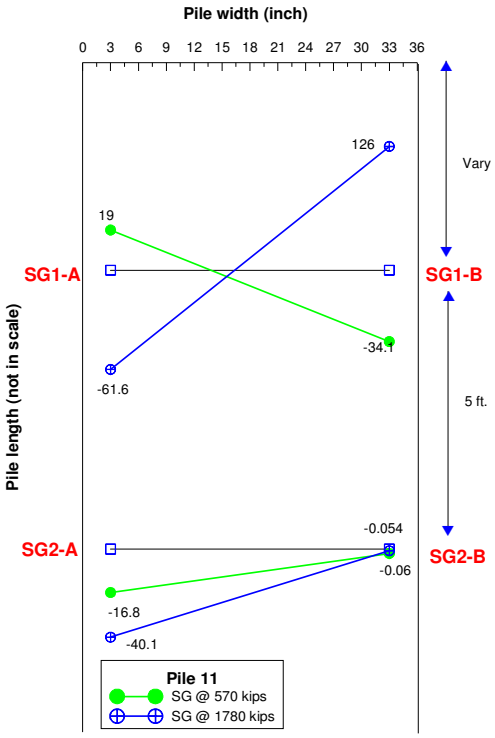

(k) Pile 11

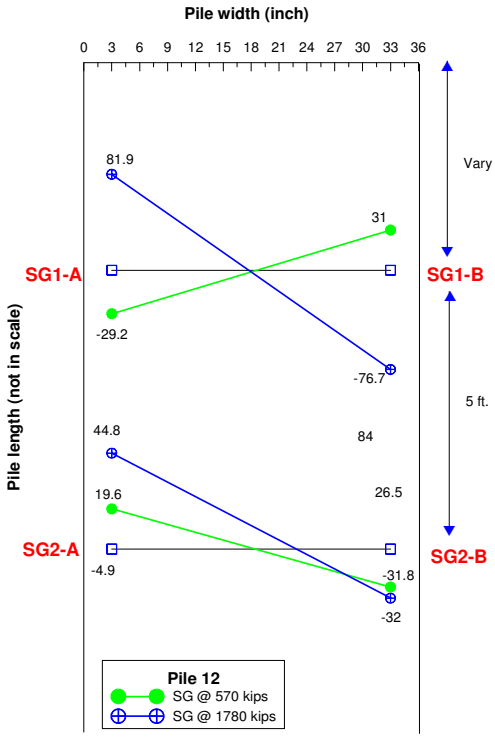

(l) Pile 12

Figure 3.15: (Continued)

3.2: Statnamic Lateral Load Test at Single Pile

A Statnamic lateral load test was performed on a single vertical pile termed as Test Pile 7 (TP-7) located nearby the M19 foundation of I-10 Twin Span Bridge over Lake Pontchartrain. The main purpose of testing a single pile is to compare the performance of the single pile with the battered pile group at similar soil condition under lateral load. The static load was derived from the statnamic load applied on the tested pile. Since the geotechnical soil condition is similar to the M19 foundation as explained earlier, this section only covers description of tested pile, instrumentation, load testing and its result of statnamic test.

3.2.1 Description of Tested Pile

The test pile (TP-7) was a 123 ft long, 36 in square pre-stressed concrete pile with a circular 22.5 in void for the length of the test pile with the exception of the bottom 2.5 ft of the test pile, which was a solid section. The pile was reinforced with equally spaced 28 one-half inch diameter prestressing strands in a square pattern and shear reinforcement consisting of W-5 steel wires.

3.2.2 Instrumentation of TP-7

The tested pile (TP-7) was instrumented with LVDT, strain gauges and accelerometers. Strain gages were installed at ten selected depths during pile casting. Two LVDT's (30 in long travel) for the directly measurement of displacement and slope at the top was installed at 3 and 7 in above the centerline elevation of the load application respectively. Also, a total of ten accelerometers were installed for the purpose of indirectly measuring the pile's deformation. These accelerometers data can be used to derive displacement by double integration. They were oriented to detect lateral motion in the direction of applied lateral load. Two accelerometers were installed on the pile at external positions approximately 5 in above the centerline elevation of the load application, one was mounted on the reference beam to detect any significant motion of that structure and eight accelerometers were installed below the mudline. The schematic diagram showing the locations of instruments in the tested pile is presented in Figure 3.16.

3.2.3 Statnamic Lateral Load Test

The completion of installing all instruments and construction of an isolated reference beam was followed by the assembly of a 500 ton statnamic device, which was horizontally mounted on a sled for lateral testing as shown in Figure 3.17. In order to transfer the load without restraining the pile to rotation, a hemispherical bearing was attached to the tested pile.

The statnamic device produced a time dependent lateral load in the order of 1/2 second or less. The load produced is not an impact, which makes the statnamic analysis very simple and more reliable than dynamic techniques. The loading was applied in five successive increasing load cycles, and the load was measured with resistance load cell of 600 tons capacity installed in between the statnamic piston and the tested pile.

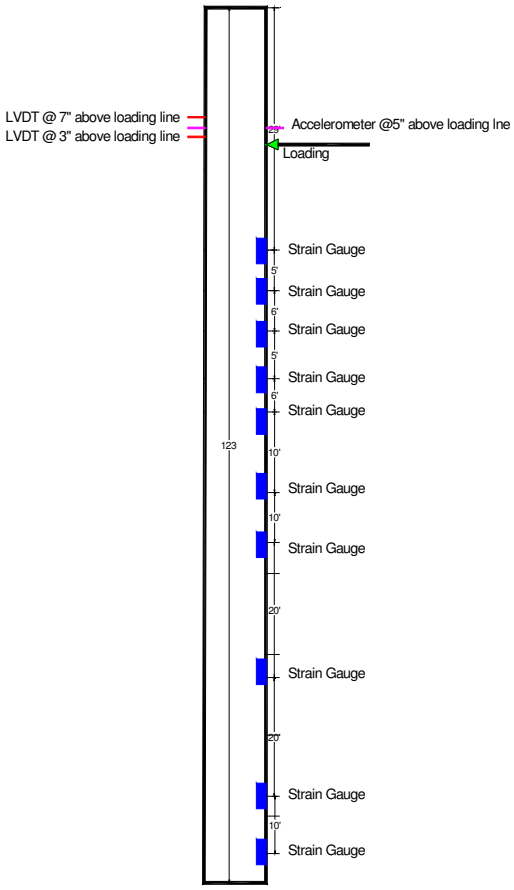

Figure 3.16:Instruments of TP-7

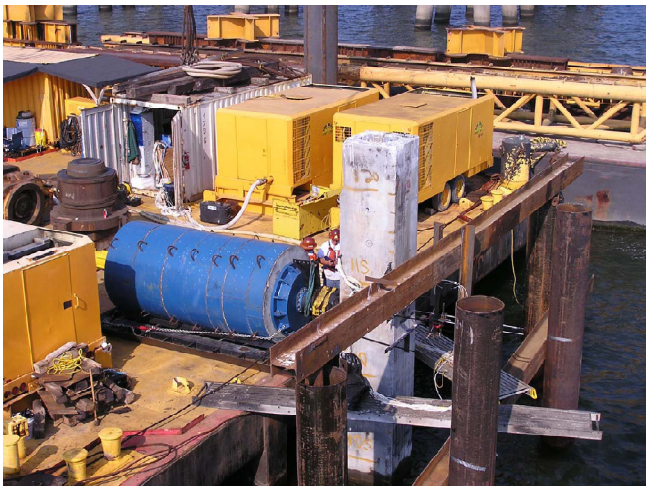

Figure 3.17: Statnamic lateral load test setup

3.2.4 Test Result

The response of the statnamic lateral load testing was measured by several instruments installed prior to the test. The installed resistance load cell measured the applied Statnamic load to the test pile at each cycle as presented in Figure 3.18. The displacement at the pile top was measured directly by the installed LVDT's at the pile head, while accelerometers measured displacement indirectly by integration function. The measured displacement from LVDT and accelerometers as a function of time shows good agreement as shown in Figure 3.19.

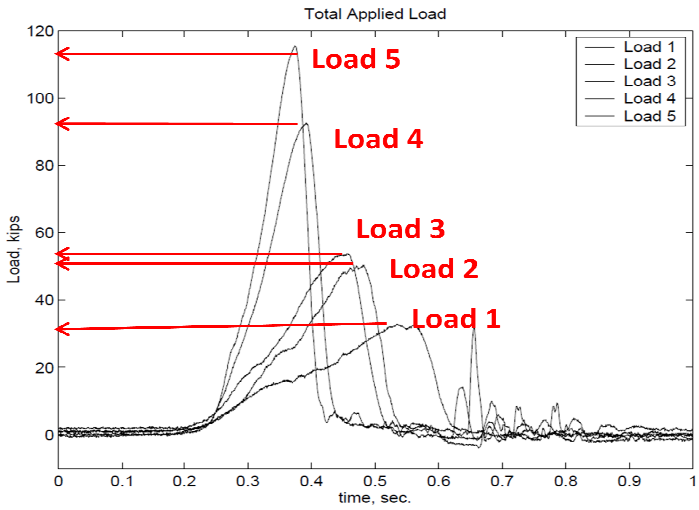

Figure 3.18: Statnamic loads applied to pile as a function of time

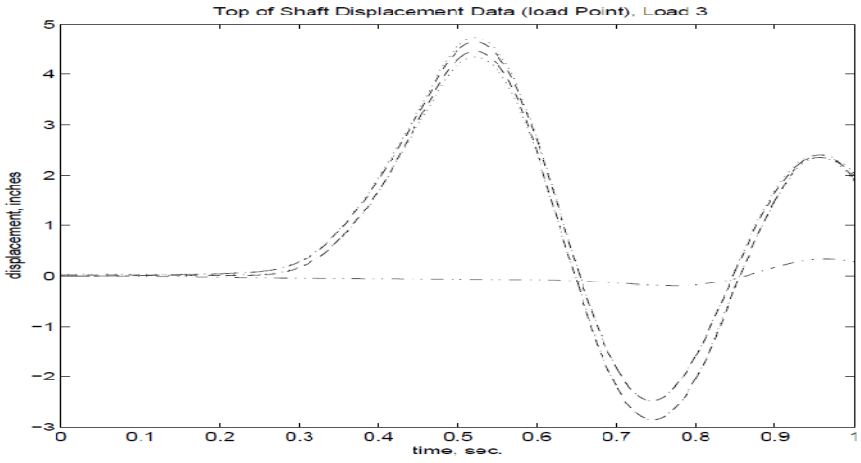

Figure 3.19: Comparison of displacements measured from LVDT's and derived from accelerometers for load 3

The displacement profiles with depth (z) for the five load cycles were derived from the accelerometers and presented in Figure 3.20. The figure suggest that the maximum displacement obtained from load cycle 5 is 10.2 in and that the displacement is negligible at elevations below approximately 30 ft. The strains obtained from the strain gauges for each load cycles were also recorded and are presented in Figure 3.21. The data suggests that the pile has yielded in bending at an elevation of approximately -20 to -25 ft, which is about 10 to 15 ft below the mudline.

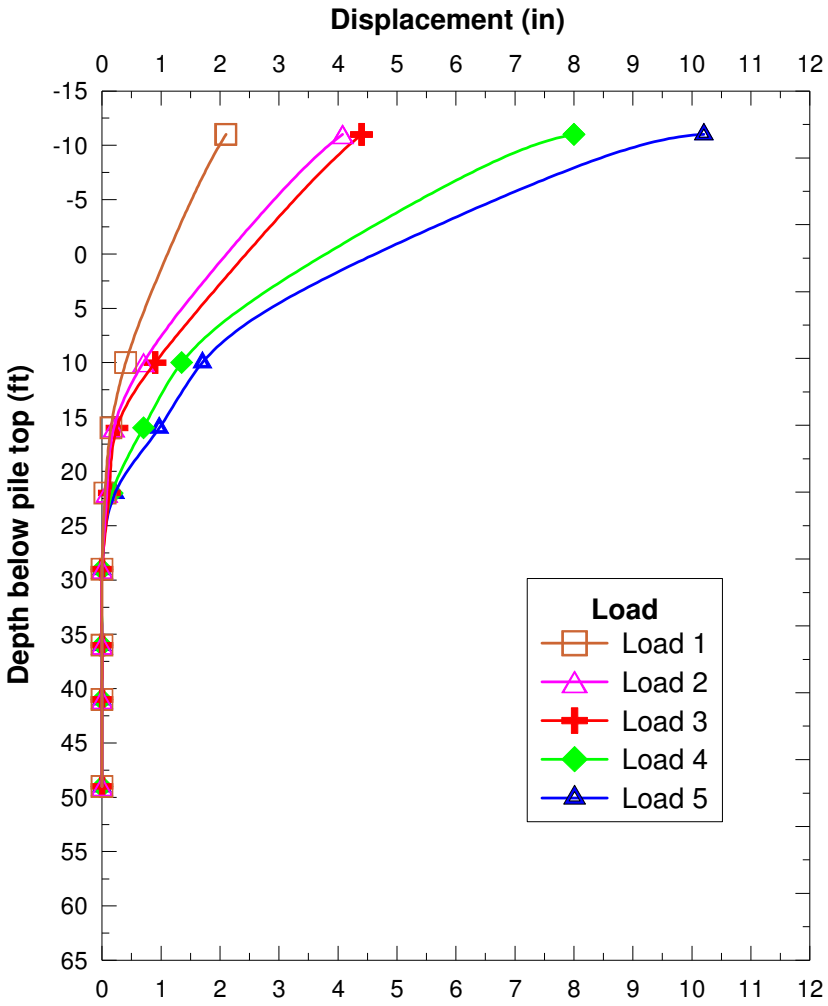

Figure 3.20: Profiles of peak displacement values with depth obtained for each load cycle

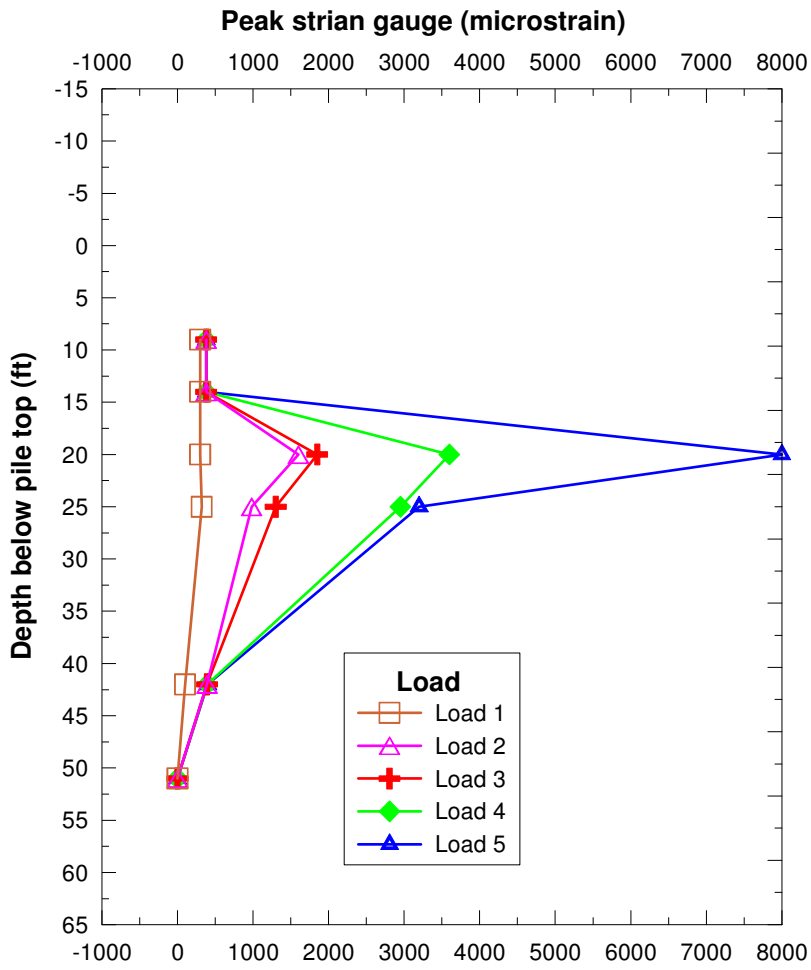

Figure 3.21: Profiles of strain with depth obtained from strain gauges for each load cycles

CHAPTER 4
METHOD OF DATA ANALYSIS

4.1 Introduction

The laterally loaded piles have been successfully analyzed using back-calculation from p-y curves of the measured data obtained using inclinometers and strain gauges. Various approaches such as piecewise polynomial curve fitting (Matlock and Ripperger, 1956; Dunnavant, 1986), high order polynomial curve fitting method (Reese and Welch, 1975; Wilson, 1998) and weighted residual method (Wilson, 1998) have been developed for p-y curve back-calculation. However, all these methods are only applied to the bending moment data calculated from strain gauge measurements. For the interpretation of inclinometer results, Brown et al. (1994) proposed the best fit curve method using least square technique based on a finite difference model of soil-pile. Liao and Lin (2003) derived the deflection function of lateral loaded piles based on the energy conservation concepts. Nip et al. (2005) assumed a fourth order polynomial to represent the shape of soil reaction profile and derived the function of the deflection profile to the match measured lateral deformation profile obtained from inclinometer measurements.

For I-10 Twin Span Bridge project, strain gauges were installed at only two locations along its depth, thus, not sufficient to interpret the lateral response of pile along its entire length. Instead, MEMS inclinometer sensors were installed at six different levels, covering nearly top 60 ft of pile length, which can be easily used to interpret the lateral response of the pile. The interpretation of inclinometer readings is performed using a high order polynomial curve fitting method and the p-y curves were then back-calculated in order to understand the lateral load behavior of battered pile group. In addition, the moment values obtained from strain gauge readings were used in this study to compare with the moments derived by inclinometer readings in order to check the accuracy of the fitting curve method used to back-calculate p-y curves. This Chapter covers the method of analysis in detail and describes the procedure adopted to calculate the effective static load from the statnamic load applied on a single vertical pile.

4.2 Interpretation of Inclinometer Data

The MEMS inclinometer measures rotation at selected depths along the pile for each load increment during lateral load test. The lateral displacement profile can be derived by integrating the rotation profile with depth (z) according to the following Equation.

$$y = \int \theta dz \tag{4.1}$$

Considering pile as a flexible elastic beam on elastic foundation, the lateral responses of the pile can be evaluated by solving the following differential equations for deflection-curve (or rotation).

$$\mathrm{M} = \mathrm{EI}\frac{\mathrm{d}^2\mathrm{y}}{\mathrm{dz}^2} = \mathrm{EI}\frac{\mathrm{d}\theta}{\mathrm{dz}} \tag{4.2a}$$

$$V = EI\frac{d^3y}{dz^3} = EI\frac{d^2\theta}{d^2z} \tag{4.2b}$$

$$\mathrm{P} = \mathrm{EI}\frac{\mathrm{d}^4\mathrm{y}}{\mathrm{dz}^4} = \mathrm{EI}\frac{\mathrm{d}^3\theta}{\mathrm{d}^3\mathrm{z}} \tag{4.2c}$$

where y is the pile lateral deflection, z is the depth below the pile top, θ is rotation, M is the bending moment, V is the shear force, P is the soil reaction force per unit length and EI is the flexural stiffness of the pile.

4.2.1 High-Order Polynomial Curve Fitting

Of the several methods mentioned earlier, only the least square technique (Brown et al., 1994), energy method (Liao and Jen, 2004), and high order method (Nip et al., 2005) were used to interpret the inclinometer data for lateral load test. Considering the non-uniformity of the soil distribution at M19 pier along with limitation of available data and inclination of pile (Nip et al. 2005) the back-analysis method, which assumes the shape of soil reaction profile rather than shape of p-y curve method, is found to be the most suitable method for interpreting the measured inclinometer data from the full-scale lateral load test of the M19 east bound pier.

The shape of soil reaction profile with depth z (P_z) is assumed to follow a 4th order polynomial, similar to Nip et al. (2005), which is defined as:

$$P_z = az + bz^2 + cz^3 + dz^4 \tag{4.3}$$

Since inclinometer sensors provide rotation data, rotation profile can be obtained by integrating Equation 4.3 three times with depth (θ_z). This yields a 7th order polynomial function as follows:

$$\theta_z = a_1 z + a_2 z^2 + a_4 z^4 + a_5 z^5 + a_6 z^6 + a_7 z^7 \tag{4.4}$$

where coefficients a_0 through a_7 need to be determined through curve fitting. Equation 4.4 was used in this study to perform non-linear fit of the measured rotation profiles obtained from the IPI measurements at different load increments using reduced chi-square minimization of residual error regression analysis (Origin Pro program). The chi-square minimization method minimizes the deviations or errors of the theoretical curves from the experimental data in order to select the appropriate parameter values for best fitting that yield least square of errors. In order to reduce the chi-square value, an iteration procedure was performed. The Origin Pro Program uses Levenberg-Marquardt (L-M) algorithm, a combination of Gauss-Newton method and the steepest descent method for iteration. The reduced chi-square value is simply the mean deviation for all data points. The precision or the goodness of the fitted values is measured by standard error; the R-square (R^2) value shows how good the fit is.

Some boundary condition assumptions were made to develop a rotation profile from the measured IPI data. Since the pile cap is 7 ft thick reinforced concrete, the pile-cap connection was considered to be a fixed end with zero rotation. In addition, the IPI measurements showed that the rotations at 65 ft are minimal thus were treated as zero rotation ($\theta_{z=65} = 0$). Examples of curve fitting of rotation for pile 8 (row 4) obtained at 1870 kips and pile 11 (row 1) obtained at 1745 kips lateral load are depicted in Figure 4.1.

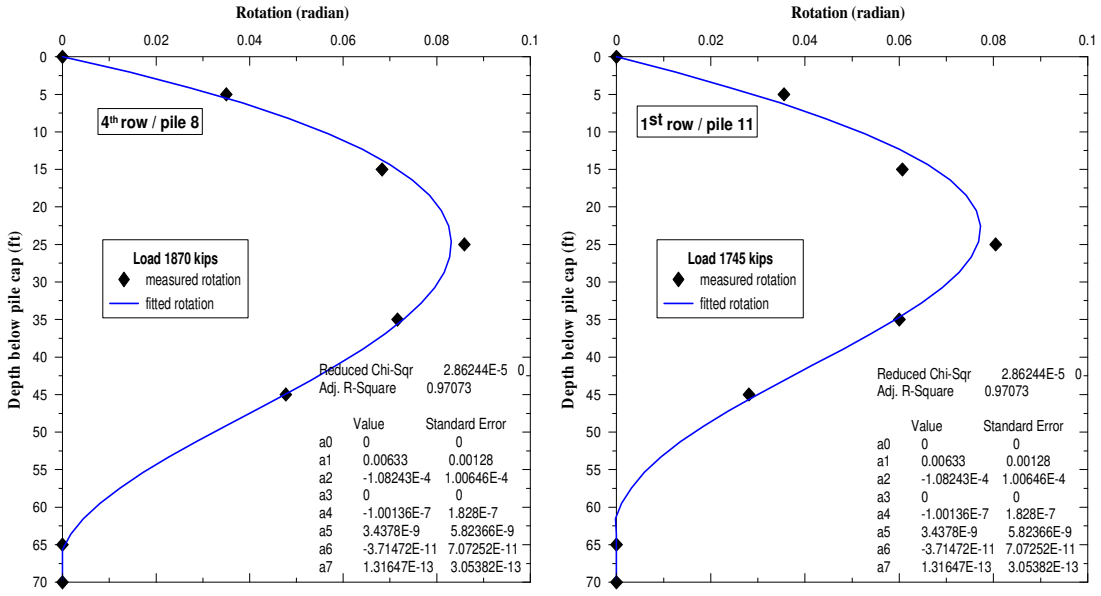

(a) (b)

Figure 4.1: Example of curve fitting of IPI measurements with polynomials

4.2.2 Derivation of Lateral Displacement Profile

Lateral deflection profiles can be calculated directly from the measured rotation by IPI sensors using the following trigonometric equation.

$$y = \Delta l \, sin\theta \qquad (4.5)$$

where Δl is the depth between two rotation values.

In order to check the accuracy of the derived lateral displacement profile, the measured deflections from inclinometer are compared with lateral deflections derived from high order polynomial fitted rotation curve for piles 8 and 11 as shown in Figure 4.2. It clearly shows that the derived lateral displacement profiles obtained from high order polynomial curve fitting matches very well with the measured displacement profiles which demonstrates that the 7th order polynomial fitted function was capable in capturing the measured rotation profiles and hence can be used to deduce the displacement profiles, moment profiles, shear force profiles and soil reaction profiles with minimal errors.

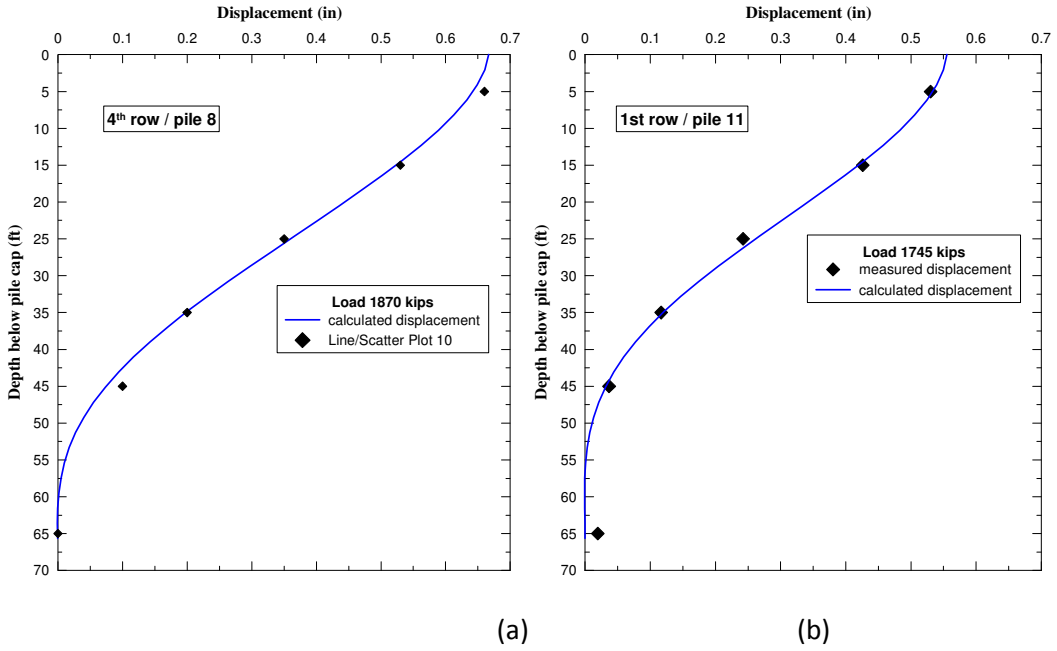

Figure 4.2: Comparing the measured displacement with the derived displacement profile

4.2.3 Development of Moment, Shear, and Soil Reaction Profiles

Once the rotation profile (θ_z) is fitted into the function and polynomial coefficients are determined, moment, shear force and soil reaction profiles can be deduced by differentiating Equations 4.2a through 4.2c with respect to rotation and multiplying the result by the flexural stiffness (EI) of the PPC pile. The resulting expressions are as follows.

$$M_z = (a_1 + 2a_2z + 4a_4z^3 + 5a_5z^4 + 6a_6z^5 + 7a_7z^6)*\text{EI} \quad (4.6)$$

$$V_z = (2a_2 + 6a_3z + 12a_4z^2 + 20a_5z^3 + 30a_6z^4 + 42a_7z^5)*\text{EI} \quad (4.7)$$

$$P_z = (6a_3 + 24a_4z + 60a_5z^2 + 120a_6z^3 + 210a_7z^4) * EI \quad (4.8)$$

The flexural rigidity or stiffness (EI) depends on the properties of the pile, its cross section and the moment developed along the length of the pile. Thus, it needs to be appropriately calculated for accurate prediction. As explained earlier in Chapter 3, the piles are composed of two different sections. The first portion of the pile is solid whereas the second portion of the pile consists of 22.5 in concentric void. The moment of inertia (I) was calculated based on the geometry as:

$I_{\text{solid pile (no void)}}$ = 139,968 in^4

$I_{\text{Hollow pile (with void)}}$ = 128475 in^4

The modulus of elasticity for the concrete (E_c) was calculated using an empirical formula as

$$E_c = 57{,}000*\sqrt{f'_c} \quad (4.9)$$

where E_c is expressed in psi and f'_c is the average 28-day compressive strength of the concrete in ksi. f'_c was calculated based on average result of six compression tests that conducted on cylindrical specimens at the time of testing (f'_c = 8000 psi). The calculated elastic modulus (E_c = 5.35×10^6 psi) was assumed to be a constant since the piles deformation were within the elastic range. However, in reality, the behavior of piles is somehow non-linear and the cracking of the pile reduces its stiffness. Nip et al. (2005) developed a curve of flexural stiffness and bending moment from strain compatibility and the equilibrium of forces to describe the relation of EI with bending moments as illustrated in Figure 4.3. It clearly demonstrates that the flexural stiffness reduces gradually for partially cracked to cracked state of concrete. However in the present study, the calculated highest moment was 1200 kips-ft, which is nearly equal to 1.4 MN-

m from where the flexural stiffness starts reducing as shown in Figure 4.3. The E_c value estimated from the results of 28 days compression strength tests on cylindrical specimens were increased by 5% to incorporate the increase in strength/stiffness at the time of lateral load testing (6 months).

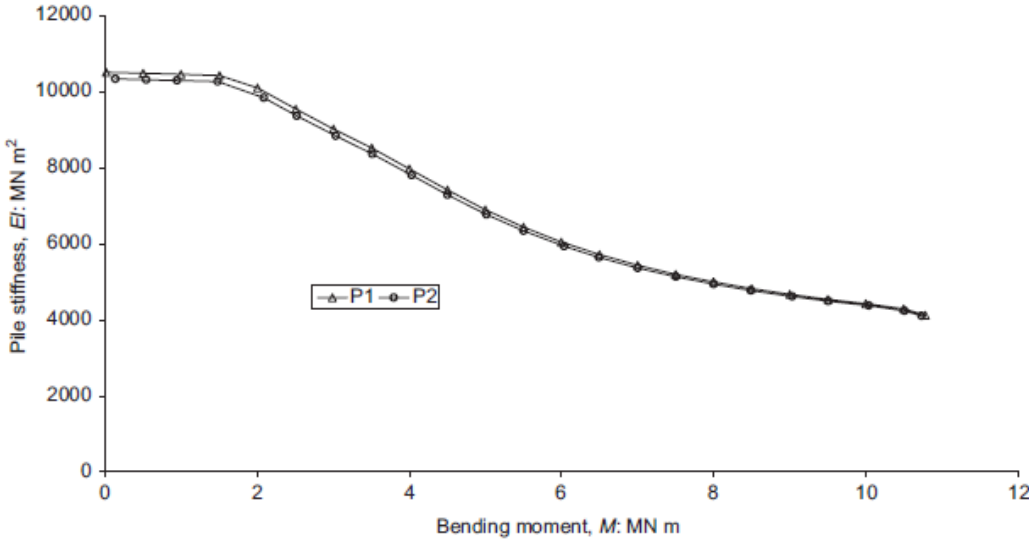

Figure 4.3: Relationship between EI and M (Nip et al., 2005)

4.2.4 Back-calculating p-y Curves

The back-calculation of p-y curves form results of lateral load test is significantly important since the back-calculated p-y curves can be used to analyze the lateral behavior of pile where lateral load tests are not feasible. The p-y curves can be derived from the inclinometer readings through the derivation of lateral displacement profiles and the soil reaction profiles for each load increment. Once the lateral displacement profile (y) and soil resistance profile (P_z) are derived, the p-y curves at different depths can be deduced. In summary, the back-calculation of the p-y curves from inclinometer data involves the following five steps:

1) Development of the rotation profile (θ_z) for each load increment by using high order polynomial curve fitting to measured inclinometer rotation data.
2) Derivation of the displacement profiles (y) with depth (z) for different load increments through single integration of the rotation profiles ($y = \int \theta dz$).
3) Development of moment profile (M_z) for each load increment with depth by single

differentiation of rotation profile and multiplying by EI (— .

4) Calculation of soil resistance (P_z) for different load increments by double differentiation of the developed moment profile — .

5) Construction of p-y curves for selected depth by taking displacement and corresponding soil resistance value for each load increment.

Using the fitted rotation profile, the lateral displacement profile was obtained from Equation 4.5 and the soil reaction profile corresponding to each load increment was calculated using Equation 4.8. Thereby, using the soil reaction per unit length obtained at different load levels and the corresponding lateral depth at selected depths, the p-y curves at selected depths were back-calculated.

4.3 Interpretation of Strain Gauge Data

Two pairs of strain gauges (SG1 and SG2) were installed at two different depth levels in twelve selected piles during casting as discussed in Chapter 3. The main purpose of installing the strain gauges was to calculate the transfer of axial load and bending moments at strain gauge locations along the pile length. The strain distribution measured by the strain gauges is the summation of the axial strain and the bending strain as given in Equation 4.10 and depicted in Figure 4.4.

$$\text{Strain}_{\text{measured}} = \text{Strain}_{\text{due to axial}} + \text{Strain}_{\text{due to bending}} \quad (4.10)$$

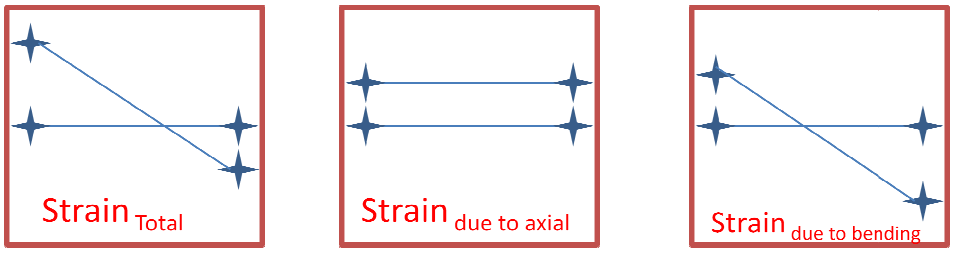

Figure 4.4: Strain distribution due to axial load and moment

4.3.1 Calculation of Moment from Strain Gauges

The moments of the pile at corresponding strain gauge locations were calculated from the strain gauges using equation 4.11. According to the Rollins et al. (1998), this approach cancels out any contribution due to axial strain, leaving strains only due to bending, and makes it possible to accurately compute the bending moment.

$$M = \frac{EI(\varepsilon_t - \varepsilon_c)}{h} \tag{4.11}$$

where ε_t is tensile strain (+ve), ε_c is compressive strain (-), and h is the horizontal distance between the two gauges spaced at equal but opposite distances from the neutral axis.

4.3.2 Axial Load from Strain Gauges

Load transfer mechanism of battered piles is different than the vertical pile. In vertical piles, the total applied lateral load is transferred to soil media only. However, for battered piles, the lateral load will also be transferred to axial compression or tension force as shown in Figure 4.5. The part of lateral load transferred to axial load reduces the developed bending moment along the pile and decreases the lateral soil resistance. The induced axial loads can be calculated from the strain gauge data as:

$$\text{Axial load} = \frac{EA(\varepsilon_t + \varepsilon_c)}{2} \tag{4.12}$$

where, A is the cross section area of pile. The axial load is compression when $\varepsilon_t < \varepsilon_c$ and tension when $\varepsilon_t > \varepsilon_c$. Figure 4.6 presents a summary flow chart for the analysis of the inclinometer and strain gauge measurements obtained during lateral load test.

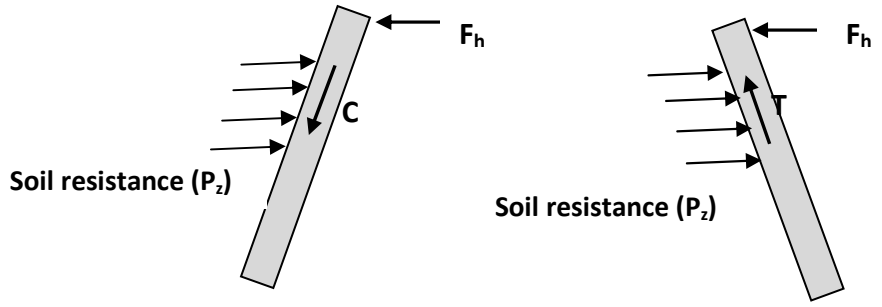

Figure 4.5: Decomposition of applied lateral load on battered pile

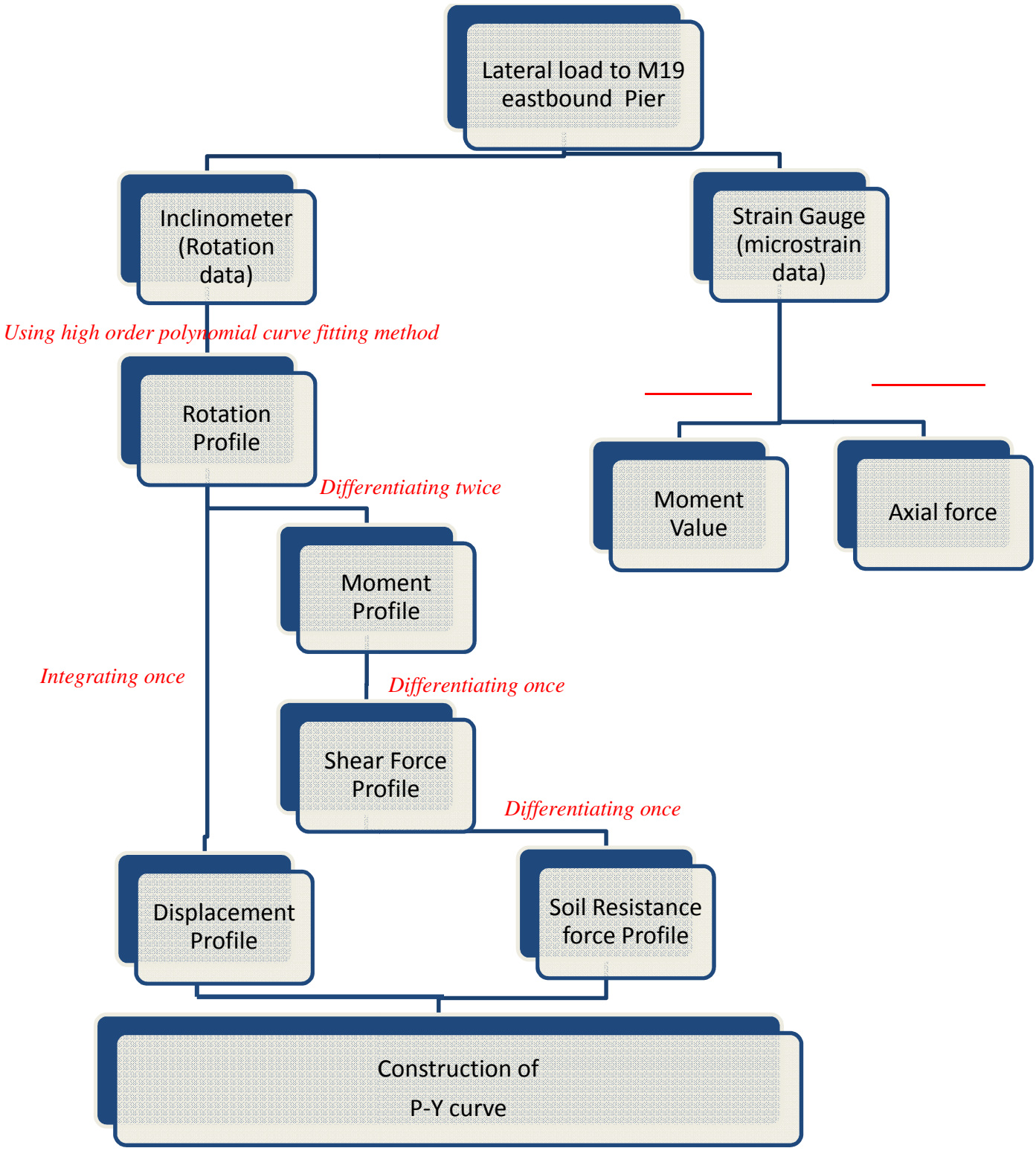

Figure 4.6: Flow-chart of analysis for battered pile group

4.4 Deriving Static Load from Statnamic Testing of Single Vertical Pile

In order to compare the static load response of battered group pile with single vertical pile, the effective static load need to be derived from the applied statnamic load on vertical pile. The measured statnamic force includes the summation of inertia resistance, damping force and static force as shown in Equation 4.13. The static force can be obtained by first determining inertia force and damping force then subtracting these forces from the measured statnamic forces. So far, single degree of freedom method has been satisfactorily used to ascertain the equivalent static force.

$$F_{Stn} = F_I + F_D + F_{St} \qquad (4.13)$$

where,

F_{Stn} = measured force on the Statnamic load cell

F_I = inertial resistance from effective mass of the foundation

F_D = effective viscous damping resistance

F_{St} = effective static soil resistance

The inertia force can be calculated assuming that the pile would act like a cylinder rotating about its base (Brown, 2000). The inertia force is calculated by taking the mass of foundation, (m) and multiplying it with the acceleration of pile (a) in relation to the displacement (i.e. $F_I = ma$). The mass of foundation includes the mass of the test pile and the soil moving during the test. Since only the top 55 ft length of pile (See Figures 3.20 and 3.21 in Chapter 3) is active during the statnamic load test, Therefore, an active length of 55 ft was used to calculate the effective mass of the foundation (m_e). The effective mass of foundation was calculated as 0.0125 kN-sec^2/m (0.00086 kip-sec^2/ft). The acceleration of such a square column in relation to a displacement y at the loading point z can be calculated by differentiating twice the displacement obtained from LVDT. Hence, the force due to inertia was calculates as:

$$F_I = m_e\, a \qquad (4.14)$$

The damping force (F_D) is proportional to the velocity (v) of the pile which can be evaluated as the product of the damping constant (C) and the velocity of the pile as follows

$$F_D = C\ v \qquad (4.15)$$

The velocity of the pile (v) can be obtained by differentiating the measured displacement (y) of the pile head. The damping constant (C) which represent the constant of proportionality between the force and velocity is related to critical damping coefficient (C_c). The C_c value represents the value for which the system will return to equilibrium after exactly one cycle. The ratio of damping constant and the critical damping is known as damping ratio (D), and the Equation 4.15 can be re-written as:.

$$F_D = C_c\ D\ v \qquad (D = C/C_c) \qquad (4.16)$$

$$C_c = 2(k\ m_e)^{½}, \text{ where k is static stiffness.} \qquad (4.17)$$

$$\text{thus, } F_D = C\ v = D\ [2(k\ m_e)^{½}]v \qquad (4.18)$$

Now, equation 4.13 can be re-written as:

$$F_{Stn} = m_e a\ (F_I) + Cv(F_D) + ky\ (F_{St}) \qquad (4.19)$$

The spring stiffness is modeled as a non-linear function since the soil response to lateral loading at large strains is known to be highly non-linear. For the analyses, the stiffness has been taken as a constant which is derived independently for each statnamic loading (and decreases with increased loads). This model was back-fitted to the results of the load test measurements, for each load cycle as shown in Figure 4.7, to obtain the non-linear spring and viscous damping parameters which best match the observed behavior. Figure 4.8 presents the stiffness, obtained for all load cycles from the back-fitted data. The stiffness is plotted against the top of pile displacement on a semi-log scale. The damping ratio for the test pile was estimated to be 0.21.

The static force can be easily calculated by multiplying the pile displacement (y) with spring stiffness (k). Using this non-linear spring, the static load corresponding to the five successive statnamic loading was derived and given as 34.5, 56.6, 59.7, 74.5 and 72.9 kips. The procedure for deriving static load and the derived values are referred from the final report submitted by Applied Foundation Testing. (Final Report of statnamic load testing, 2006)

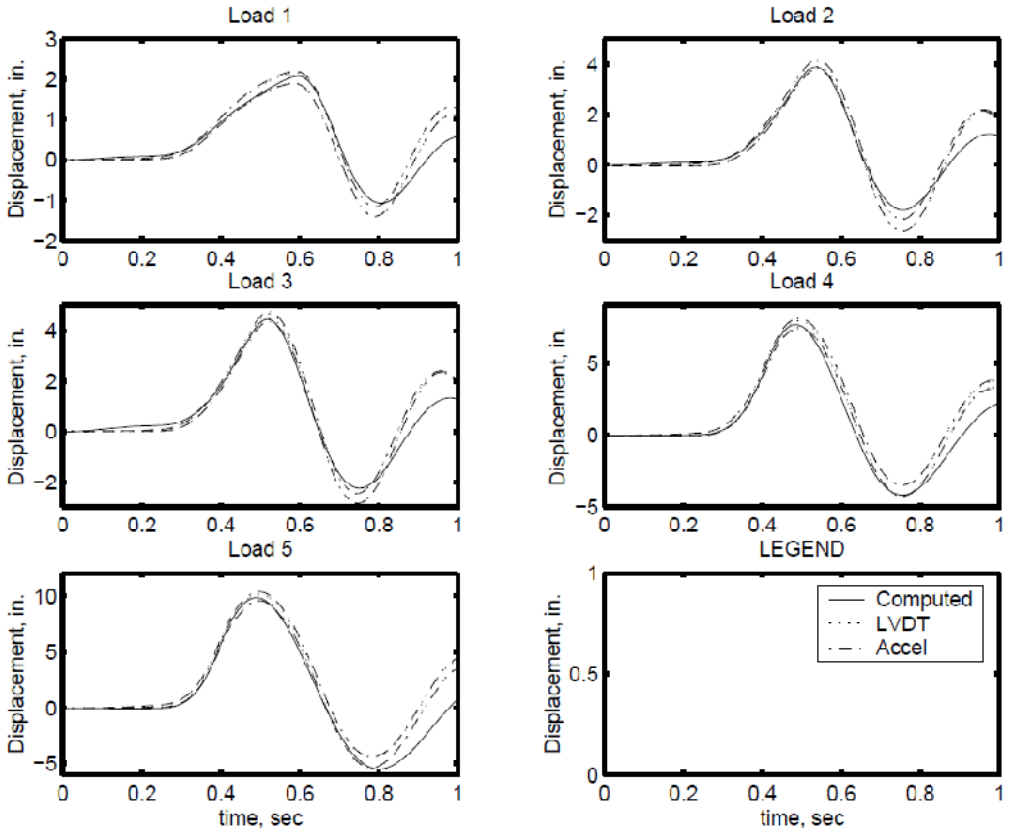

Figure 4.7: Results of back fitting process single degree of freedom model (Comparison of computed and measured top of pile displacement)

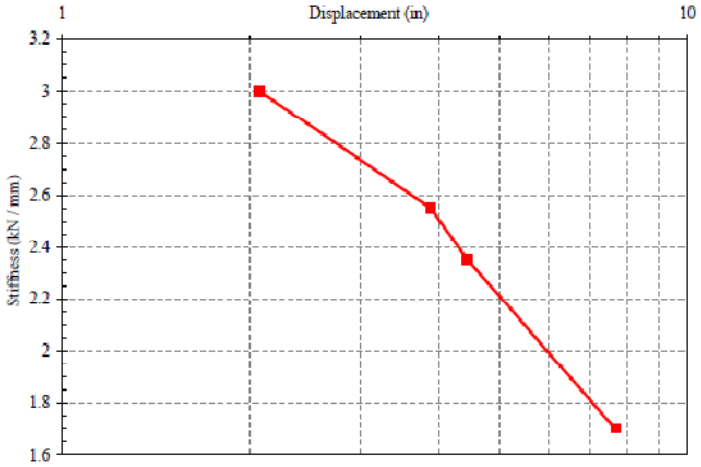

Figure 4.8: Pile stiffness versus displacement at point of load application

CHAPTER 5
RESULT OF ANALYSIS

The analysis of battered pile group foundation of I-10 Twin Span Bridge that were subjected to lateral loading is performed using the methods presented in Chapter 4. A thorough discussion on the developed profiles of lateral displacement, bending moment, soil resistance and back-calculated p-y curves are presented. These curves are used to analyze the lateral performance of piles located at different rows as well as within the same row. For better understanding, the individual piles are classified based on their location within the foundation as illustrated in Figure 5.1. The row located near the position of applied load is termed as 4th row (back row or trailing row); whereas the row situated at the farthest is termed as 1st row (front row or leading row). The piles located at the edge are called corner piles else designated as inner piles.

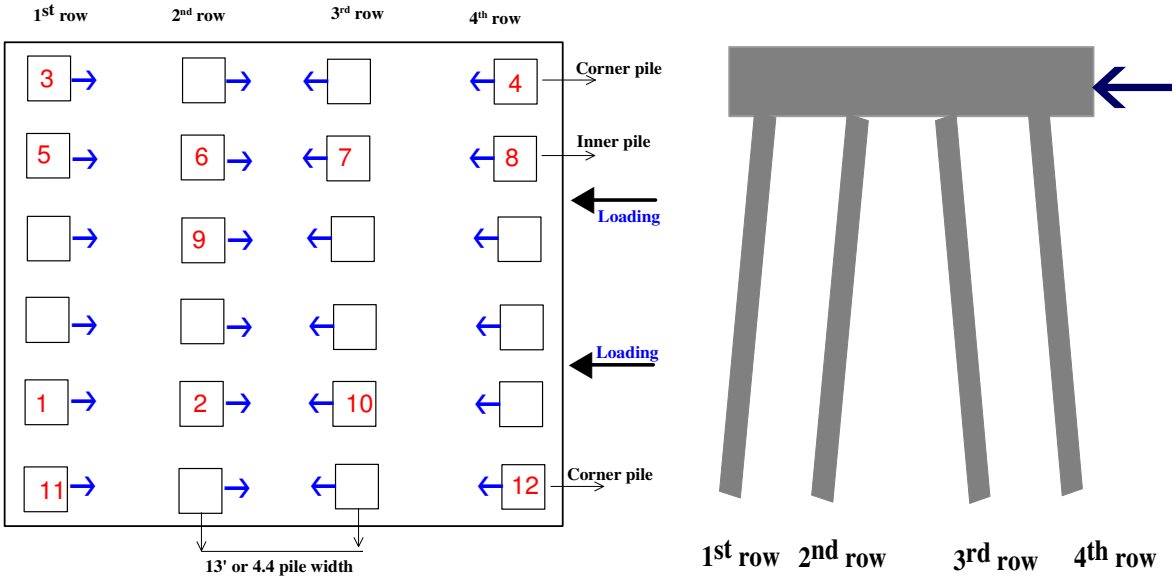

(a) (b)

Figure 5.1 a) Plan view of pile layout b) Side view of pile layout

5.1. Profiles of Lateral Displacement

Lateral displacement profiles along the depth of each pile (below pile head) are derived from inclinometer data using Equation 4.5. The lateral displacement profiles are determined at

increasing static lateral load of 570, 770, 970, 1180, 1580, 1745 and 1870 kips. The profiles are determined for piles 11, 6, 7, and 8, which are located in the 1st row, 2nd row, 3rd row and 4th row respectively. The developed lateral displacement profiles for these piles are shown in Figure 5.2. The maximum displacement values obtained at the peak lateral load of 1870 kips for the piles located at the back row when compared to the front row do not differ; the variation of displacements is within merely 10% range. The maximum displacement at the pile head of 4th row (pile 8) and 1st row (pile 11) are 0.67 in and 0.6 in, respectively. This is in excellent agreement with the result of the automated survey measurements, which were 0.69 in and 0.59 in, respectively as explained earlier in Chapter 3. The displacement profile of 2nd row pile is almost similar to 3rd row pile with mere 3-5% variation at lower load such as 570 and 770 kips.

Further examination of the derived displacement profiles reveal that the depth from pile head to the zero displacement for piles depends upon the magnitude of loading and row location. At higher loading such as 1870 and 1745 kips, the depth from the pile head to zero displacement for 4th row pile is about 55-60 ft (18B to 20B, where B is pile width), whereas, it is about 45-50 ft (15B-16B) for the 1st row pile. The depth to the zero displacement for the 2nd row and the 3rd row piles are similar; this may be due to the increasing spacing between the opposite battered (positive battered pile in 2nd row and negative battered pile in 3rd row) along the depth.

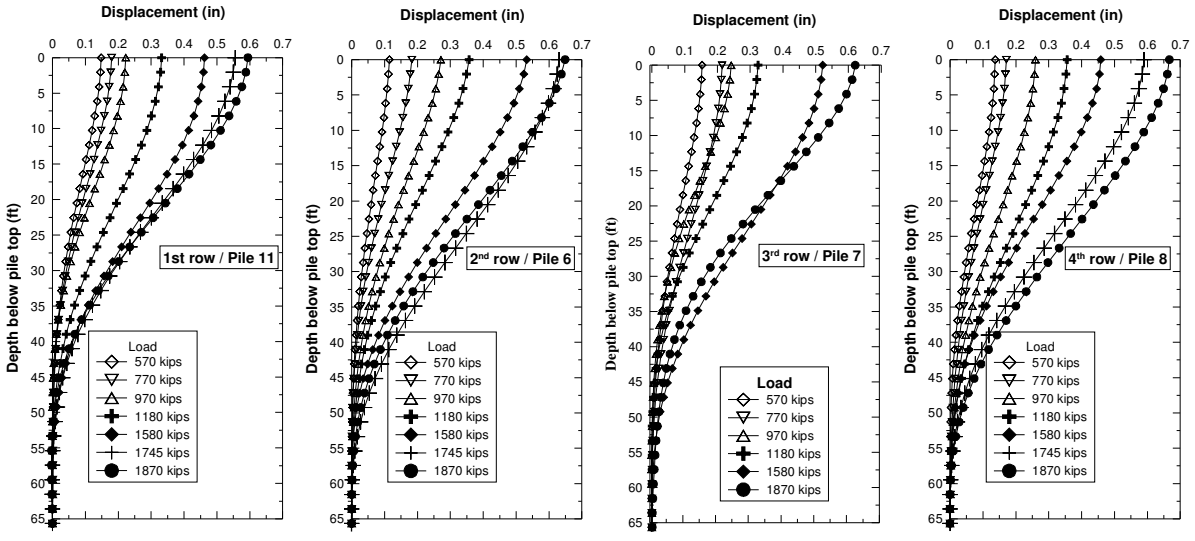

(a) Pile 11 (b) Pile 6 (c) Pile 7 (d) Pile 8

Figure 5.2: Lateral displacement Profiles

In order to have a better understanding of the load-displacement relationship, the curve of total load applied at pile cap versus derived peak displacement at pile head is plotted. It is then compared with the automated laser survey measurements as shown in Figure 5.3. The figure demonstrates the linear nature and also slight indication of bi-linear behavior of piles. All piles exhibit similar lateral displacement profile. It is noteworthy, as shown in Figure 5.3, that the front row pile (pile 11) comparatively takes more lateral load at same displacement, whereas, the 4th row pile has larger lateral deformation at similar load. The margin however is not substantial. The graph does not have a peer peak load point. The load seemed to increase not yet reaching the yield point.

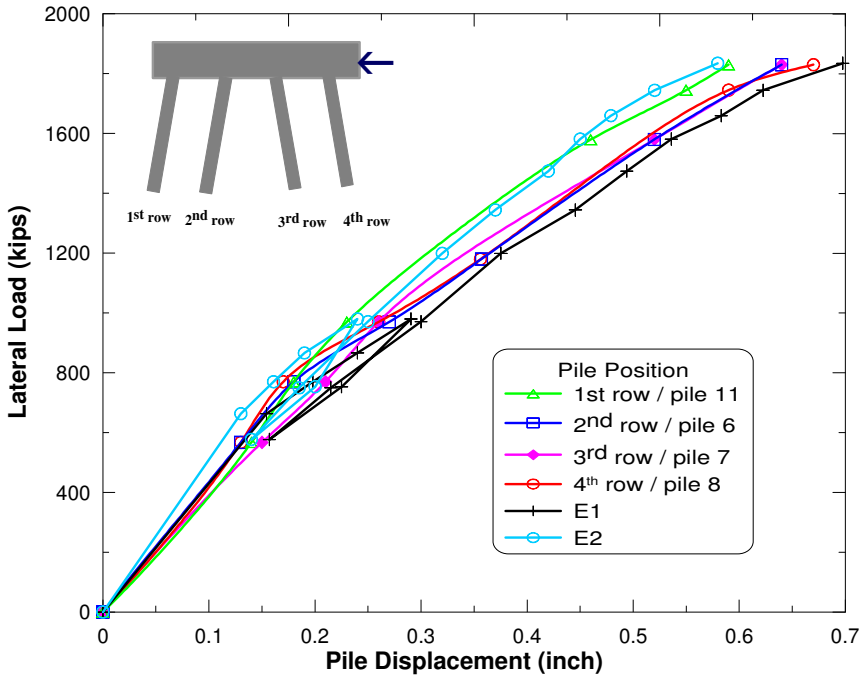

Figure 5.3: Applied load versus maximum displacement at pile head

- **Lateral Displacement Profile of Piles Located within the Same Row**

In order to understand the lateral load behavior of piles within the same row, the lateral deformation profiles of three instrumented piles, 4, 8 and 12 located in the 4th row are derived as depicted in Figure 5.4. Piles 4 and 12 are located at the corner of the 4th row, whereas pile 8 is located next to pile 4 as shown in Figure 5.1. All these three piles have almost similar lateral

displacement profiles. Figures 5.5a and 5.5b shows curves of applied load versus displacements determined at pile head and at ground level for piles in the 4th row. These Figures indicate that all three piles in 4th row undergo similar displacements for corresponding applied loads. The displacement were larger for pile 4 than other piles at 1200 and 1600 kips. This may be attributed to instrumental minor human and errors accumulated during measurements and calculations.

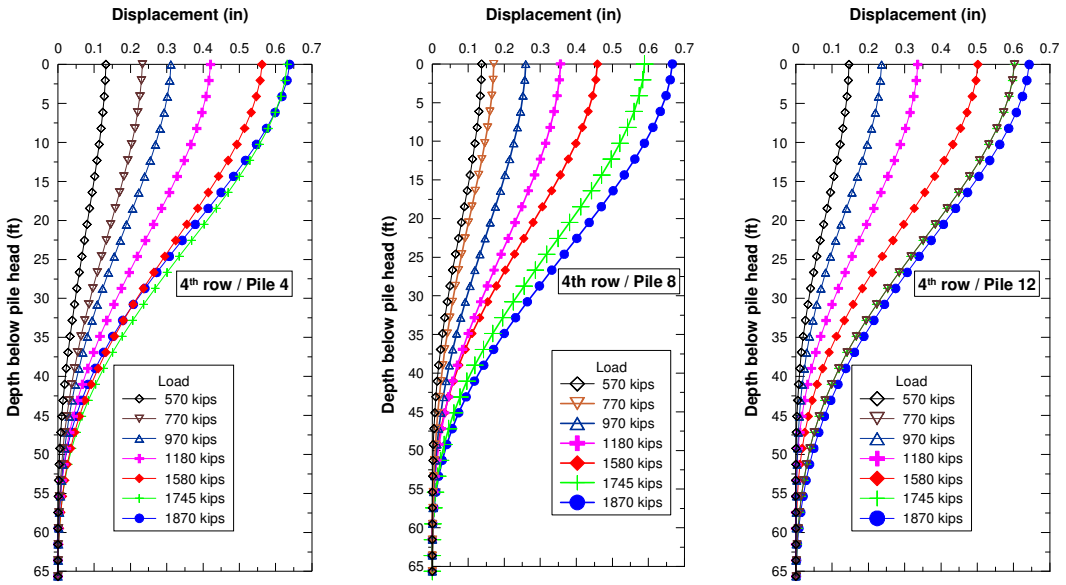

(a) Pile 4 (b) Pile 8 (c) Pile 12

Figure 5.4 : Lateral displacement profile of piles located in 4th row

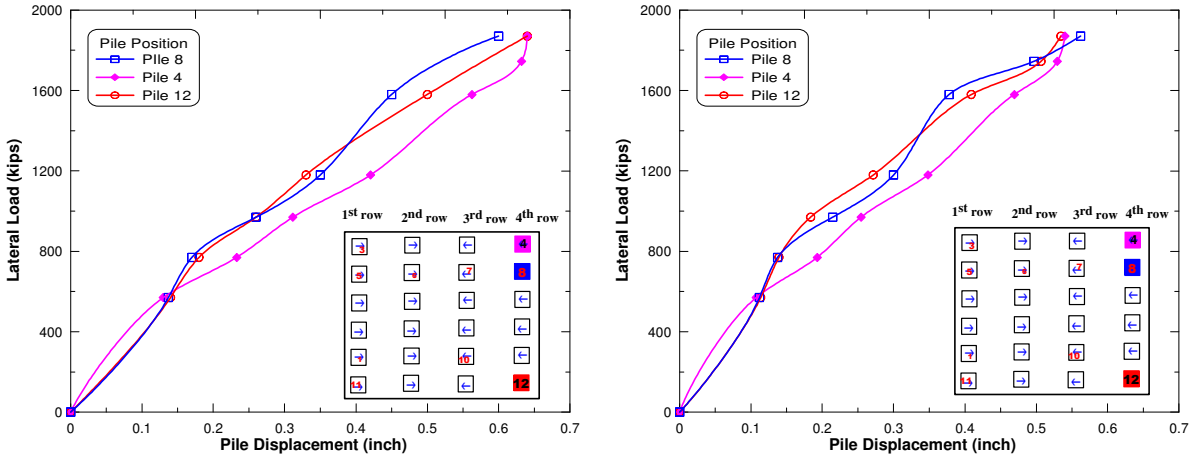

(a) At pile head (b) At ground level

Figure 5.5: Comparison of displacements of piles in the 4th row

5.2. Profiles of Bending Moment

The profiles of bending moments for piles at different applied lateral loads were derived using Equation 4.6. The moments of individual piles located at different rows are drawn with reference to y- axis at a static lateral loads of 570, 770, 970, 1180,1580, 1745 and 1870 kips. The moment profiles for piles 11, 6, 7 and 8 representing 1st, 2nd, 3rd and 4th rows respectively are shown in Figure 5.6. Evidently, the maximum positive bending moments occur at pile head for all piles due to rigid pile-cap connection. It is inferred from the figure 5.6 that the magnitude of the moment and also the depth to the first zero moment (from where the moment changes form positive to negative), increases with the increment of applied lateral loads. The 1st row pile has comparatively the highest moment value, whereas the 4th row pile has the lowest moment value. Also, the depth to the zero moment for 1st row pile occurred at shallower depth than the 4th row pile. Such trend is also observed for the depth from pile head to maximum negative moment. This finding is consistent with previous study on the analysis of laterally loaded vertical pile groups (McVay et al., 1998). The 3rd row pile has larger moment than the 4th row pile at all loads. However, the rate of increment of moment value is comparatively reduced at higher loads. At lower applied loads such as 570 and 770 kips, the 3rd row pile has about 15% larger moment than the 4th row pile, whereas the rate of variation is limited to 5-7% at higher applied loads. Similarly, the 1st row pile moment exceeds the 4th row pile moment by 30 to 40% at 570 and 770 kips, 10% at 970 and 1180 kips, but it only exceeds by 3% at the highest applied loads of 1745 and 1870 kips. Some unexpected results, might be attributed to some minor measurement error, as seen for the 2nd row pile, which has larger moments than 1st row pile at 970 and 1180 kip loads.

The moment profiles obtained for piles located in different rows are also compared. The comparison are made at lower peak load 570 kips and at higher peak load 1870 kips as shown in Figures 5.7a and 5.7b, respectively. As expected, all piles display similar profile except pile 11 of the 1st row, which exhibits larger negative moments when compared to other piles. Figure 5.7 also indicate that the depth to zero moment as well as depth to the maximum negative moment increases as the load increases. The graph of applied load versus maximum moment at pile head is constructed as presented in Figure 5.8a.

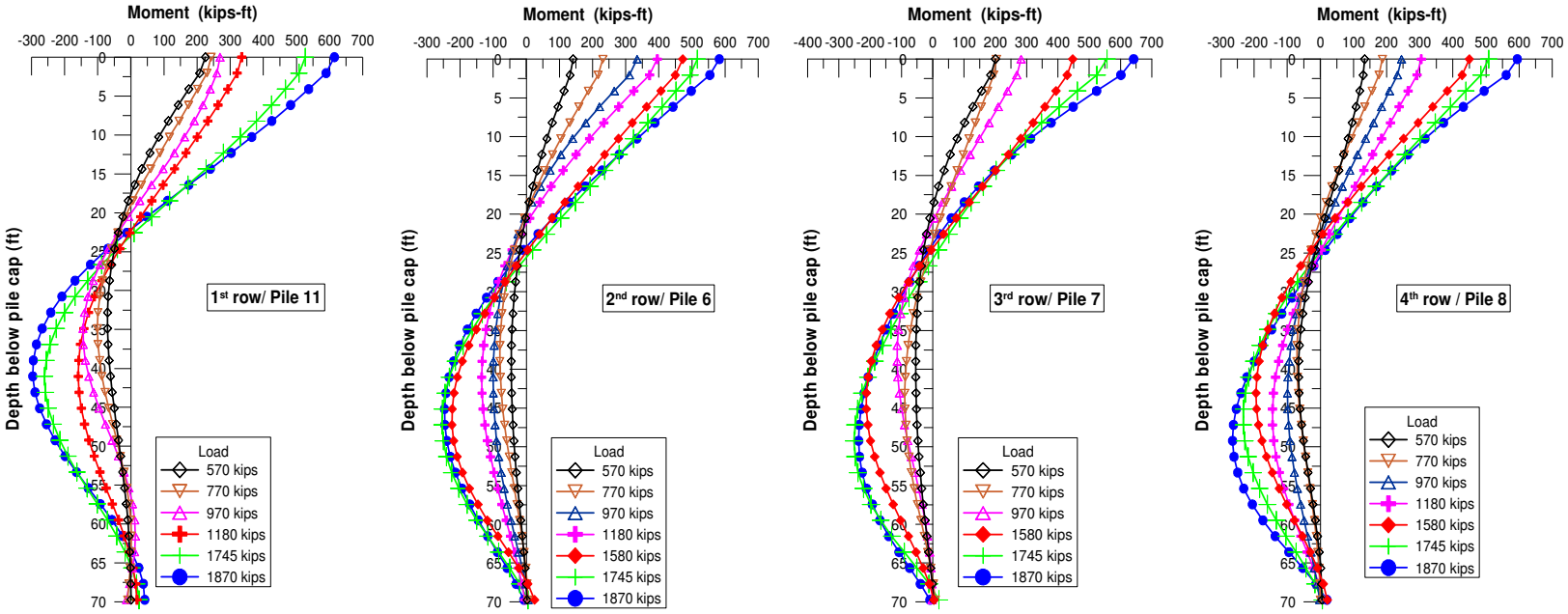

(a) 1st row / pile 11 (b) 2nd row / pile 6 3rd row / pile 7 4th row / pile 8

Figure 5.6: Profile of Bending Moment for different pile

Similar to the trend of load-displacement curve, the moment–load curve also shows bi-linear behavior. The curve of applied lateral load versus moment developed at near to ground level (12 ft from pile head) is also drawn as shown in Figure 5.8b. The moments value at ground level is found to be 50 to 55% lower than moment at pile head. However, the variation of moment within the piles at ground level is not negligible. The variation of moments remain within the range of 15%. The 1st row pile still possesses the largest moment at all applied loads.

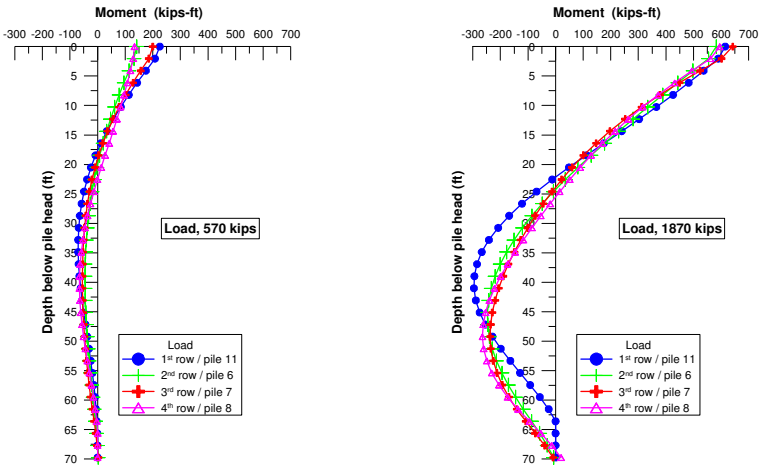

(a) at 570 kips load (b) at 1870 kips load

Figure 5.7: Comparison of derived moment profile of different row piles

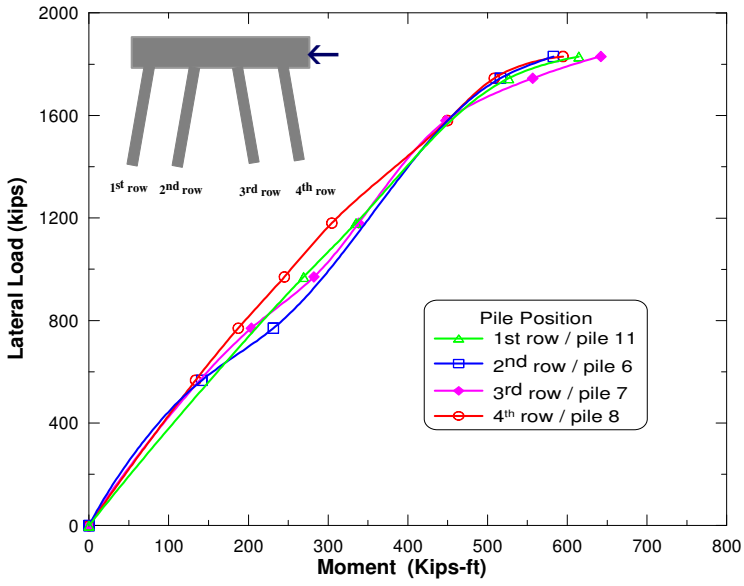

Figure 5.8a: Applied average load versus maximum moment curve

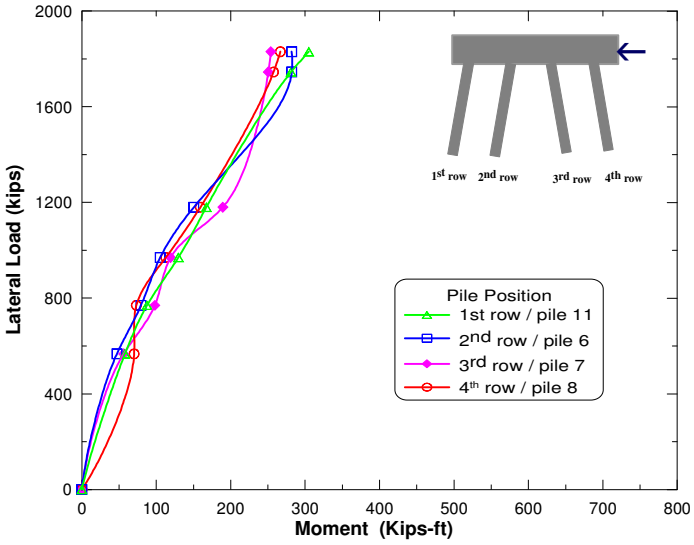

Figure 5.8b: Applied average load versus maximum moment curve

- **Profiles of Bending Moment within the Same Row**

Similar to the displacement profiles, the bending moment profiles of piles located within the 4th row are determined. The displacement profiles for piles 4, 8 and 12 are presented in Figure 5.9. One can observe that the outer piles 4 and 12 have almost similar moment profiles. The maximum moment of pile 4 is about 700 kips-ft while the maximum moment of pile 12 is about 630 kips-ft The inner pile (pile 8) also shows similar bending moment profile, however, the moment values at pile head as well as at ground level are found to be 7% to 25% smaller than the corner pile as shown in Figure 5..

5.3. Bending Moment from Strain Gauge Measurements

The strain gauges measurements were also used to calculate bending moment at certain depths of the piles. The moments were calculated from the strain gauges using Equation 4.11. They are calculated at two locations where strain gauges were installed. One pair of strain gauges (called SG1) were installed at 10 to 12 ft from pile head, depending upon length of pile, whereas, another pair (called SG2) were installed at 5 ft below SG1. The moment calculated from strain gauges at these locations are also compared with the moment developed from inclinometer readings. The comparison of moments from strain gauges readings and inclinometer readings for piles 4, 7 and 12 are shown in Figure 5.11. These figures show a good agreement of moment's calculated from both instruments.

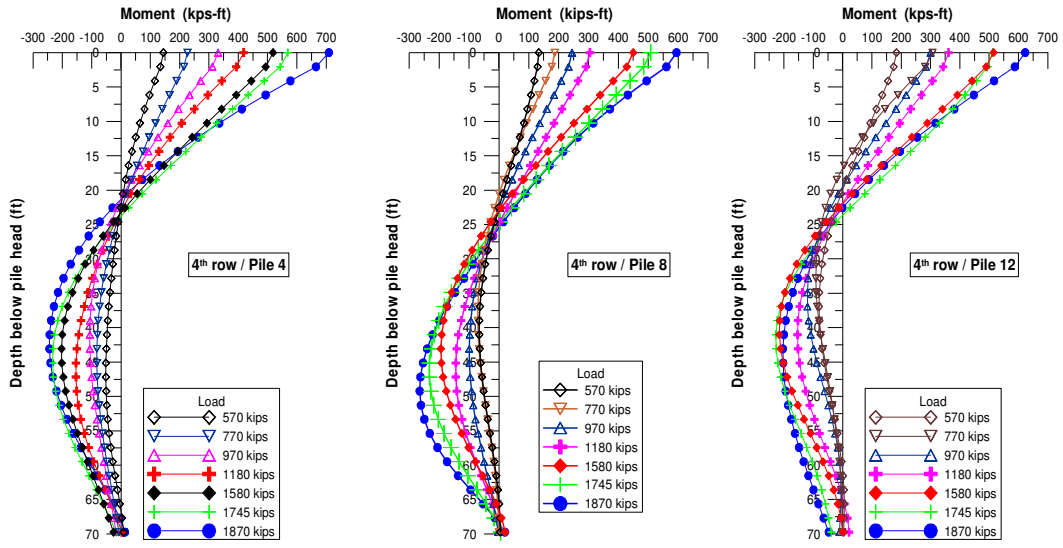

(a) Pile 4 (b) Pile 8 (c) Pile 12

Figure 5.9: Bending moment (kips-ft) profiles of piles of the 4th row

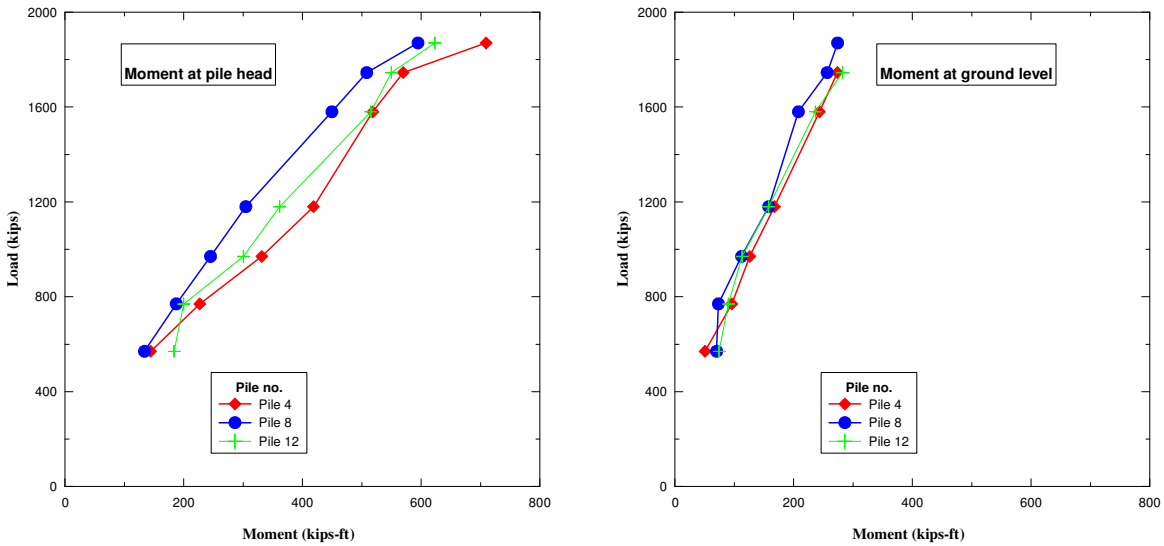

(a) at pile head (b) at ground level

Figure 5.10: Comparison of moments of piles located in the 4th row

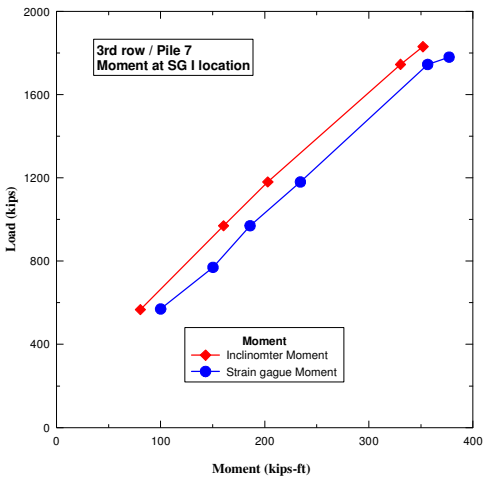

(a) Pile 7 at SG1 location

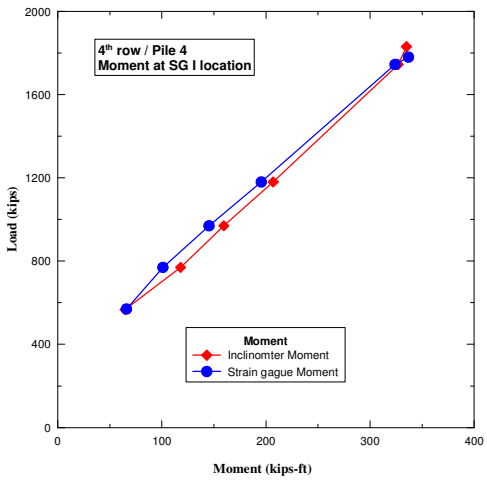

(b) Pile 4 at SG1 location

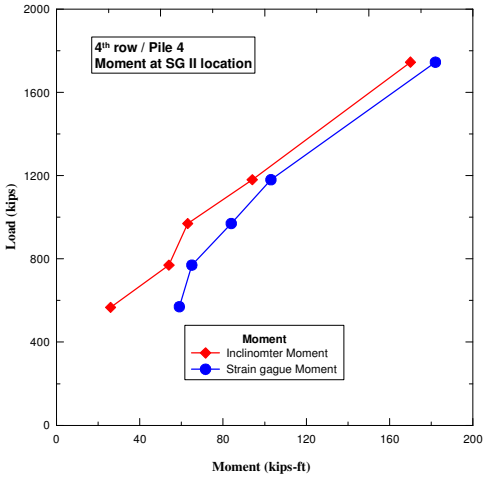

(c) Pile 4 at SG2 location

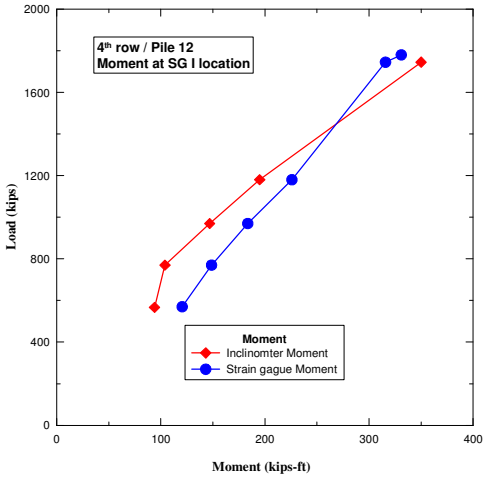

(d) Pile 12 at SG2 location

Figure 5.11: Comparison between measured and calculated moment values

5.4 Measurement of Piles' Axial Loads

The piles' axial loads at SG1 and SG2 locations were calculated from the readings of strain gauges using Equation 4.11. The axial forces in piles are calculated at increasing static loads as shown in Figure 5.12. The measured axial forces in piles from strain gauge reading are due to

applied lateral load only, since the strain gauges were set to zero prior to lateral load test. The Figures indicate that the magnitude of induced axial loads is linearly proportional to the incremental of applied lateral loads In general, nearly 5% to 12% of applied lateral load was transmitted to axial load in all piles; however the direction of developed axial loading depends upon the row position. It is also observed that that the piles inclined in the direction of lateral loading (row 3 and 4) are subjected to tension and those inclined in the opposite direction of loading (row 1 and 2) are subjected to compression.

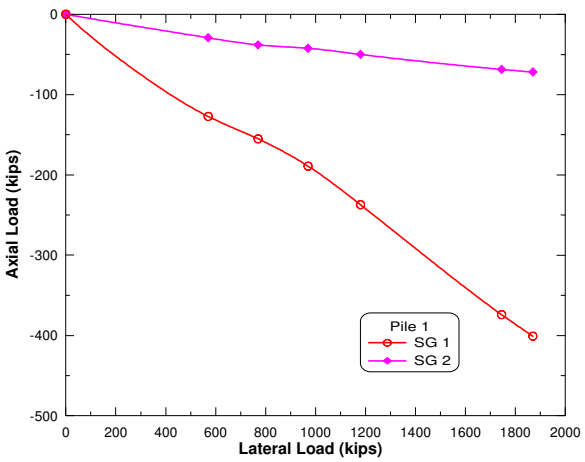

(a) Pile 1

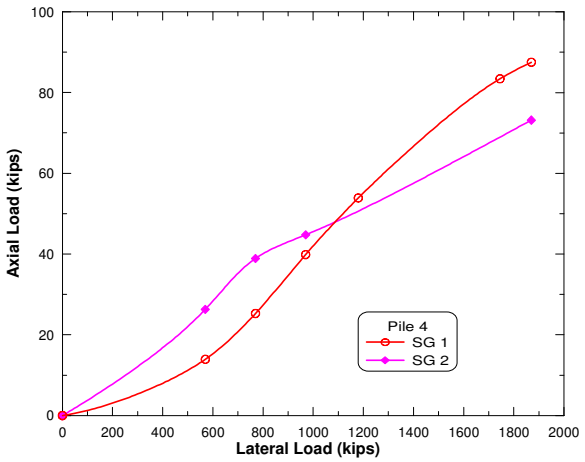

(b) Pile 4

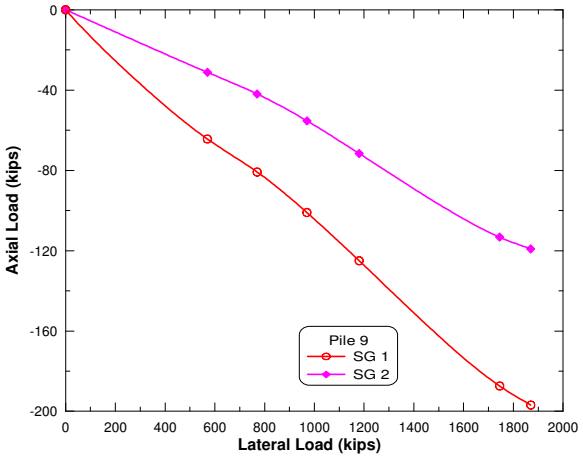

(c) Pile 9

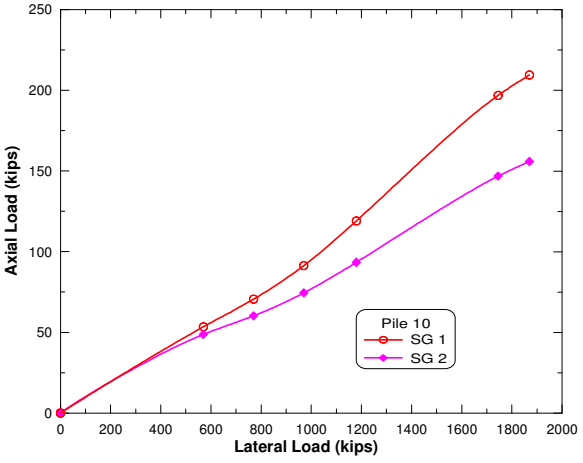

(d) Pile 10

Figure 5.12: Developed axial load in piles

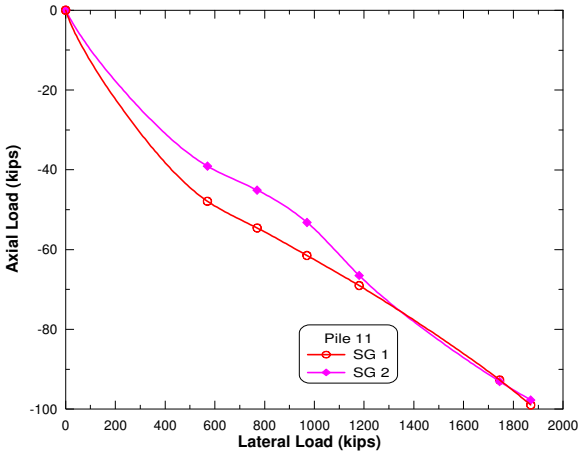

(e) Pile 11

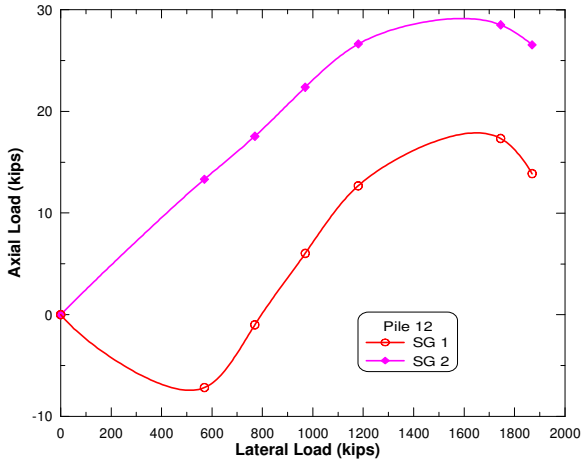

(f) Pile 12

Figure 5.12: (Continued)

At SG1 location for pile 11 in the 1st row, a compressive axial load of about 50 kips and 100 kips were developed at the applied lateral load of 570 kips and 1780 kips, respectively. This indicates that about 8% and 5% of applied lateral load was transmitted to compressive axial load at lower and higher loads respectively as shown in Figure 5.13a. However, at SG2 (5 ft below the SG1) location for that pile, only 6% of lateral load was transmitted to axial load at higher load, and 5% for lower load as illustrated in Figure 5.13b. Hence, the rate of transmitting applied lateral load to axial pile loads decreases with pile depth. Some anomolies is found for pile 1 of same row. It noticed that the maximum compression axial load developed for pile 1 at SG1 location is 400 kips or 22% of lateral load, which simply suggests the overestimation or malfunction of installed strain gauges. However, the result obtained at SG2 location of pile 1 shows good trend, but indicates 15-22% lower compressive load than pile 11 as shown in Figure 5.14a. Most importantly, the results of pile 1 and pile 11, which are located in the 1st row (the farthest row from the loading position) evidently, indicate that the front row piles developed compressive axial force under lateral loading.

The axial load measured for the middle row piles, i.e., the 2nd and 3rd rows (piles 7, 9, and 10) are almost similar, but higher than those piles in the outer rows. At the peak lateral loading of 1780

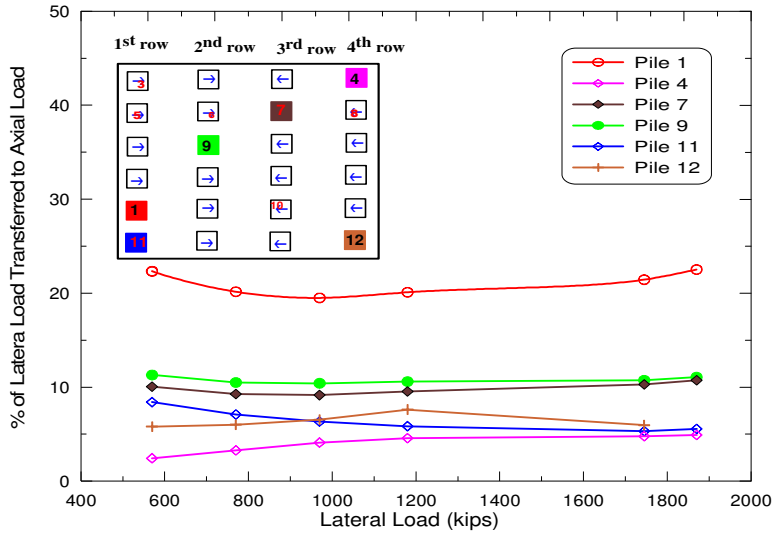

Figure 5.13.a Percentage of lateral load transferred to axial load at SG1

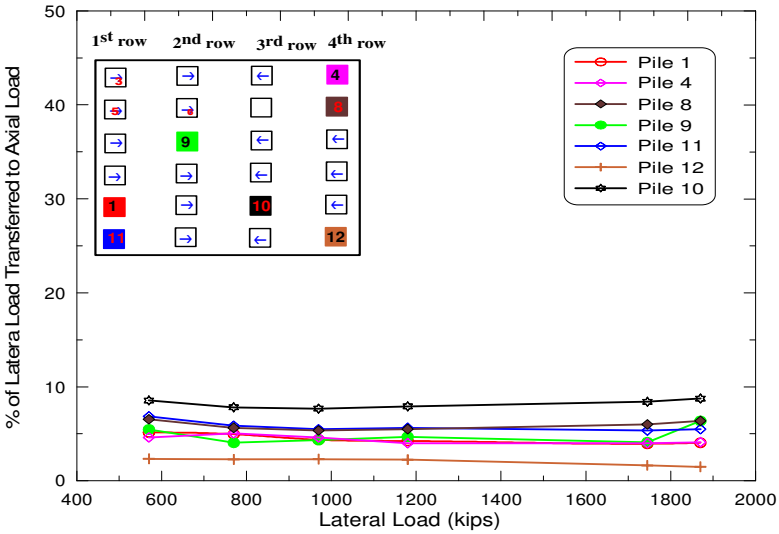

Figure 5.13b. Percentage of lateral load transferred to axial load at SG2

kips, the axial loads developed in piles 7, 9, 10 at SG1 location are near to 200 kips. However, the developed axial load was tensile in the 3rd row and compressive in the 2nd row, i.e., the row closer to the back row develops tensile force and the row next to the front row develops compressive force. As shown in Figure 5.14b, piles 7 and 10 of the 3rd row have almost the same amount of axial load at SG1 location. The past experimental results show that the row closer to the point of loading develops tensile force (Zhang and McVay, 2001). Evidently, piles 4 and 12 located in the 4th row developed tensile force. Pile 4 has 90 kips tension load at SG1 location whereas pile 12 has 40 kips in tension. This was expected since the laser survey shows that north side of pile foundation undergoes larger deformation than the south side of the pile foundation

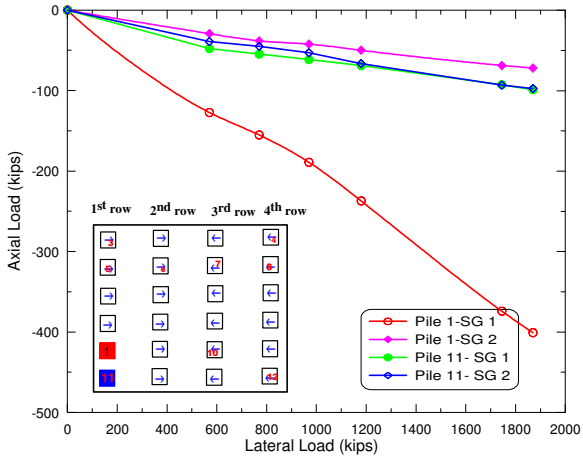

Figure 5.14a. Comparison of induced axial load on Piles 1 and 11

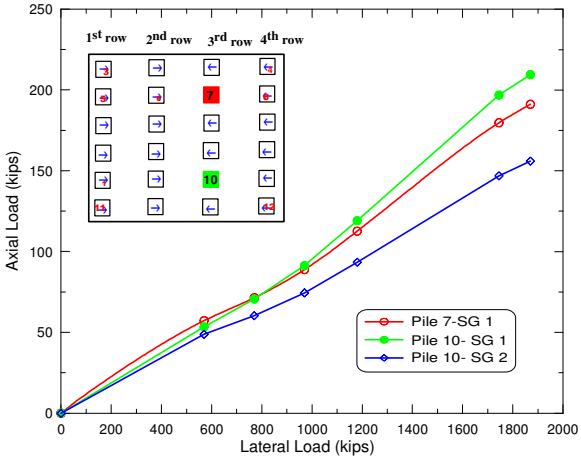

Figure 5.14b. Comparison of induced axial load on Piles 7 and 10

The aforementioned results explicitly suggest that the statically induced axial forces in the piles are non-uniform, and depend on row position: the piles locating in the row nearby the applied lateral induced tensile forces and piles located at the farthest row, such as 1st row, induced compressive forces, which is consistent with the results of studies (Pinto et al., 1997; and McVay et al., 1996). The bar chart showing induced axial force in piles corresponding to applied lateral load is presented in Figure 5.15. It can be explained that the lateral displacement along with the rotation of the rigidly connected pile group cause the back row piles (pile 7 and pile 8) to move upward subsequently inducing tensile force, whereas it cause the front row piles (piles 9 and 11) to move downward resulting in compressive forces. The schematic diagram illustrating the compressive and tensile movement of piles is depicted in Figure 5.16.

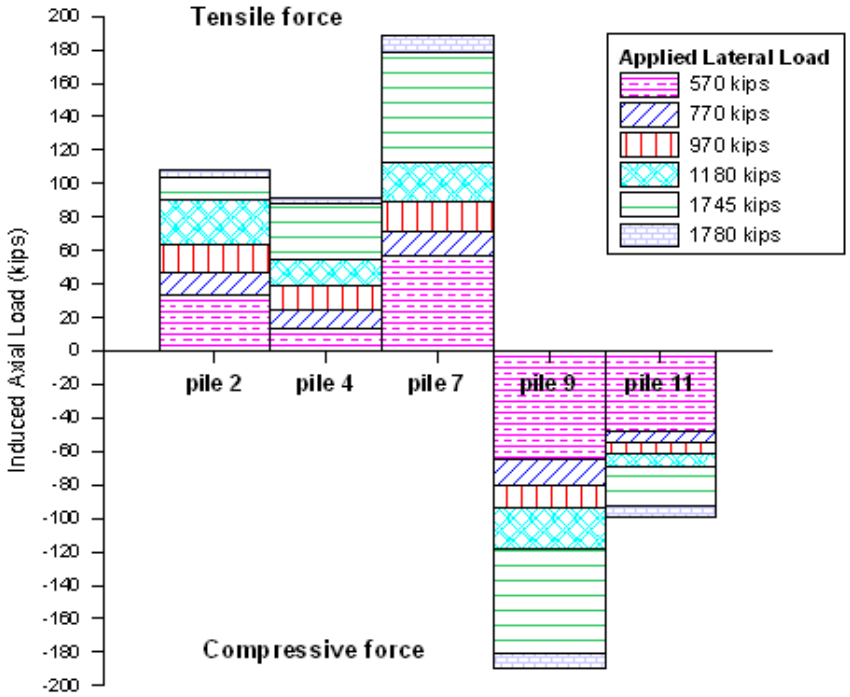

Figure 5.15: Induced axial force in pile under lateral loading

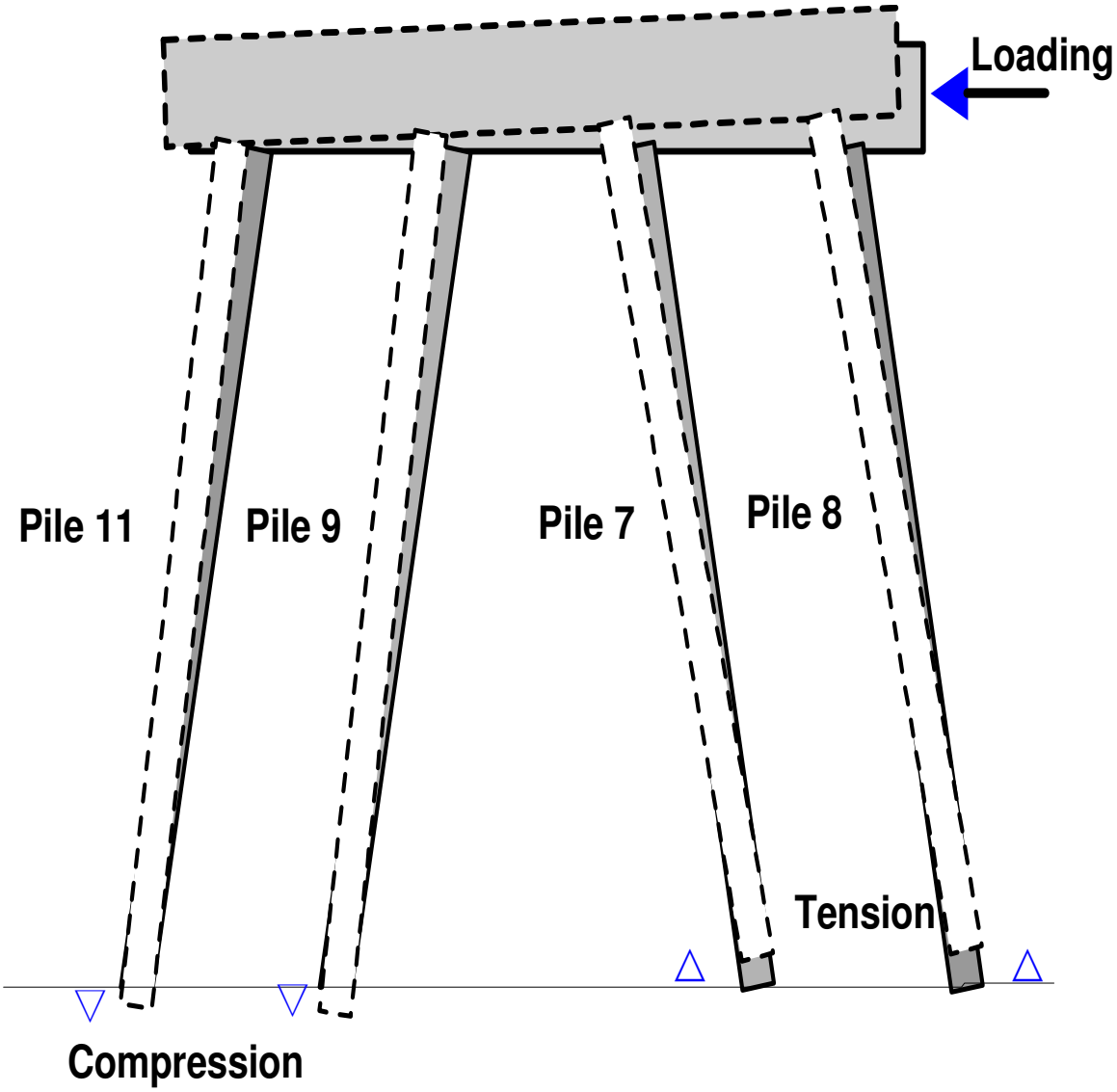

Figure 5.16: Schematic Diagram illustrating the movement of pile under lateral loading

In addition, the distribution of axial forces along the pile length are also not uniform since the induced axial force at SG2 location are lower than the axial force induced at SG1 location. The reason is evident since the SG1 is located nearby the ground level where the soil is too much soft, thus the tendency of the pile to deform laterally is larger due to the low lateral soil resistance. With the depth of soil, the soil lateral resistance increases due to the increment of the

stiffness of soil, thus lower axial forces as compared to SG1 is induced. However due to the lack of sufficient number of strain gauges at the lower level of the piles, the distribution of the axial force along the length of the pile could not be illustrated.

5.5. Profile of Soil Resistance Force per Unit Length

The profiles of soil resistance force per unit length for piles were derived by differentiating the moment profile twice as described in Equation 4.8. The soil resistance profiles of piles 11, 6, 7 and 8 representing the 1st, 2nd, 3rd and 4th row are illustrated in Figure 5.17. The 1st row (pile 11) exhibits the maximum soil resistance value; approximately 20% to 40% higher than the 4th row pile. However, the value of soil resistance corresponding to the same depth for all piles does not vary substantially; mere 7-8% variation is observed. Similar to moment profiles, the value of soil resistance increases with increasing the applied lateral load. The depth from pile head to the position of maximum soil lateral resistance developed in pile also increases as the applied load increases. For example, at the applied load of 570 kips, pile 8 of the 4th row shows maximum soil resistance of 0.42 kips/ft, which occurred at 24 ft (8B) below the ground level. On the other hand, the maximum soil resistance developed a the applied load of 970, 1180, 1745 and 1870 kips are 0.50, 0.77, 1.22, 1.4 kips/ft, respectively. These maximum soil lateral resistances occurred at 29 ft (9.7B), 32 ft (10.7B), 34 ft (11.3B) and 34 ft (11.6B), respectively. Hence, the greater the applied load, the deeper the maximum soil resistance occurred. Such trend is also seen in other pile rows. In comparison to other piles, the depth to the maximum soil resistance is found to be the lowest in the 1st row piles as depicted in Figure 5.16a. It also indicate that the distributing range of soil resistance along the length pile is smaller for front row pile (pile 11) than other row piles. The soil resistance distribution extends to 16B in back row pile, whereas, the soil resistance distribution for leading row piles extends to 14B depth. Thereby, it can be inferred that the soil resistance depends upon the loading and position of row.

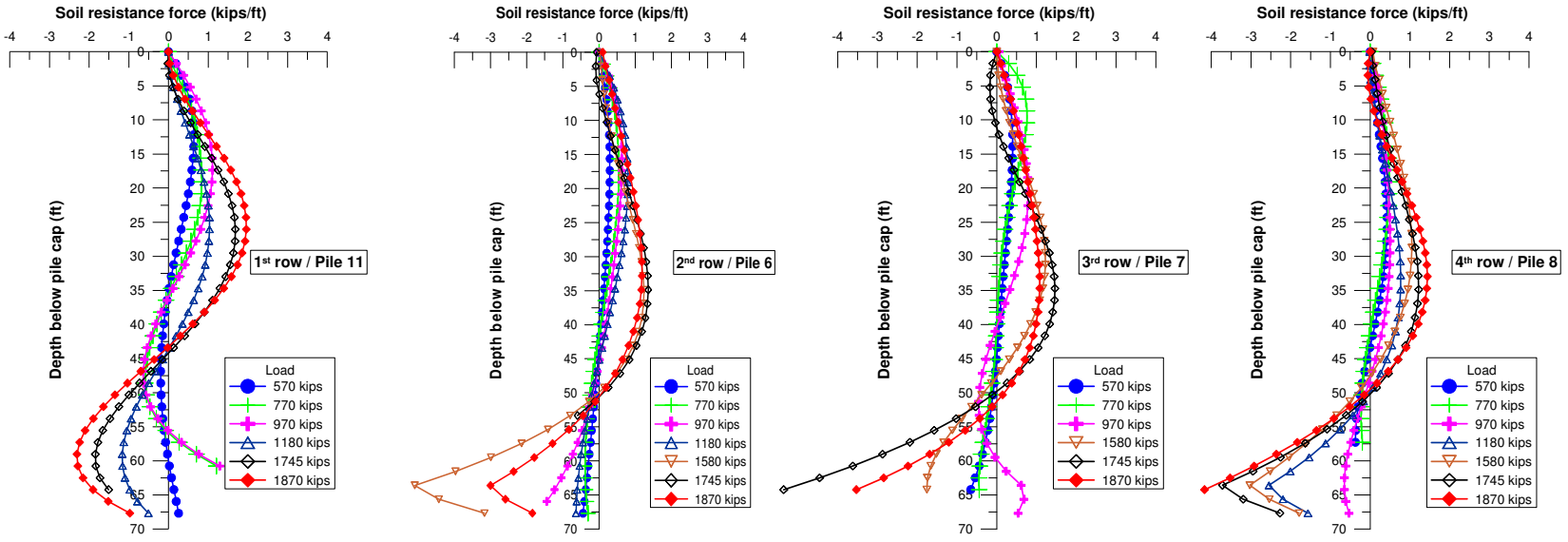

(a) 1st row/ pile 11 (b) 2nd row / pile 6 (c) 3rd row / pile 7 (d) 4th row / pile 8

Figure 5.17: Soil resistance force (kips/ft) profile for each row in pile group

- **Profiles of Soil Resistance Force within the Same Row**

The soil resistance profiles are derived for piles 4, 8, and 12 located within the 4th row as shown in Figure 5.18. Figure 5.18a show that the soil resistance force developed for pile 8 is negligible at the top 10 ft depth. However, such trend is not seen for piles 4 and 12, which have comparatively much higher soil resistance at this depth as depicted in Figure 5.18b and 5.18c. This could be due to the presence of soft soil nearby the top layer of pile 8. The maximum soil resistance is almost similar in all piles. However, the depth to the maximum soil resistance differs between piles. The depth to the maximum soil resistance is within 20-25 ft below ground level for piles 4 and 12, whereas the depth to the maximum soil resistance for pile 8 is in the range of 30-35 ft below ground level, which is comparatively deeper than for piles 4 and 12.

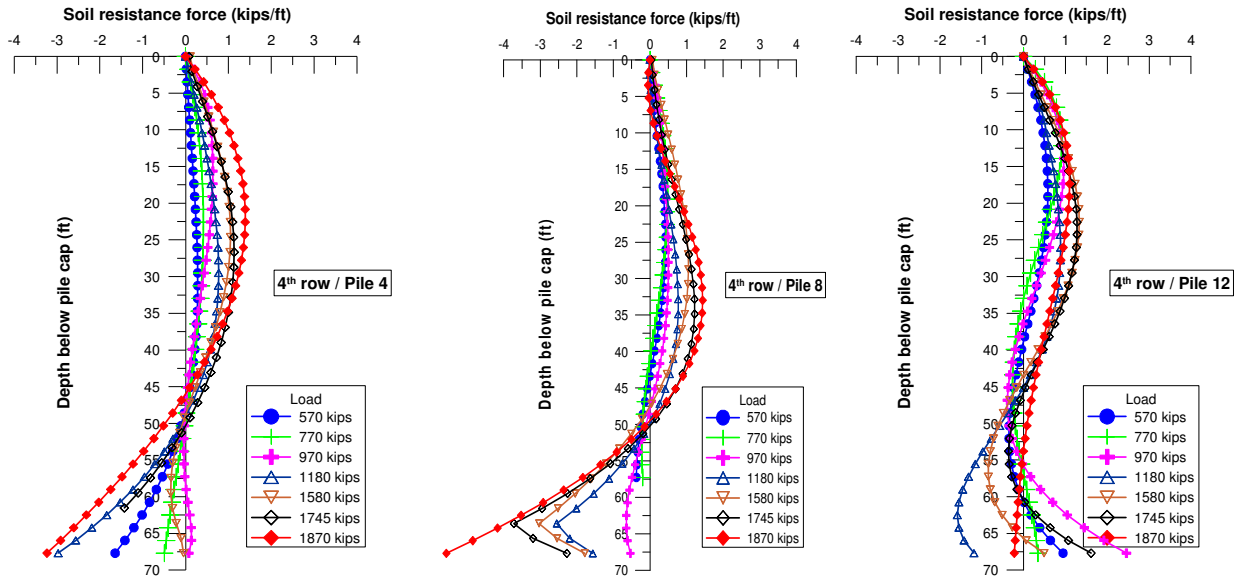

(a) pile 4 *(b) pile 8* *(c) pile 12*

Figure 5.18: Soil resistance force (kips/ft) profile of piles within 4th row of pile group

5.6 Back-Calculation of p-y Curves

The p-y curves are used to analyze the pile group response and the pile-soil interaction at selected depths. They were constructed from the soil reaction profile (P) for each applied lateral load increment and the corresponding lateral displacement profile (y) as explained earlier in Section 4.2.4. The p-y curves for depths of 5 ft, 10 ft, 15 ft and 20 ft below ground level were developed for different piles. The p-y curves for piles 6, 7, 8, and 11 are compared with each other at depths of 5 ft intervals as presented in Figure 5.19. They indicate that the 1st row (pile 11) has the largest soil reaction corresponding to same pile displacement. However, 2nd, 3rd and 4th row piles display similar p-y curves at all depths. Since, the CPT soundings showed that soil profile close to pile 11 has a higher undrained shear strength compared to the soil close to the other pile locations, This might explain the higher soil lateral resistance and lower deformation for pile 11.

Figure 5.18 also indicates that the determined p-y curves were fully developed only at 5 ft and 10 ft depth. The p-y curves below 10 ft depth were not fully developed. The soil resistance increases with increasing depth; it may be because the stiffness increases with increasing the depth. This conforms to the findings of experiments that were conducted by McClelland and Focht (1956) for Louisiana offshore soils.

Considering the center-to-center pile spacing of 4.3B at loading direction, which is 4.3B, it is inferred that that the group effect is negligible. However, further study is needed to verify this statement.

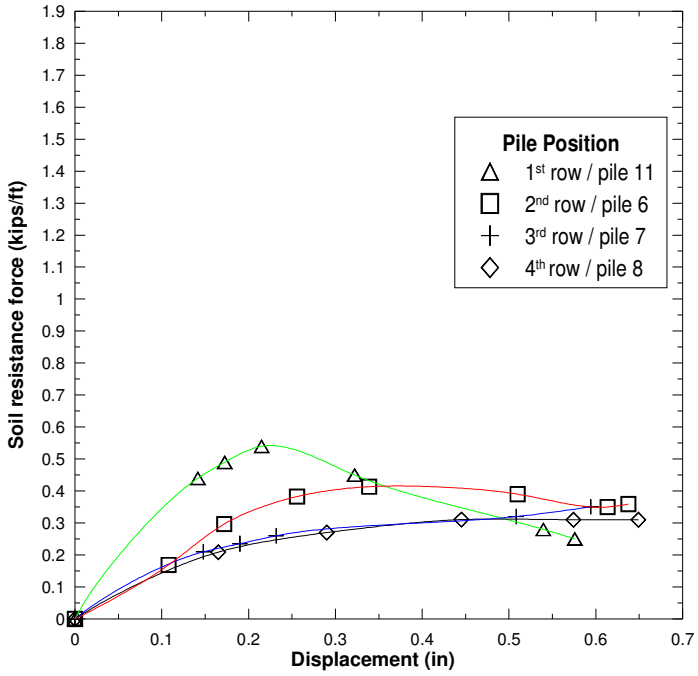

(a) 5 ft below Ground level

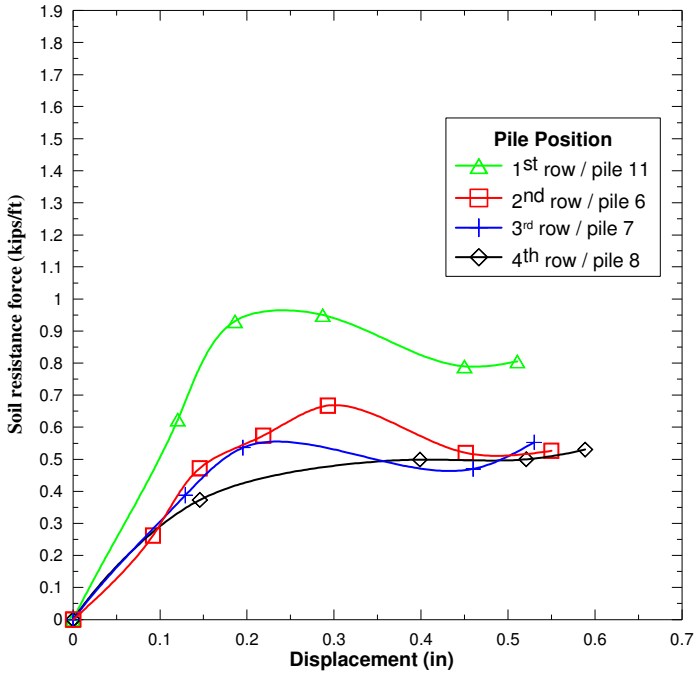

(b) 10 ft below Ground level

Figure 5.19: Comparison of p-y curves of piles

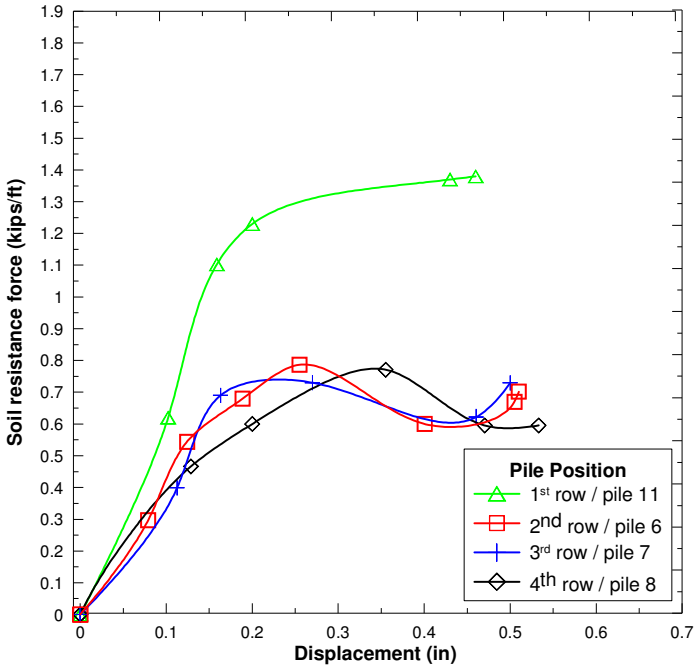

(c) 1 5 ft below Ground level

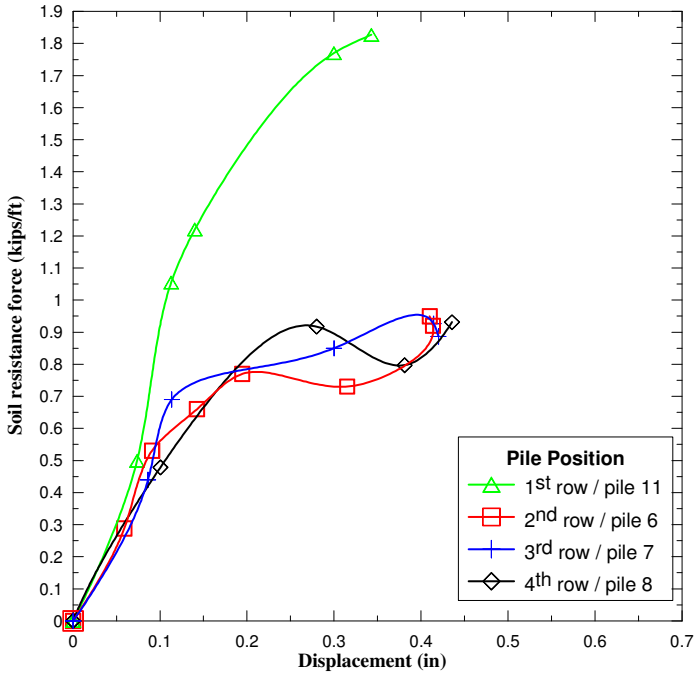

(d) 20 ft below Ground level

Figure 5.19: (Continued)

- **Comparison of Back-Calculated p-y curves for Piles in the Same Row**

The p-y curves for for piles 4, 8, and 12 located within the same 4th row are compared at the depth intervals of 5 ft, 10 ft, 15 ft and 20 ft as shown in Figure 5.20, which shows that the outer piles (piles 4 and 12) have larger soil reaction than the inner pile (pile 8) at the same lateral displacement. The outer pile 12 has the largest soil reaction, with approximately 30% larger than the inner pile 8.

In addition, the p-y curves back-calculated for piles 11 and 12 are also compared since both piles have similar lateral displacement. It can be seen that piles 11 and 12 develop similar p-y curve at 5 ft and 10 ft below ground level as shown in Figure 5.21a. However, with the increase of depth (15 ft and 20 ft), pile 11 exhibited larger later soil resistance, and hence producing stiffer p-y curves compared to pile 12 as presented in Figure 5.21b.

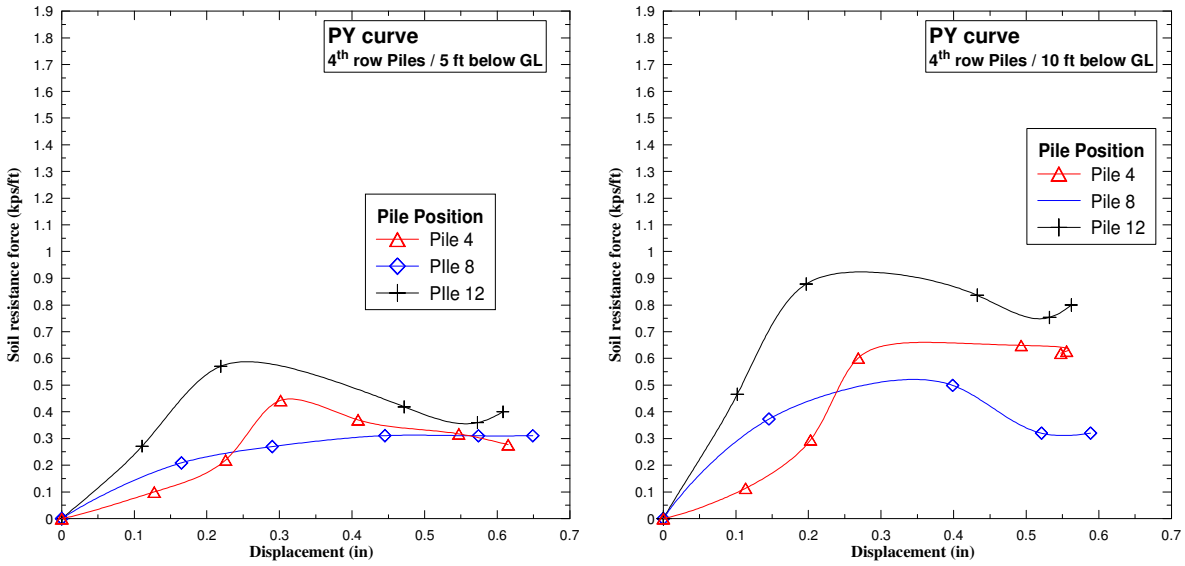

(a) (b)

Figure 5.20: Comparison of p-y curves of same row piles

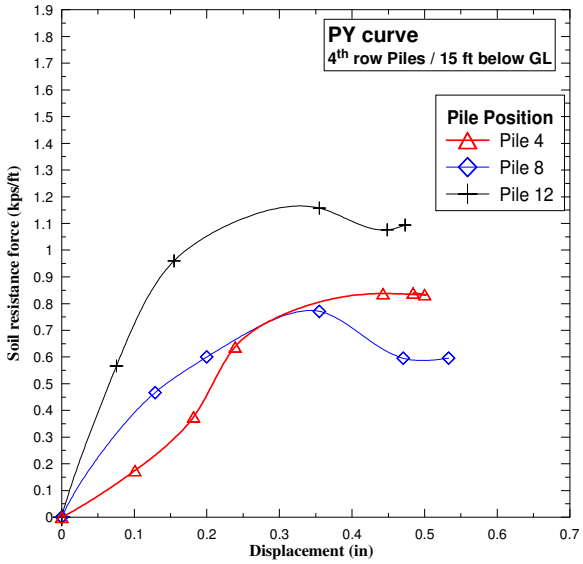

(c)

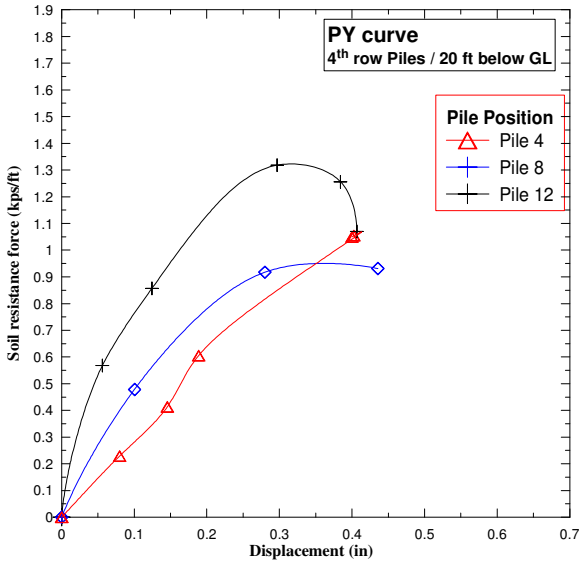

(d)

Figure 5.20: (Continued)

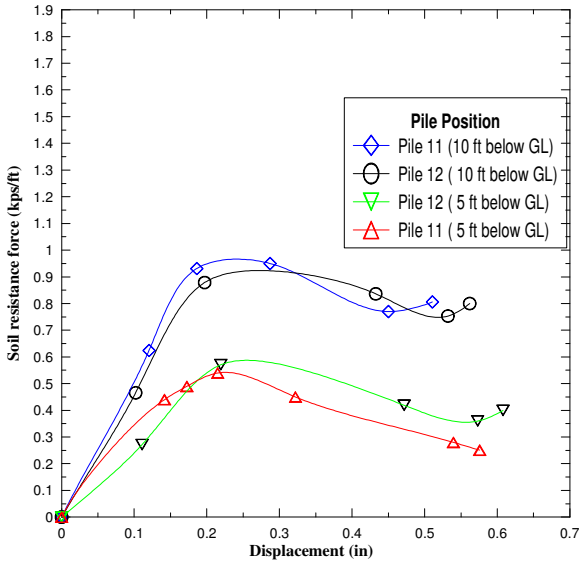

(a)

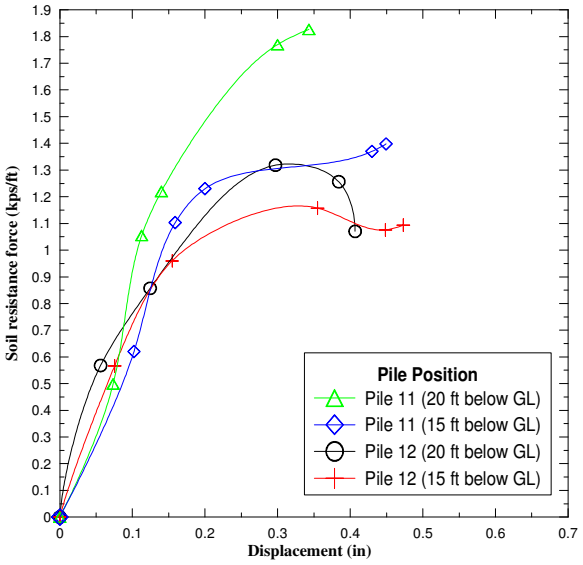

(b)

Figure 5.21: Comparison of p-y curves of pile 11 and pile 12

CHAPTER 6
FB-MULTIPIER ANALYSIS

6.1 Introduction

Several computer programs are available for the numerical analysis of single pile and pile group as discussed in literature review. The FB-MultiPier was selected to perform the numerical analysis of the battered pile group foundation at M19 eastbound pier. It is an advance form of FB-Pier, which was developed by the University of Florida. The FB-MultiPier was preferred for numerical analysis because the entire I-10 Twin Span Bridge was designed using this software. The objective of the FB-MultiPier analysis was to compare its result with the results of full-scale lateral load test.

6.1.1 Brief Introduction of FB-MultiPier

The FB-MultiPier program can be used to analyze the entire components of the bridge from bridge slab to soil layer by incorporating the finite-element analysis. It performs analysis by generating the finite element models for given geometric description of the structure and the foundation system. For the generation of finite element models, the FB-MultiPier incorporates several types of elements such as membrane element, flat shell element, plate element, and special element generated by adding normal rotational stiffness to the shell element, which account for the torsional force transmitted from pile to pile cap. The soil modeling in the FB-MultiPier provides the ability to define the soil layers at varying depths. Each soil layer can be modeled either as sand or clay, using one of the several built in p-y curves or apply user-supplied p-y cruves to respective layers. The p-y curves incorporated in the FB-MultiPier and their input parameters are summarized in Table 6.1.

The pile-soi interaction in a pile group is characterized by user defined p-multipliers to account for group effect. FB-MultiPier uses an iterative solution technique to predict the lateral displacements. During iteration, it calculates stiffness of soil and piles, and eventually generates the stiffness matrix to predict the lateral displacement of the pile as output. The displacement is then used to predict the internal forces of structures' members

Table 6.1. Summary of Input Parameter of p-y curves used in FB-MultiPier

Soil type	Soil stiffness	Soil location	Parameters	p-y curve
Sand	Loose–dense	Above ground water table	ϕ, K_s, γ	O'Neill and Murchison (1984)
		Below ground water table	ϕ, K_s, γ	Reese et al. (1974)
Clay	Soft/medium stiff	Above ground water table	S_u , ε_{50}	O'Neill and Gazioglu (1984)
		Below ground water table	S_u , ε_{50}	Matlock (1970)
	Stiff	Above ground water table	S_u, ε_{50}	Reese and Welch (1972)
		Below ground water table	$\boldsymbol{S_u}$ **,** $\boldsymbol{\varepsilon_{50}}$**,** $\boldsymbol{\gamma}$**,** $\boldsymbol{K_s}$	**Reese et al. (1975)**

6.1.2 Modeling of M19 Eastbound Pier Foundation in FB-MultiPier

The M19 eastbound pier structure was modeled with 24 battered piles, pier cap, 2-pier column, shear wall, and a cantilever bent as illustrated in Figure 6.1. The piles are modeled as 3D discrete elements. The discrete element models the non-linear behavior of concrete material by using input or default stress-strain curves that are a function of compressive stress of concrete (f'_c) and modulus of elasticity of concrete (E_c). The input data defining the pile geometry and structural properties such as f_c, E_c, pile length and width, reinforcement area, were input to generate the pile model. The fixed head pile cap was modeled using nine nodded shell elements which is based on Mindlin's theory that can take into account the bending and shear deformations. Similarly, each soil layer surrounding the piles was modeled as an attached non-linear spring which can be characterized by selecting a proper p-y curve. The p-y curve was selected based on soil type and properties. The input required for modeling soil layers are undrained shear strength (S_u), strain corresponding to 50% of the maximum stress (ε_{50}), unit weight of the soil (γ) and the subgrade modulus of soil (K_s) for clayey soil; or friction angle (ϕ), K_s and γ for sandy soil.

The values of these soil input parameters were based on laboratory and in-situ test results. The undrained shear strengths (S_u) were obtained from unconsolidated undrained (UU) triaxial tests that were conducted on undisturbed samples obtained from soil borings. The S_u were also estimated from CPT tests. The value of strain that correspondence to 50% of the maximum principle stress (ε_{50}) were determined from UU tests, and were compared with the typical values of ε_{50} recommended by Matlock (1970) as presented in Table 2.2. The subgrade soil modulus (K_s) was estimated based on undrained shear strength value as given in Table 2.4. Similarly, SPT

blow counts (N_{60}) were used to estimate the internal friction angle for sand. The values of soil parameters for each layer and selected p-y curve for that layer are presented in Table 6.2 and Figure 6.2.

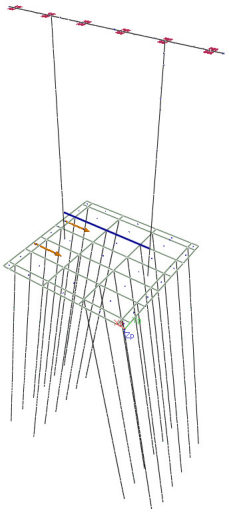

(a) Structure view

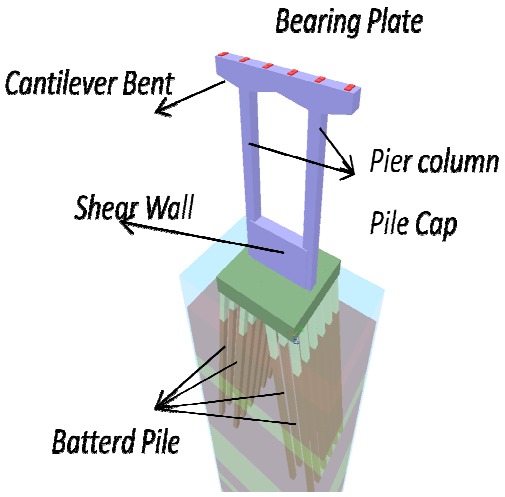

(b) 3D pier view

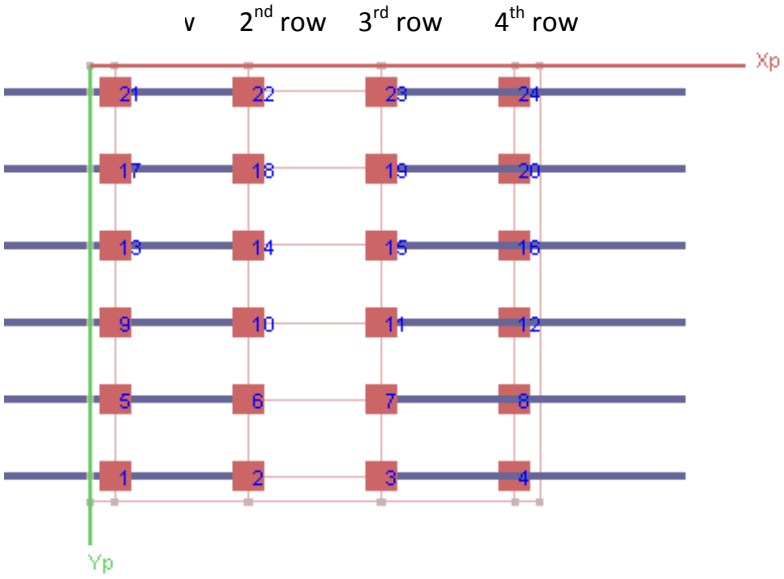

(c) Top view of Pile layout

Figure 6.1: FB-Multipier model for M19 Pier

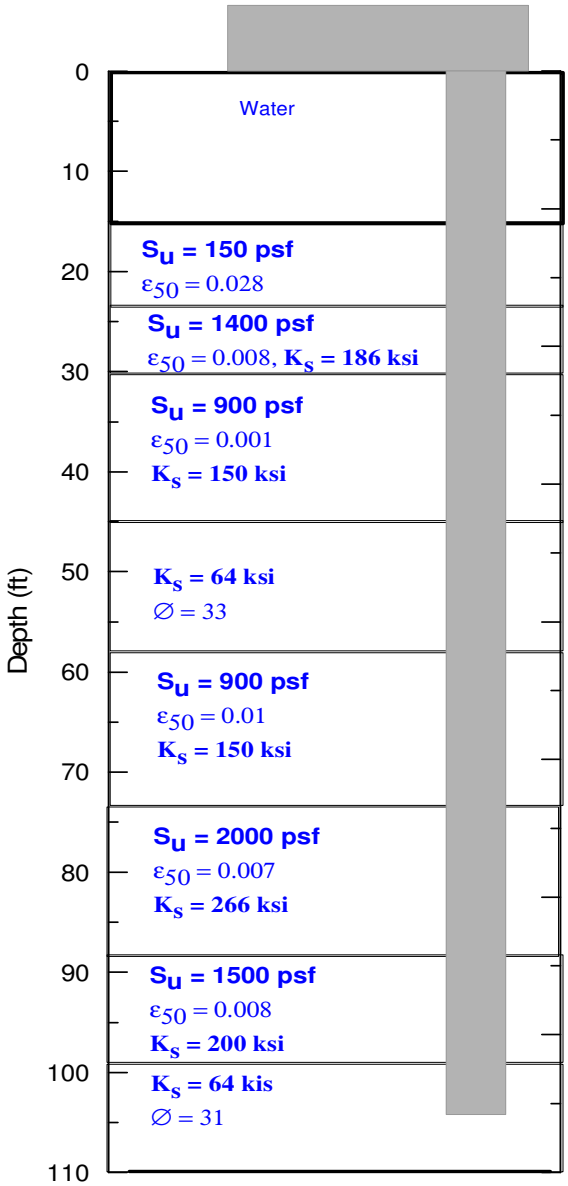

Figure 6.2: Soil input values used for generating FB-MultiPier model

Table 6.2: value of input parameters for FB-MultiPier Analysis

Depth below excavated Ground (ft)		Soil type	Lateral model (p-y curve)	Unit weight (pcf)	Undrained shear strength (psf)	Friction angle ϕ (deg)	subgrade modus K_s	strain ε_{50}
-15	23	Cohesive		120	150			0.028
-23	30	Cohesive		11	1400		186	0.008
30	32			120	900		150	0.010
32	35			118	280			0.02
35	45		Clay soft	108	950		150	0.01
45	57	Cohesionless	Sand (Reese)	120		33	64	
57	73	Cohesive	Clay soft	114	900			0.01
73	93		Clay stiff	123	2000		266	0.007
93	99	Cohesive	Clay stiff	128	1500		200	0.008
99	101	Cohesive	Clay soft	124	1140			0.009
101	105	Cohesionless	Sand(Reese)	120		31	64	
105	138	Cohesionless	San (O'Neil)	120		38	123	
138	145	Cohesive	Clay stiff	113	1400		186	0.008
145	155	Cohesive	Clay stiff	107	1900		253	0.007
155	163	Cohesionless	Sand (Reese)	127		28	46	
163	174	Cohesive	Clay stiff	115	2600		346	0.006
174	178	Cohsieve	Clay stiff	127	1600		213	0.007
178	186	Cohesinless	Sand (Reese)	120		29	64	
186	194	Cohesinless	Sand (ONeill)	120		38	149	

6.2 Sensitivity Analysis

The values of S_u, ε_{50} and K_s are, in general, important input parameters of FB-MultiPier, and can substantially affect the predicted lateral deformation behavior of piles. A preliminary analysis of lateral behavior of M19 pier by FB-MultiPier was first performed using the input soil parameters values presented in Table 6.2. The preliminary analyses showed large discrepancy in the analyzed of lateral displacements from the measured values recorded during the lateral load test. Therefore, before analyzing the lateral load behavior of M19 pier, sensitivity analysis was first performed for these soil input parameters. The following Section will discuss the results of analysis performed by varying soil input parameters.

6.2.1 Sensitivity Effect of Undrained Shear Strength (S_u)

Sensitivity analysis was performed to investigate the effect of S_u. Three cases were considered: (1) using laboratory derived S_{u_lab} as given in Table 6.2; (2) by increasing the laboratory-derived S_u values of all layers to $2S_{u\_lab}$; and (3) by decreasing the S_{u_lab} value to $\frac{1}{2}S_{u\_lab}$, while keeping all other parameters constant. It was observed that the variation of S_u highly affects the lateral displacement profile. As shown in Figure 6.3a, the lateral displacement value for the top 5 ft depth decreased by 23% to 25% at $2S_{u\_lab}$ whereas, the displacement value increased by 38% to 40% when the S_u value is reduced to $\frac{1}{2}S_{u\_lab}$. As expected, the lateral displacement is inversely proportional to the undrained shear strength. Also, the ultimate soil resistance per unit length is directly proportional to the undrained shear strength (i.e., the higher the S_u value, the higher the soil resistance at any depth as depicted in Figure 6.3b). This trend is clearly observed in the p-y curves generated for soft clay and stiff clay as presented in Figures 6.4.

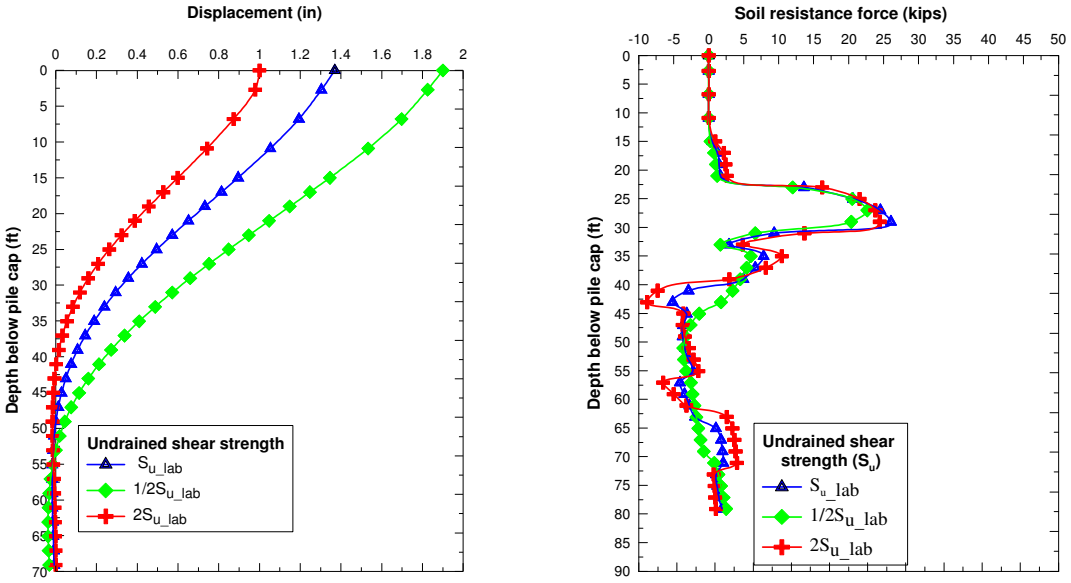

(a) Lateral deformation (b) Soil resistance force

Figure 6.3: Behavior of pile at varying undrained shear strength of pile 11

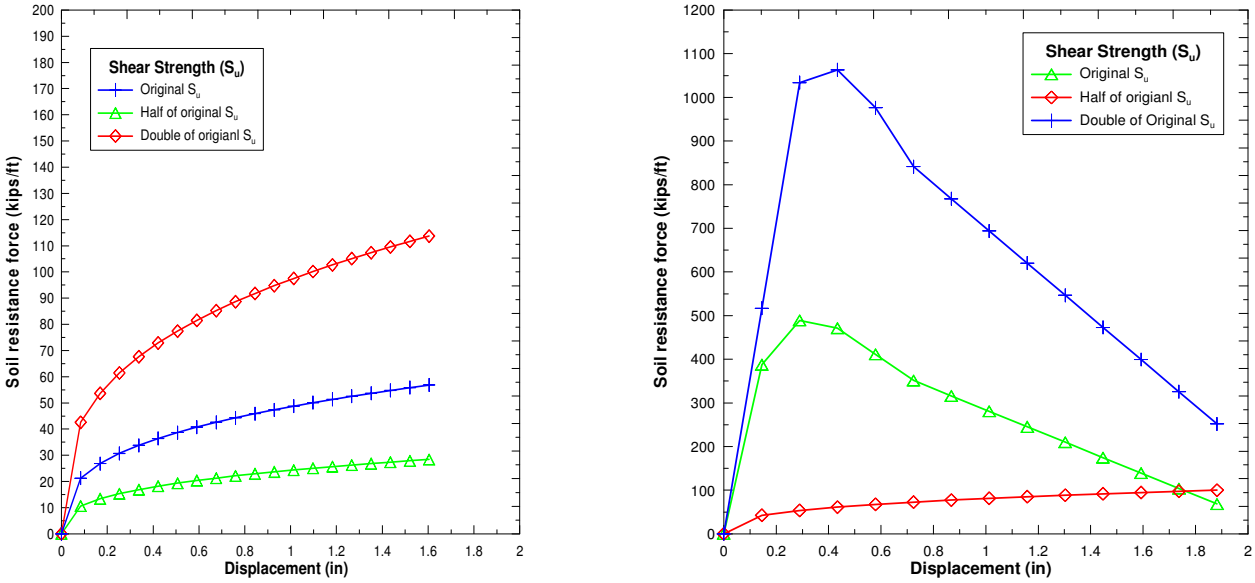

(a) for soft clay (b) for stiff clay

Figure 6.4: P-Y curve at varying undrained shear strength

6.2.2 Influence of Strain at 50% Stress (ε_{50})

Sensitivity analyses were also performed by varying ε_{50} input values. Three cases were analsyed by considering ε_{50}, $2\varepsilon_{50}$ and $\frac{1}{2}\varepsilon_{50}$ of values listed in Table 6.2, while keeping other parameter constant. The results of analyses indicate that reducing the ε_{50_lab} does not have substantial influence on the magnitude of the lateral deformation, and that displacement is merely reduced by 3% to 4%. However, the lateral displacement is increased by 10% when the ε_{50_lab} value is doubled as shown in Figure 6.5a. Furthermore, the soil pressure value increases with decreasing the $\boldsymbol{\varepsilon}_{50\_lab}$ and vice versa as shown in Figure 6.5b. As the soil resistance (P) is inversely proportional to the y_{50}, which itself is related to ε_{50}, the pressure at lower strain is higher than the pressure at larger strain i.e. at the same displacement the pressure corresponding to the lower strain is higher. It was also noticed that changing the strain value does not alter the shape of p-y curve for soft clay. However, the shape of p-y curves was altered for the stiff clay due to the variation of the strain value. The reason for this effect is that the peak point of the curve varied with the variation of strain values, which changes the shape of p-y curve. The p-y curves at varying strain values for the soft clay and for stiff clay are presented in Figure 6.6.

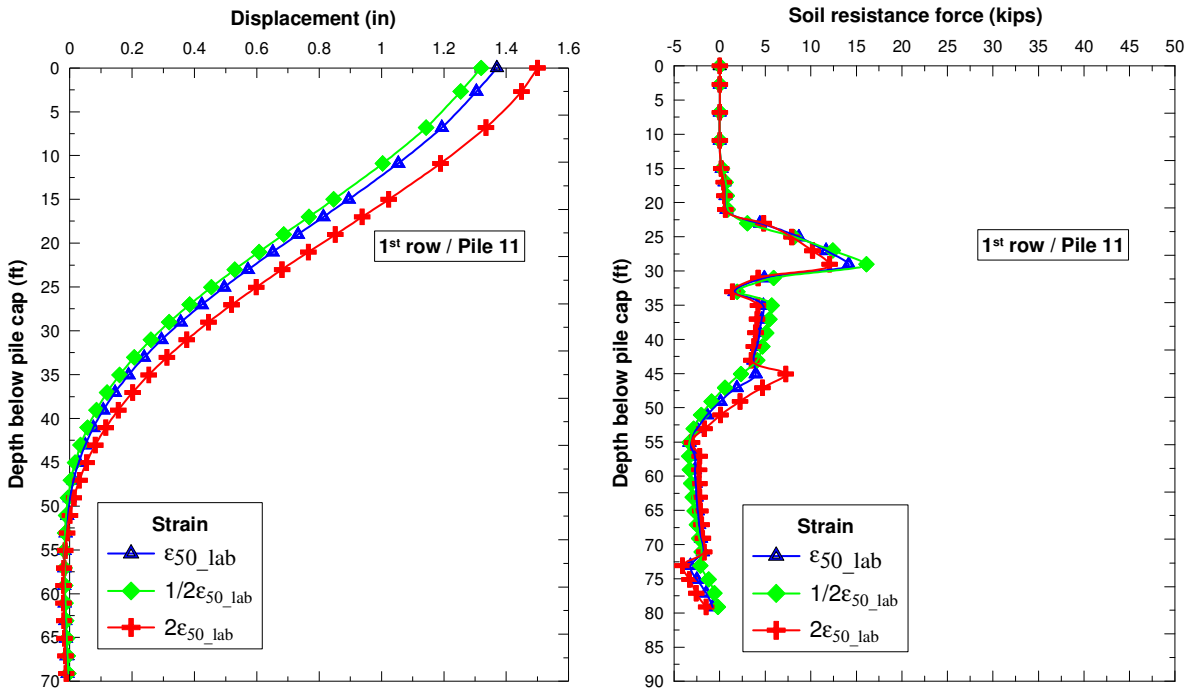

(a) Lateral deformation (b) Soil resistance force

Figure 6.5: Behavior of pile at varying strain values

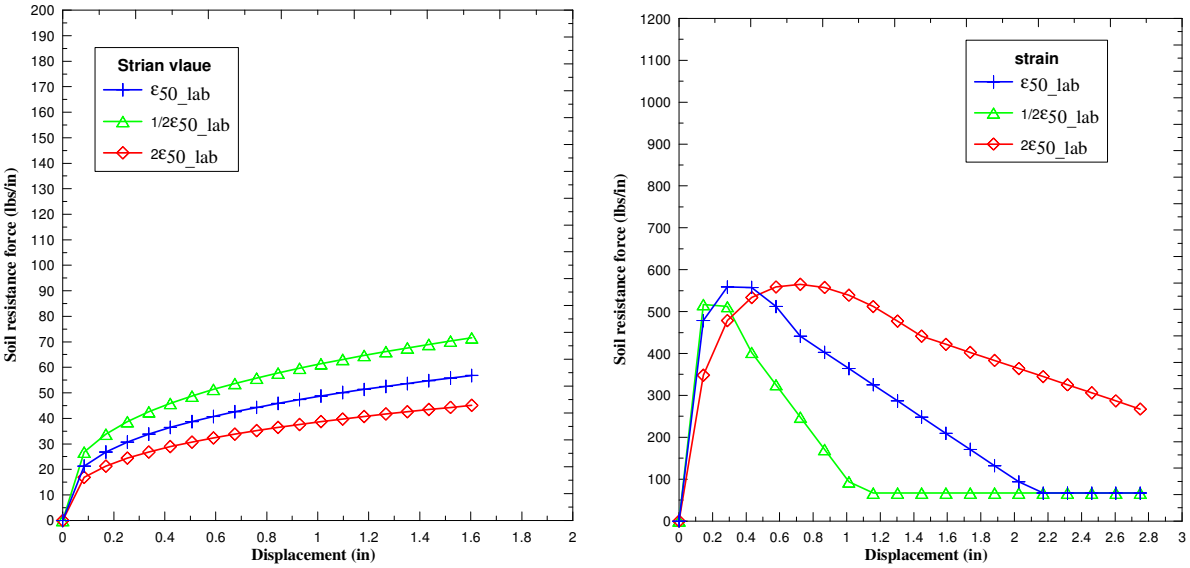

(a) for soft clay layer (b) for stiff clay layer

Figure 6.6: p-y curve at varying strain values (ε50)

6.2.3 Sensitivity Effect of Young's Modulus of Concrete (E_c)

Several analyses were performed on M19 eastbound pier by varying the value of E_c in order to assess the influence of E_c on the lateral deformations of M19 pier, and the results are depicted in Figures 6.7. The Figure suggests that increasing E_c from 5090 ksi (from the measured compressive strength) to 7000 ksi resulted in decreasing the lateral deformation by 23% to 25% for the top 20 ft depth. However, when E_c is further increased to 10000 ksi, the lateral deformation is reduced by 40%. As expected, the variation of E_c does not affect the shape of p-y curve at all.

6.2.4 Sensitivity Effect of of Subgrade Modulus of Soil (K_s)

Analyses were also performed on M19 eastbound pier by varying the subgrade soil modulus parameter (K_s) to $\frac{1}{2}K_s$ and $2K_s$ while keeping all other input parameters constant. The results of the analysis are presented in Figures 6.8 and 6.9 for lateral displacement and p-y curves, respectivly. The figures show that the variation of K_s does not affect the lateral deformation of M19 pier. This may be because of ignoring the effects of subgrade soil modulus during the development of selected p-y curves for soil in this study incorporated in FB-Multipier.

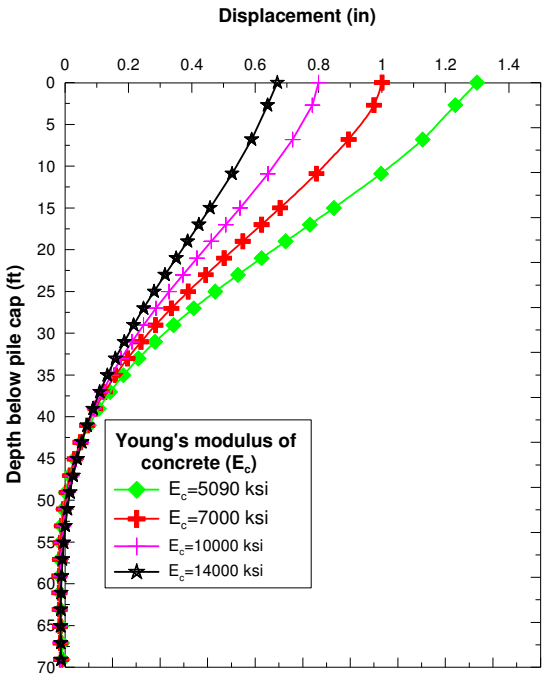

Figure 6.7: Displacement at varying E_c

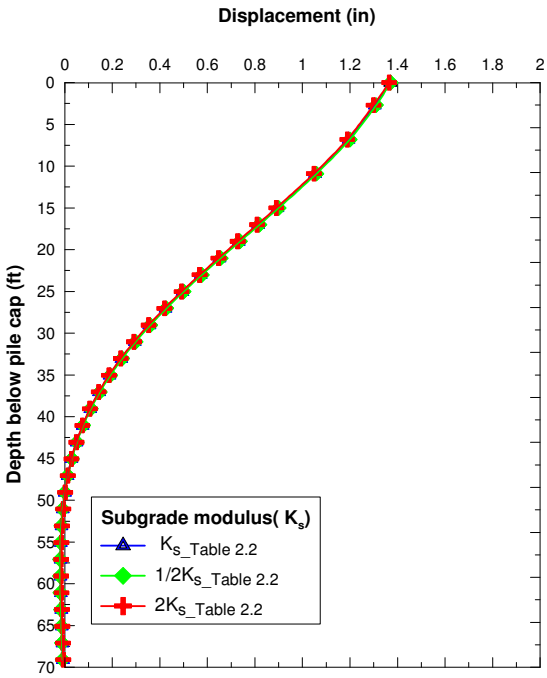

Figure 6.8: displacement at varying K_s

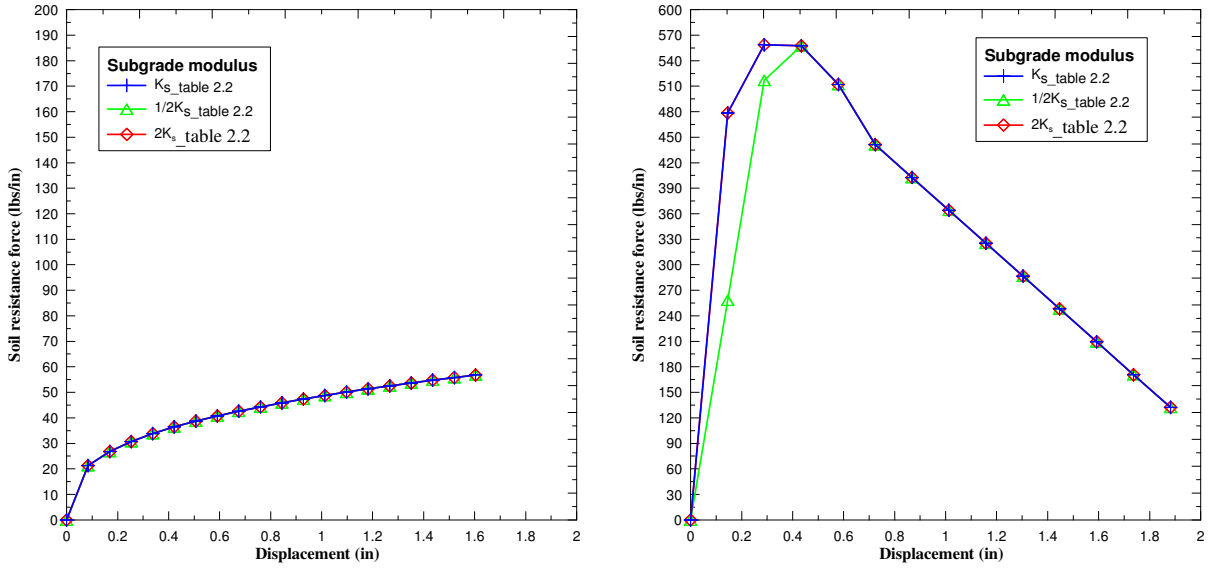

(a) for soft clay layer (b) for stiff clay layer

Figure 6.9: P-Y curve at varying subgrade soil modulus (Ks)

6.2.5 Battered Pile Group versus Vertical Pile Group

To explore the extent of the effectiveness of battered pile group as compared to vertical pile group, all battered piles of M19 pile foundation were replaced with vertical piles and re-analyzed using FB-MultiPier software keeping all other parameters constant. Similar to the battered pile group, the analyses of vertical pile foundation were performed by applying lateral static loads in incremental order to study the lateral response of vertical pile group (e.g., displacement, moment and shear force profiles). Since the input p-multipier was selected to be 1 based on the results of lateral load test, all vertical piles in the group show very close performance. Therefore, the comparison was only made for pile 11 of the 1st row at lateral load of 1870 kips as depicted in Figure 6.10. The figure compares the profile of lateral displacement, moment and shear force of battered pile groups with vertical pile group.

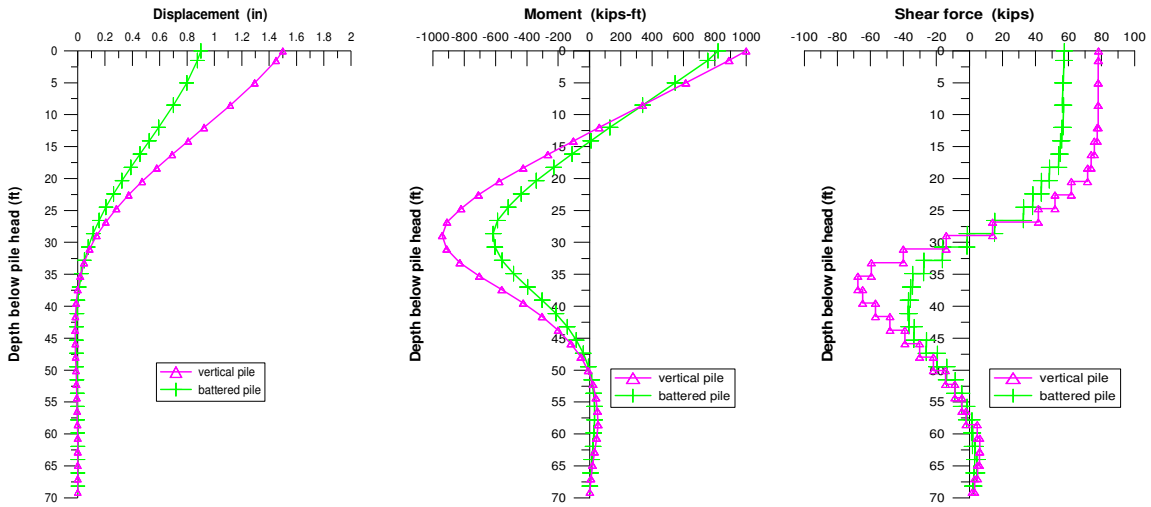

(a) Displacement profile (b) Moment profile (c) Shear force profile

Figure 6.10: Comparison of battered pile group versus vertical pile group

Figure 6.10 shows that the displacement and the shear force predicted values for the vertical piles are about 70% and 30%, respectively, higher than the values of battered piles at the same lateral loading condition. However, the moment value is merely increased by 8%, suggesting that the moment behavior of both battered pile and vertical pile are not substantially different.

The sensitivity analyses performed using various input parameters showed that the lateral deformation is highly sensitive to S_u of the surrounding soil and E_c. The higher the undrained shear strength, the lower the lateral deformation and vice versa. Hence the value of S_u is substantially sensitive input soil parameters in the FB-MulitPier analyses. In contrast to S_u, the lateral deformation of M19 eastbound pier is not much sensitive to the $\boldsymbol{\varepsilon_{50}}$ value, and that the reduction of the $\boldsymbol{\varepsilon_{50}}$ value does not substantially affect the magnitude of the lateral displacement of M19 pier. Moreover, K_s also does not affect either the lateral displacement of M19 pier or the p-y curves of soils. On the other hand, the value of young's modulus of concrete (E_c) was found to be sensitive to the predicted lateral deformations of M19 pier. The result of sensitivity analyses demonstrated that the differences between the measured displacements of M19 pier and the FB-MultiPier predicted displacement are affected by the selection of proper input parameters, most importantly, the S_u and E_c.

6.3 Analysis of Battered Pile Group

The FB-MultiPier program was used to simulate the behavior of the laterally loaded batter pile foundation of the M19 eastbound pier at I-10 Twin Span Bridge. The FB-MultiPier analyses were performed in order to predict the profiles of lateral displacement, shear forces, moment profiles and shear resistance force. These predicted profiles were then compared with the results of high order polynomial curve fitting method. Figure 6.11 shows the numbering of piles applied during FB-Multiper anlaysis as well as the instrumented piles' number. The input parameters given in the FB-Multiper for modeling pile and pile cap are summarized in Table 6.3; while the input parameters given for the pier are given in Table 6.4.

Table 6.3: Input parameter explaining material properties of pile and pile cap

Input parameter	**Pile**	**Pile Cap**	**Unit**
Breadth (B)	3	44	ft
Width (W)	3	42.5	ft
Height (H)	105-107	7	ft
Unit weight(γ)	150	150	pcf
Elastic Modulus(E_c)	5090	5090	ksi
Poisson's ratio (v)		0.2	ft
Thickness(t)		7	ft
Compressive strength (f'_c)	8	6	ksi

Table 6.4: Input parameter explaining material properties of pier columns

Pier height (ft)	Cantilever length (ft)	Column spacing (ft)	Column offset (ft)	Pier Column (no.)	Elastic Modulus (E_c) (ksi)	Compressive strength (f'_c) ksi
68	13.5	31.25	58.75	2	4696	8

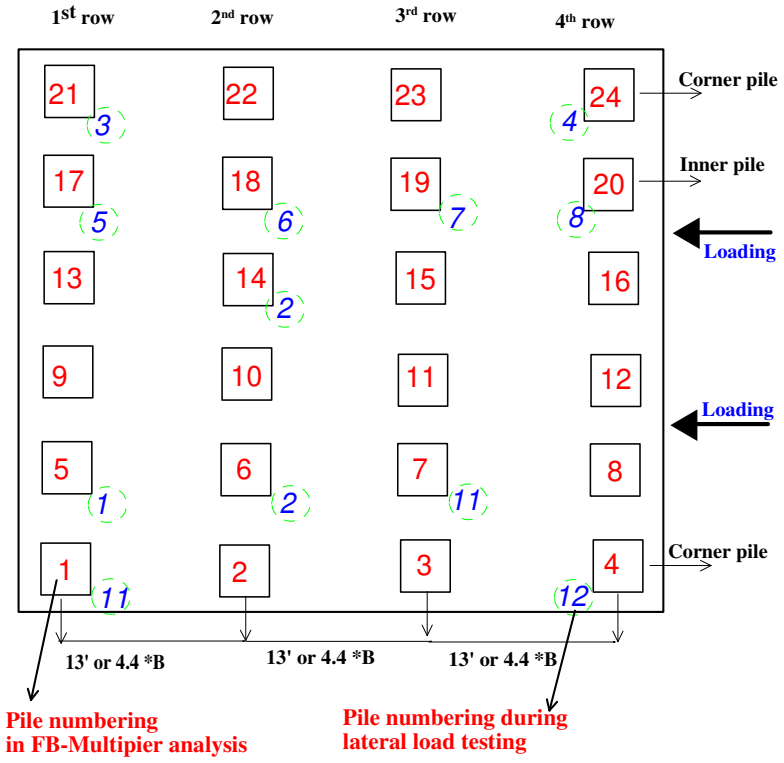

Figure 6.11: Plan view of pile layout modeled in FB-MultiPier

The results of sensitivity analyses indicated that the predicted lateral deformation behavior of piles are highly sensitivity to the S_u value of the soil layers. Moreover, the S_u value estimated from laboratory tests (S_{u_boring}) and CPT test (S_{u_CPT}) are distinctly different as shown in Figure 6.12. Several FB-MultiPier analyses were first performed using soil properties estimated from both borings and CPT input data at lateral loads of 570, 770, 970, 1180, 1580, 1745 and 1870 kips. For characterizing pile group effect, the following two different conditions were considered:

(1) Including the pile group effect (e.g., p-mutliplier <1),

(2) Ignoreing the pile group effect (e.g., p-multiplier-1)

FB-MultiPier facilitates the use of p-multiplier value for different row piles to characterize the pile group effect, and such effect can be ignored if unit p-multipliers are chosen for all row piles. The reasons behind considering no group effect in this study are: a) The measured lateral displacement under maximum load was small (0.66 in) and within the elastic deformation range of piles; b) the back-calculated p-y curves from lateral load test demonstrated no group effect

especially between rows 2, 3, and 4; and c) the pile spacing in the loading direction is 4.3 times of the pile width at cap level, which is also increases with depth between rows 2 and 3.relatively insignificant for the group interaction.

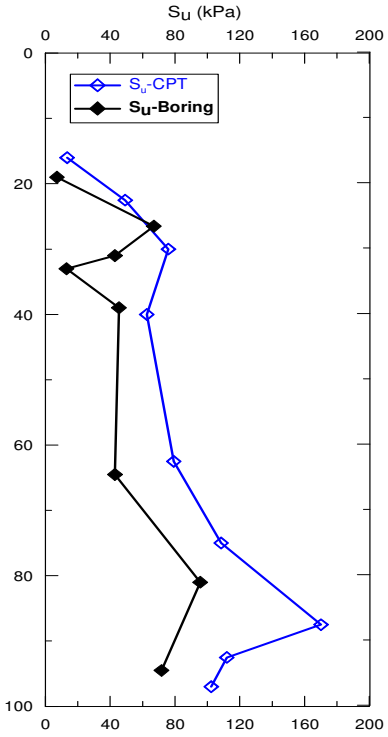

Figure 6.12: Comparison of undrained shear strength obtained from CPT and UU tests

The pile head displacements predicted by FB-MultiPier using S_{u_boring} as well as S_{u_CPT} while keeping all other parameter the same are compared with the measured displacement from automated survey and displacement derived using high order polynomial curve fitting methods as shown in Figure 6.13. It indicates that FB-MultiPier over-predicted the lateral deformations compared to the measured displacements. It also indicated that the lateral displacements predicted at pile head using S_{u_boring} are much larger than the displacements predicted using S_{u_CPT}. Moreover, the pile head displacements predicted from the FB-MultiPier analyses using S_{u_CPT} and other soil properties by ignoring the pile group effect are comparatively closer to the measured lateral displacements from the lateral load test at M19 eastbound pier of I-10 Twin Span Bridge.

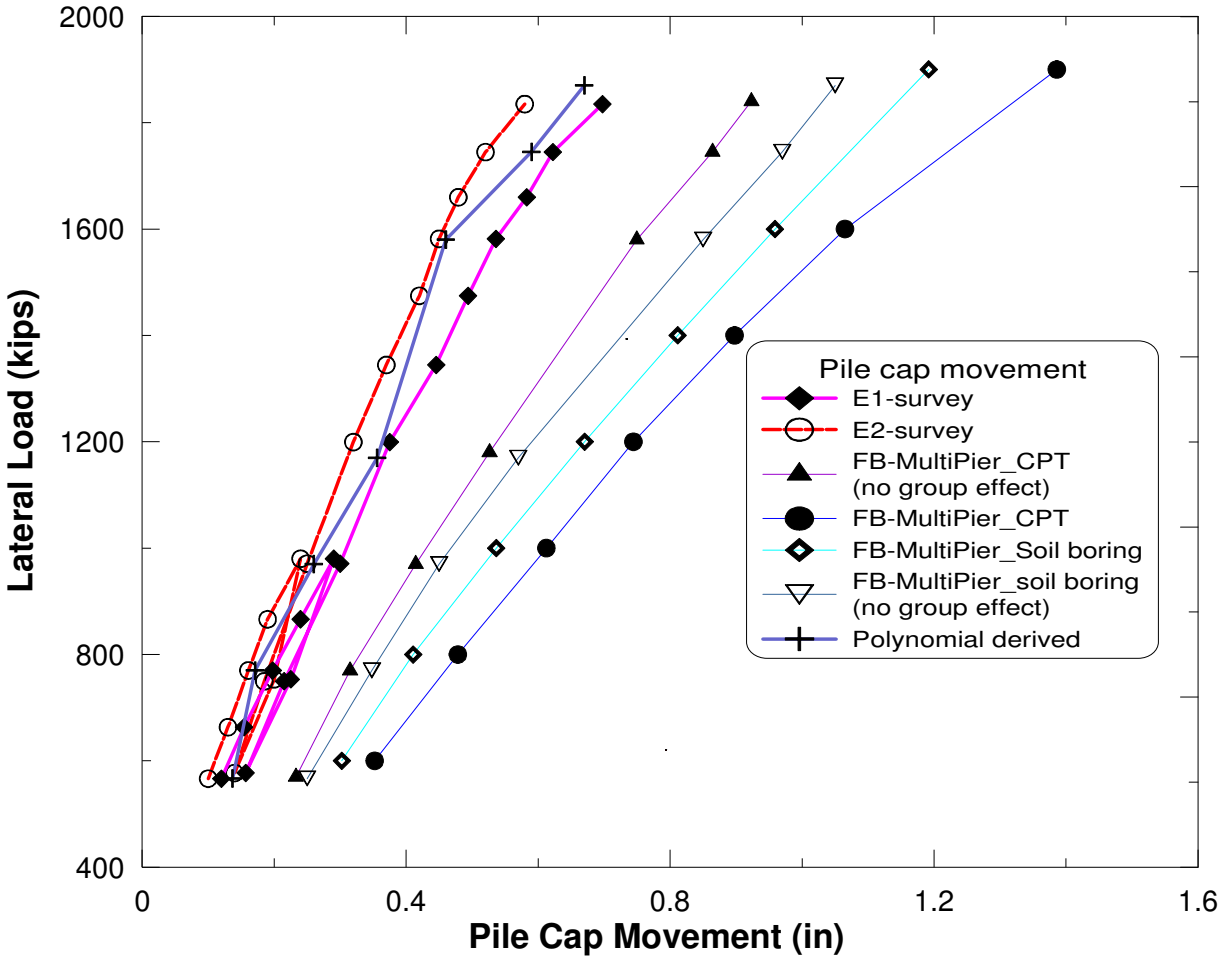

Figure 6.13: Comparison of predicted pile top displacements with IPI measurements.

The profiles of lateral displacement predicted at the maximum applied lateral load of 1870 kips by FB-MultiPier analyses using the aforementioned different conditions are compared with the IPI measured and polynomial derived displacement profiles developed at same load as shown in Figures 6.14a and 6.14b for piles 4 and 8, respectively. It clearly indicates that the lateral displacement profile predicted using S_{u_CPT} and ignoring the group effect agreed better with the derived displacement profile. Since the FB-MultiPlier analysis carried out using the S_{u_CPT} data, which is more trusted, and ignoring group effect as discussed earlier, comparatively predicted the lateral deformation of M19 piles more accurately. The displacement profiles, moment profiles, shear force profiles etc. for the rest of this Chapter will be analyzed using the S_{u_CPT} values and ignoring the pile group effect.

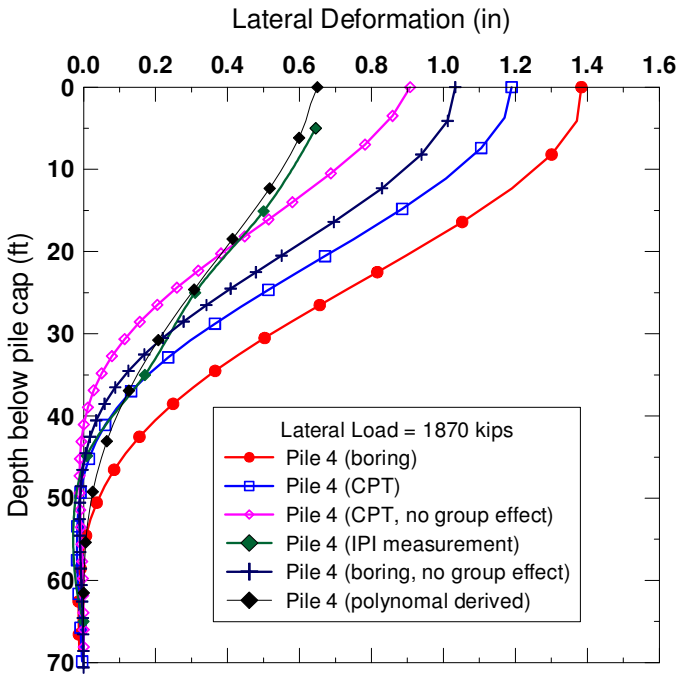

(a) $Pile_{FB}$ 24 (Pile 4)

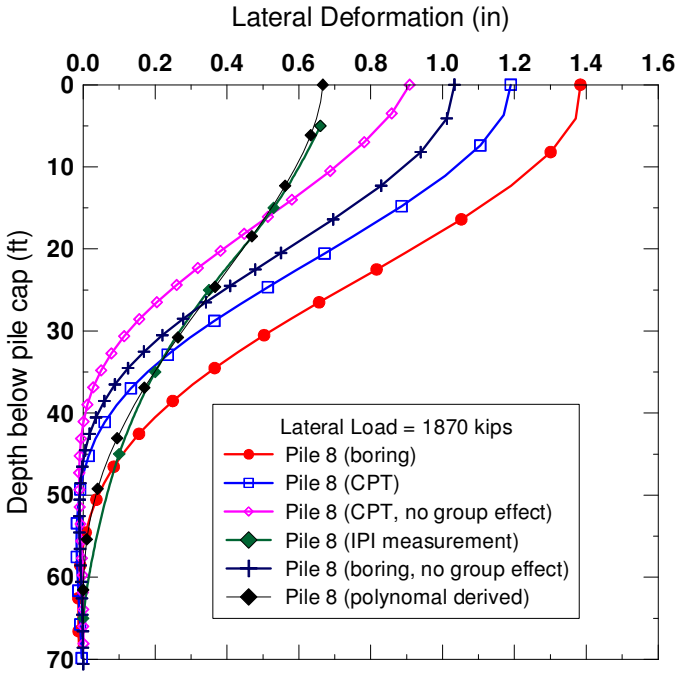

(b) $Pile_{FB}$ 20 (Pile 8)

Figure 6.14: Comparison of predicted deflection profiles at different conditions

6.3.1 Profiles of Lateral Displacement

The lateral displacement profiles predicted at increasing lateral load of 570, 770, 970, 1180, 1580, 1745, and 1870 kips were determined for all four row piles. Since, the predicted displacement profiles for all row piles are similar, so only for pile 11 (row 1) and pile 8 (row 4) are presented in Figures 6.15a and 6.15b, respectively. The FB-MultiPier predicted 0.21 in displacement at 567 kips and 0.90 in displacement at 1870 kips at pile head for all piles. For pile 8, the results suggest that the predicted deformation is 40% larger than the measured one which is 0.66 in. Similarly 35% discrepancy is found for pile 11 (1st row pile). In general, 30% to 50% variation was found between the predicted and measured lateral deformation for all piles at all loads. In addition, the depth at which the lateral displacement gradually reduced to zero was found to be smaller than the measured one. The depths to the zero displacement of predicted profiles were in the range of 35-40 ft from pile top proportioning to magnitude of loads, whereas this range is 45-60 ft for the measured displacement profiles.

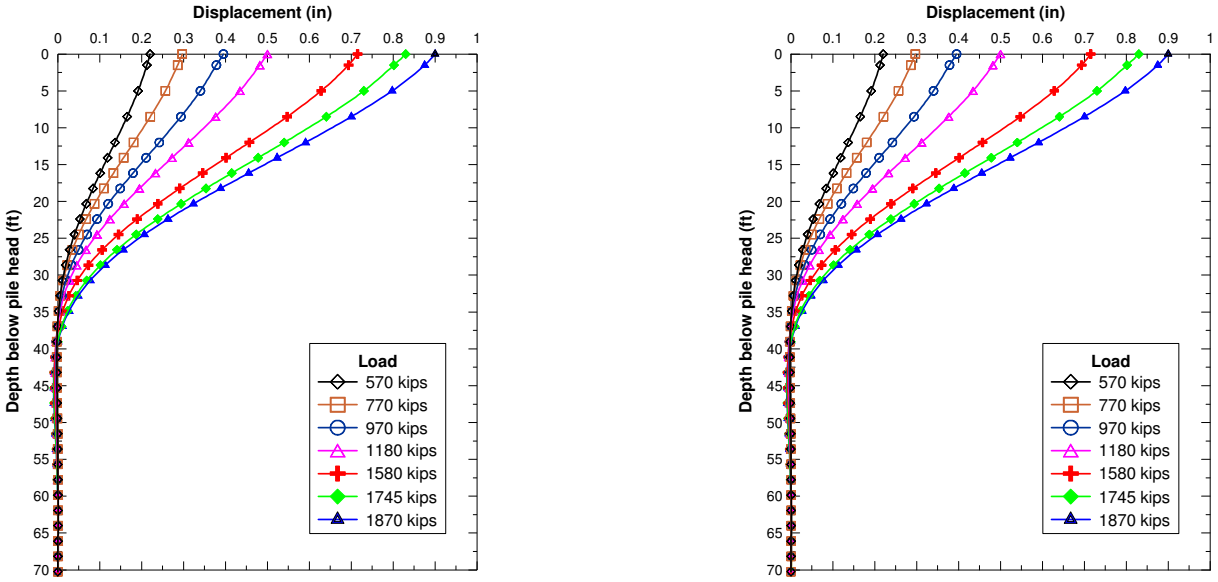

(a) 1st row / pile 11 (b) 4th row / pile 8

Figure 6.15: Predicted deflection profiles from FB -MultiPier

6.3.2 Profiles of Bending Moment

The bending moment profiles predicted by the FB-MultiPier at different loadings were also drawn for all piles. Similar to the displacement profiles, the generated moment values for piles at different rows are almost equal. Figures 6.16a and 6.16b show the predicted bending moment profile for pile 11 (row 1) and pile 8 (row 2). Figure 6.17 compares the bending moment profiles for piles located in rows 1, 2, 3 and 4 at the lateral load of 1870 kips. The figure shows that the piles locating in these rows have almost equal moment at the lateral load of 1870 kips. The maximum positive moment is located at the pile head level, as expectedly, where the pile and pile cap are rigidly connected.

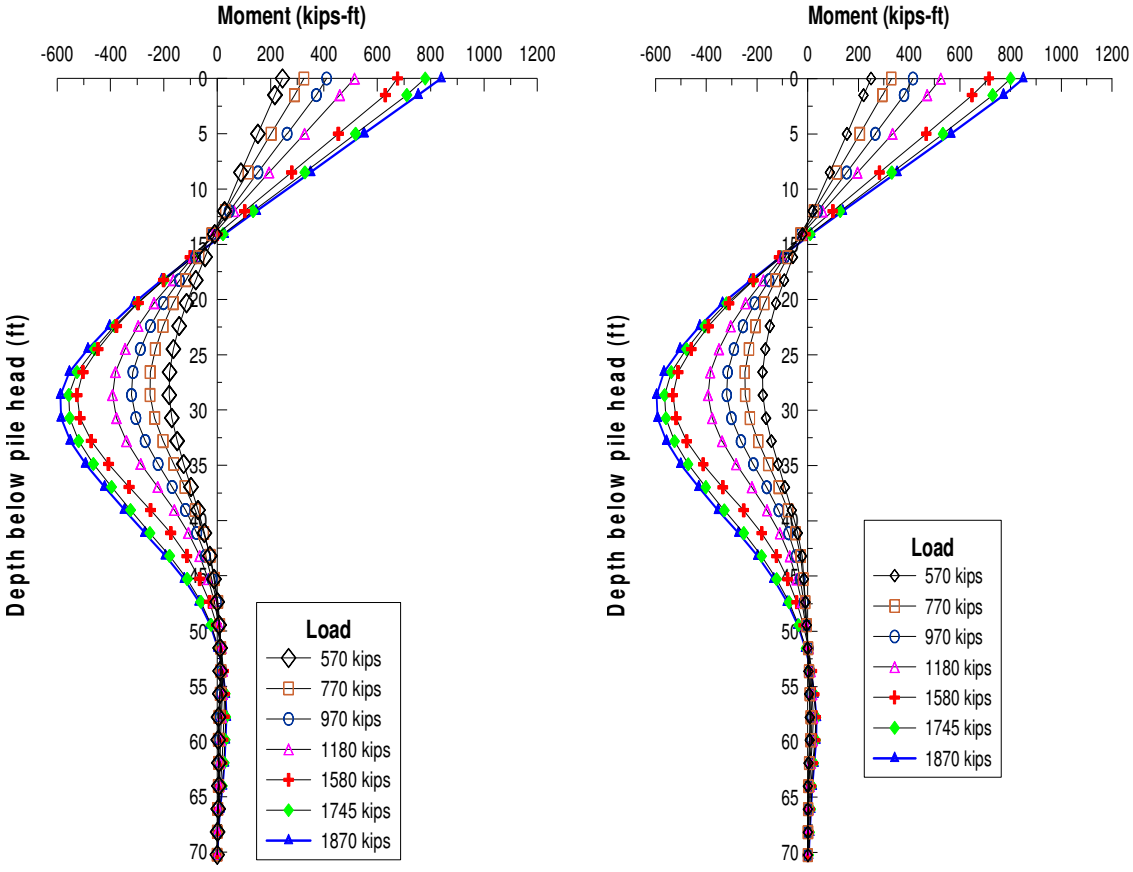

(a) 1st row / pile 11 (b) 4th row / pile 8

Figure 6.16: Predicted bending moment profiles from FB -MultiPier

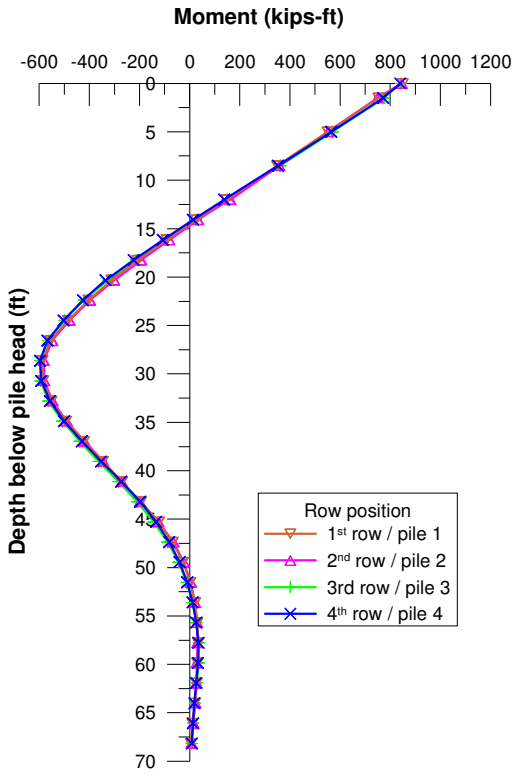

Figure 6.17: Comparison of moments at 1870 kips

The moments' profile predicted by the FB-Mutipier program are compared with those calculated from the IPI and strain gauge readings as shown in Figures 6.18a and 6.18b for piles 4 and 12, respectively. The FB-MultiPier predicted moments are comparatively larger than back-calculated results from IPI measurements. The maximum moment for 1st row pile predicted by FB-Multipier at lateral load increments of 570 kips and 1870 kips are 240 and 900 kips-ft, respectively, which are nearly 10% and 40% larger than the calculated moments. Similarly, the maximum moment predicted at ground level is nearly 50% lower than that calculated moments for all loads. However, the back-calculated moments from IPI measurements show good agreement with strain gauge measured moments. Hence, it can be inferred that the FB-MultiPier predicted higher moment than calculated moments from IPI and strain gauges.

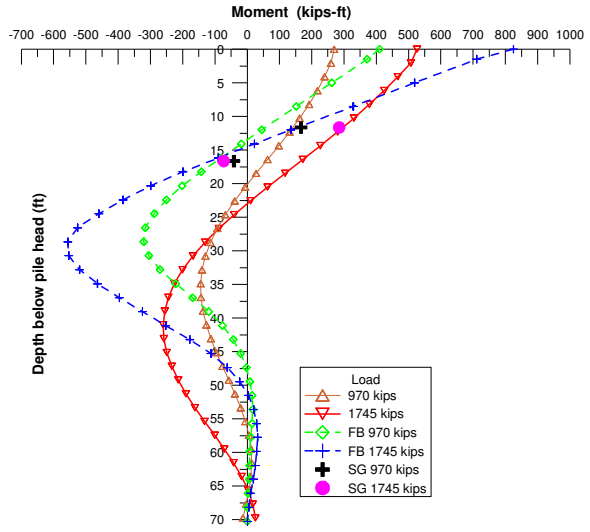

(a) 1st row pile (Pile $_{FB}$1 or pile 11)

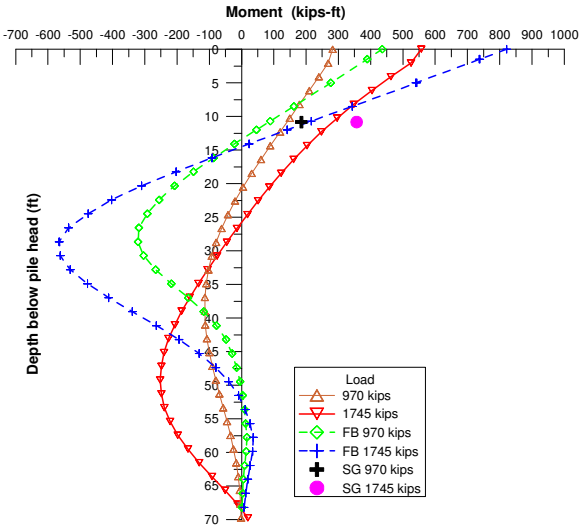

(b) 3rd row pile (Pile $_{FB}$19 or pile 7)

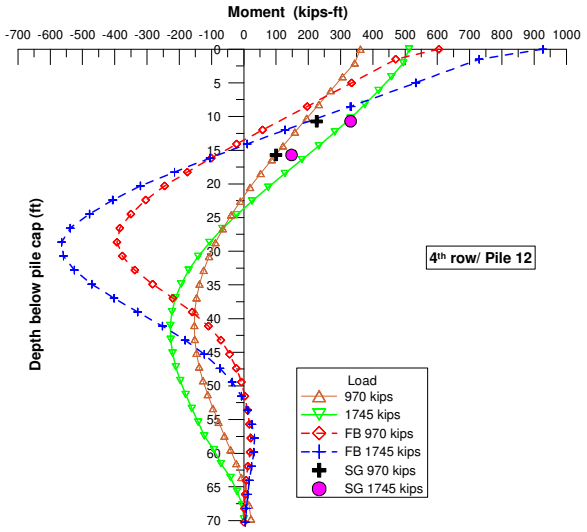

(c) 4th row pile (Pile $_{FB}$4 or pile 12)

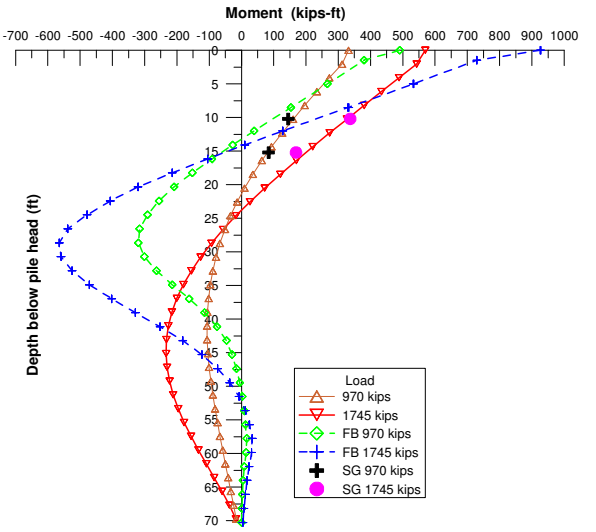

(d) 4th row pile (Pile $_{FB}$24 or pile 4)

Figure 6.18: Comparison between IPI, strain gauges and FB-MultiPier calculated moments

6.3.2 Profiles of Soil Resistance Force

The profiles of soil resistance force predicted by the FB-MultiPier at the different lateral loadings for the 1st row pile and 4th row pile are presented in Figures 6.19a and 6.19b, respectively. The figures show that the maximum soil resistance predicted by FB-MultiPier was 25 kips at the maximum load of 1870 kips, which occurred at about 26-32 ft below the pile head. It is also observed that the positive soil resistance force changes to negative at 35-40 ft from pile head depending on the magnitude of applied load. Furthermore, Figure 6.19 clearly illustrates that at higher applied load such as 1870 and 1745 kips, the soil resistance changes to negative at deeper depths than that at lower applied load.

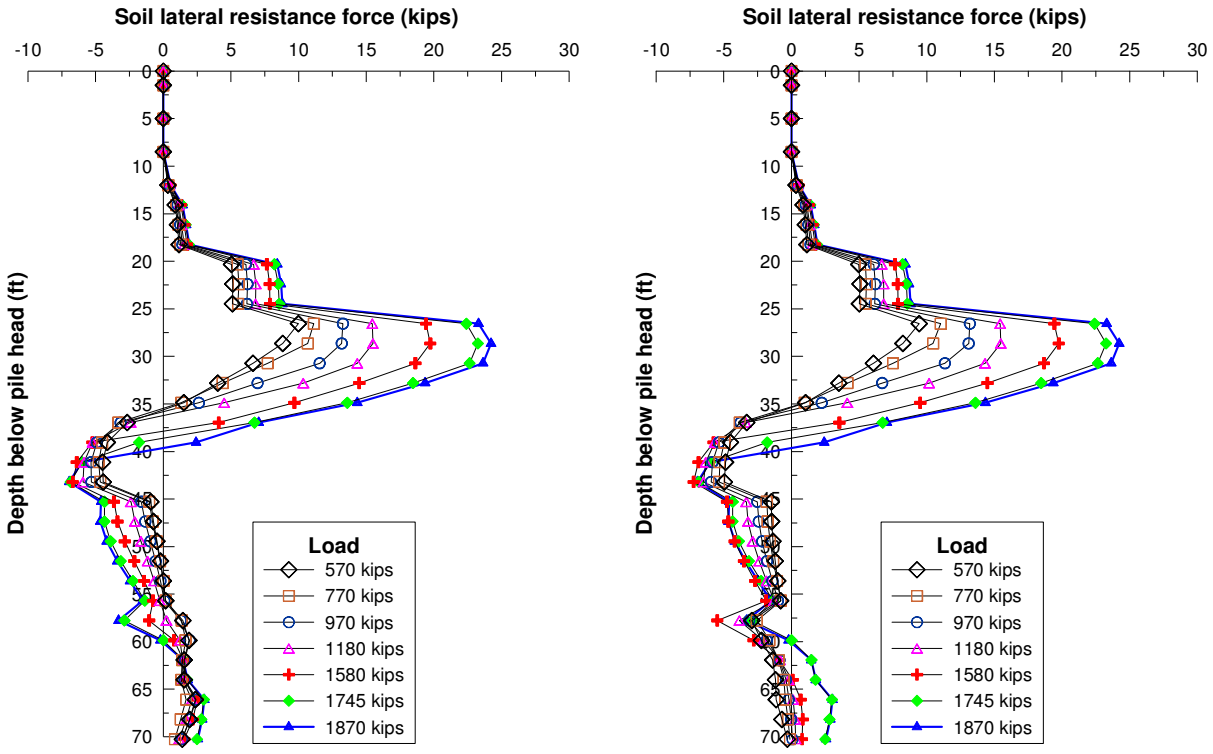

(a) 1st row pile FB-1 (d) 4th row pile FB-20

Figure 6.19: Predicted soil resistance force profiles from FB -MultiPier

The soil lateral resistance force per unit length predicted by FB-MultiPier were compared with those derived using the high order polynomial method as shown in Figures 6.20a and 6.20b for

pile 1 (row 1) and pile 8 (row 4), respectively. It depicts that the FB-MultiPier predicted maximum soil resistance forces are nearly four times greater than those calculated using high order polynomial curve fitting. In addition, the maximum soil resistances derived by the polynomial method occured at deeper depths than the predicted values. Moreover, the calculated resistance profiles gradually reduced to zero at larger depths than the predicted soil resistance profile for both 1st and 4th row piles.

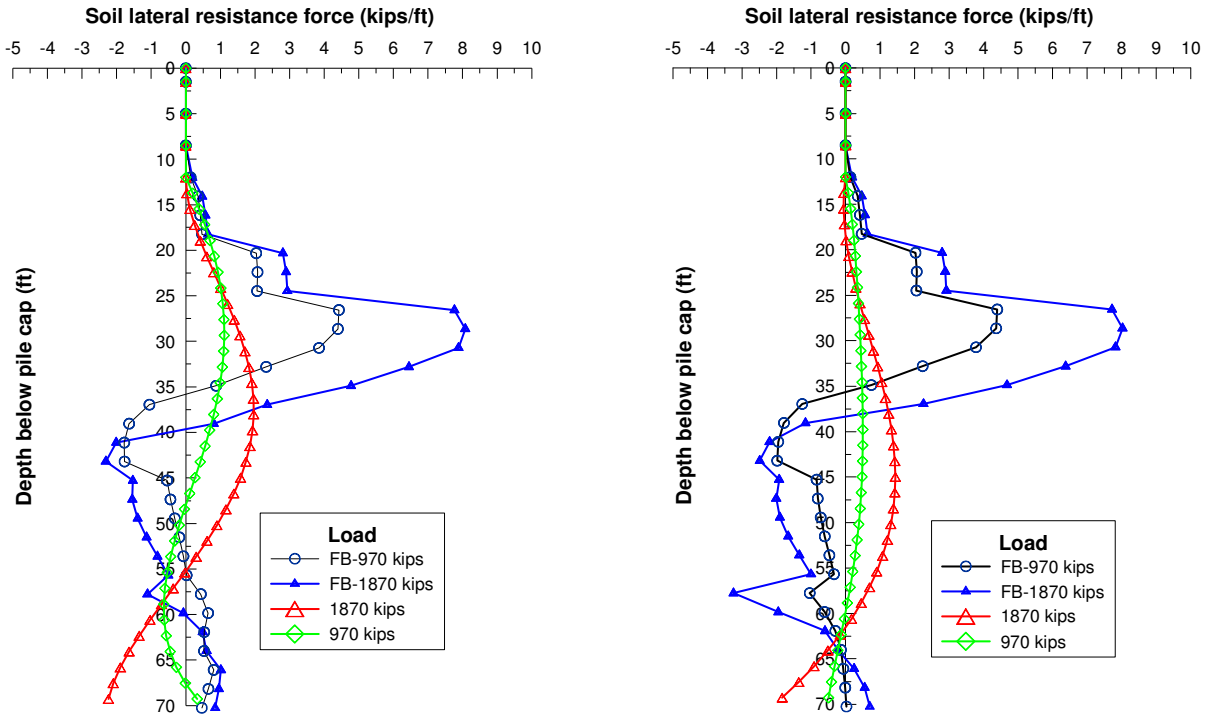

(a) 1st row (Pile FB-1 or pile 11) (b) 4th row (pile FB-2 or pile 8)

Figure 6.20: Comparison between IPI, and FB-MultiPier calculated soil resistance force

6.3.3 Profiles of Axial Force

The profile of axial force developed in piles when applying incremental lateral loading were also determined from the FB-MultiPier analysis. The axial force profiles developed along the piles located in different rows at the applied lateral load of 570 kips and 1870 kips are presented in Figures 6.21a and 6.21b, respectively. As expected, the back row piles have developed tensile axial force, whereas the front row piles have developed compressive axial force. These results agree completely with the measured axial force calculated from the strain gauges readings. Hence FB-Multipier verified that the piles nears the loading zones develop tensile forces and those located farther from the loading zone develop compressive forces.

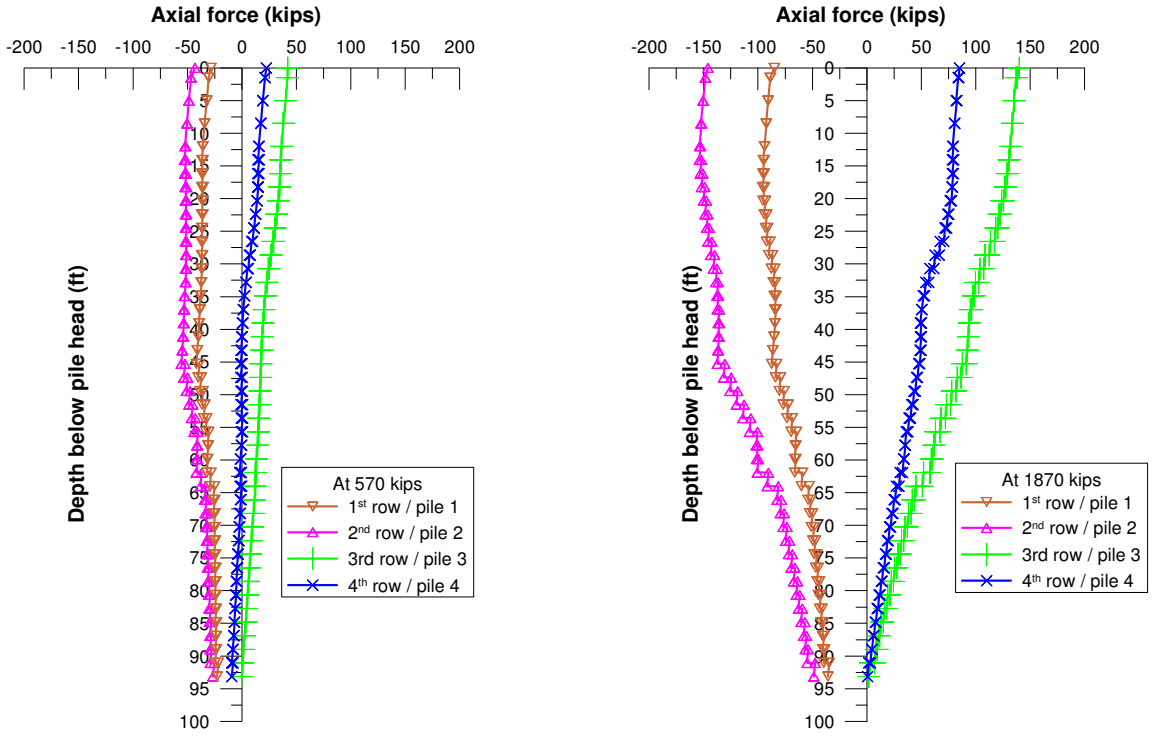

(a) At 570 kips (b) At 1870 kips

Figure 6.21: Comparison of predicted axial force of piles in rows

The axial forces predicted by FB-MultiPier at static lateral load increment were compared with those measured form the strain gauges located at different depths of the piles. As explained earlier, a pair of strain gauges (SG1) was located at 10 ft-12 ft from pile top, depending on the pile cut-off length, and another pair of strain gauges (SG2) was located at 5 ft below the strain gauges (SG1). The comparison between the predicted axial forces at SG1 and SG2 locations of the piles subjected to increasing static lateral load to the measured axial forces are presented in Figure 6.22. The figure shows that the FB-MultiPier predicts very close axial forces at both levels (SG1 and SG2), which somehow contradicts with the measured axial forces at these levels. However, in general there is acceptable level of agreement on trend and range of predicted axial forces, compared to measured axial force.

The axial forces predicted for the 1st row piles are in the range of the measured axial forces at SG2 as shown in Figure 6.22a. Since, the measured axial forces at SG2 location are not varied significantly from SG1, it can be said that the predicted axial forces are in a good agreement with the measured axial forces for the 1st row pile. The predicted axial forces for the 2nd row pile (Figure 6.22b) are larger than the measured axial force at SG2, and apparently closer to the measured axial force at SG1. However, the variation between the measured axial forces at SG1 and SG2 for row 2 pile is high compared to piles in other rows. The 3rd row pile's (Figure 6.22c) predicted axial forces smaller than the axial forces at SG1, but, it almost matches with the measured axial forces at SG2. Similar to the 1st row pile, the predicted axial forces at increasing lateral load for the corner pile ($Pile_{FB}$-24) of 4th row are found to be within the range of measured axial forces as shown in Figure 6.22d.

In general, the predicted axial force using FB-MultiPier is somehow smaller than the measured axial forces from strain gauges. However, it can be observed that the FB-Multipier predicts the axial forces within acceptable range. But, the proper distribution of axial force along the pile length are not distinctly defined, since the predicted axial forces SG1 and SG2 location are very close, which are 5 ft apart.

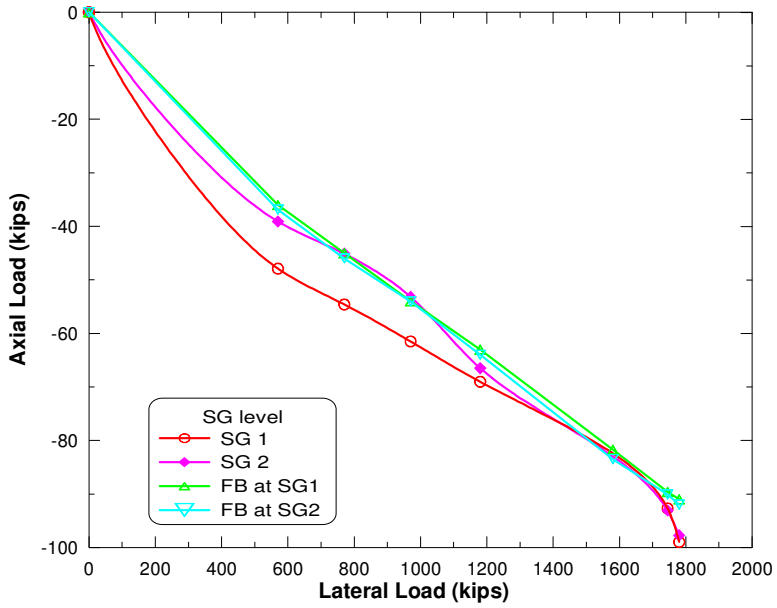

(a) 1st row (pile$_{FB}$-1 or pile 11)

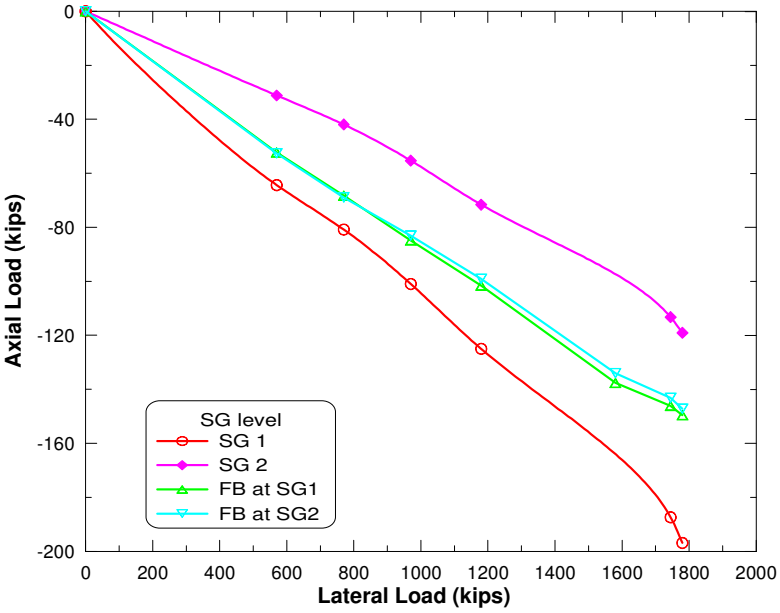

(b) 2nd row (pile$_{FB}$-6 or pile 9)

Figure 6.22: Comparison of Predicted axial force of piles in rows

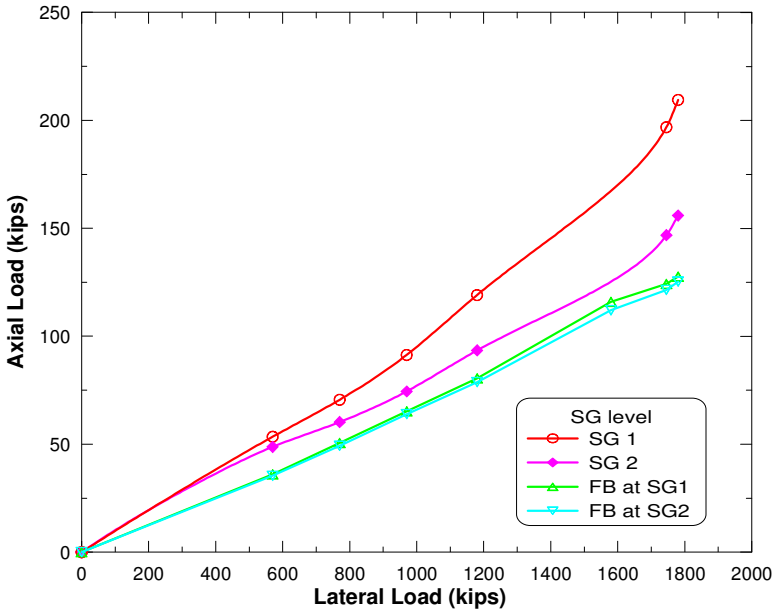

(c) 3rd row (pile$_{FB}$-7 or pile 10)

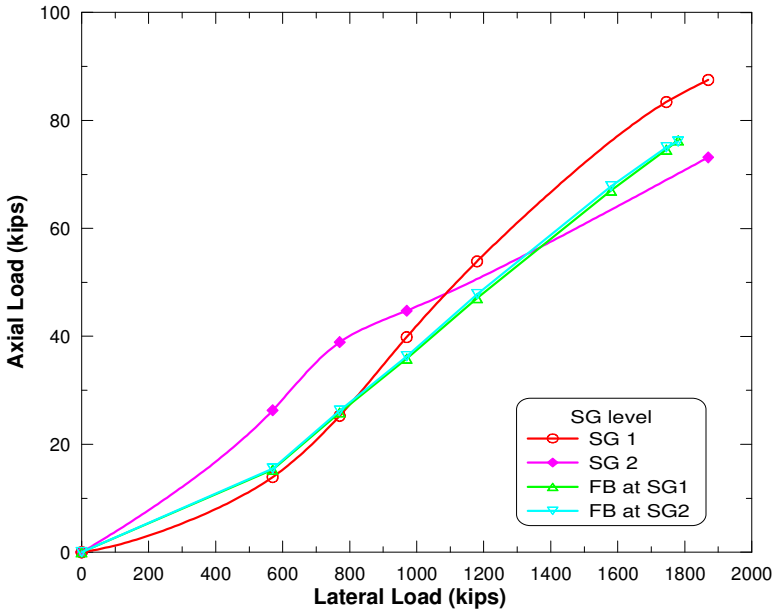

(d) 4th row (pile$_{FB}$-24 or pile 4)

Figure 6.22: (Continued)

6.3.4 Profiles of Shear Force

The profiles of shear force predicted by the FB-MultiPier at different applied lateral loadings are drawn and presented in Figure 6.23. Since the shear force predicted for all piles are very close, only the profiles of shear forces for the 1st row and 4th row piles are presented in Figures 6.23a and 6.23b, respectively. The shear force predicted at the pile top are 19 to 20 kips and 57 to 60 kips corresponding to the applied lateral load of 570 kips and 1870 kips, respectively. It can be observed that the depth to the first zero shear force occurred between 25-35 ft from pile top for both row piles.

The shear force predicted by FB-MultiPier are compared with the shear force derived using the high order polynomial curve fitting. The comparisons are made at the applied lateral loads of 970 kips and 1870 kips as shown in Figure 6.24. The figure indicates that the predicted shear forces are much larger than the derived shear force from high order polynomial fitting curve.

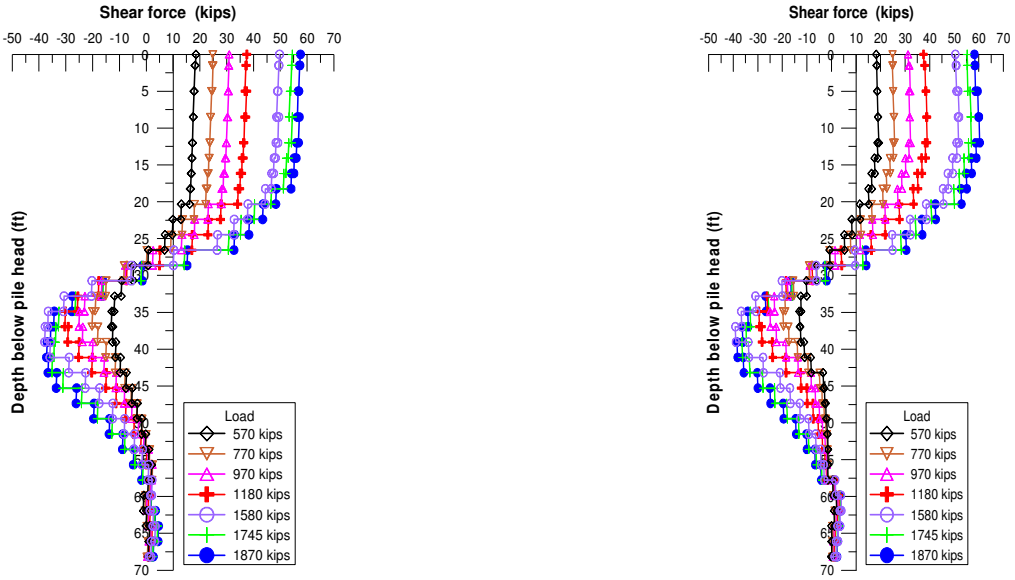

(a) pile$_{FB}$-1 or pile 11 (b) pile$_{FB}$-20 or pile 8

Figure 6.23: Predicted Shear force profile at static load increment

The maximum shear force predicted for pile$_{FB}$-1 of 1st row pile is about 60 kips, whereas, the maximum shear force calculated for the same pile is nearly half. Such trend is also observed for all piles. Moreover, the depths to the first zero shear force derived by using high order polynomial are also much larger than the predicted FB-MultiPier profiles. In the derived profiles,

the depths to the zero shear force are in the range of 45 ft - 55 ft, nearly one and half times greater than that in the predicted profiles. In addition, the profiles of predicted shear force have similar trend and shape at all applied loads. However, the derived profiles do not follow the same trend and shape as the predicted ones. For example, the shape of shear force profiles derived for pile 11 of 1st row are totally different than the shape of other piles' shear force profiles.

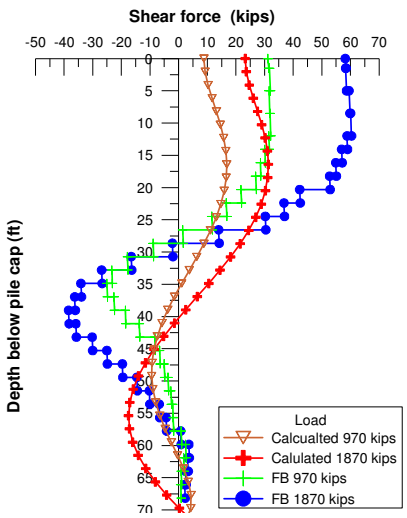

(a) 1st row (pile$_{FB}$-1/pile 11)

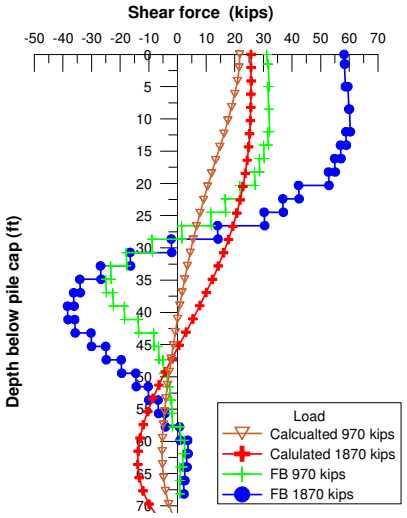

(b) 2nd row (pile$_{FB}$-18/pile 6)

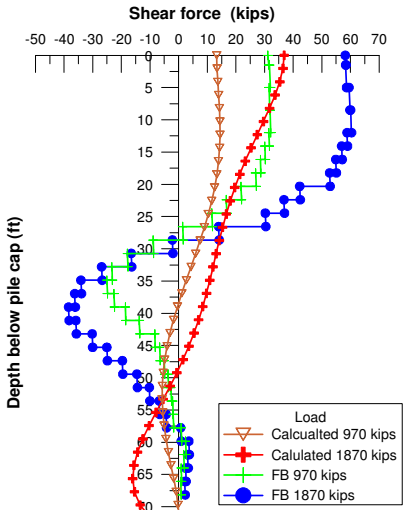

(c) 3rd row (pile$_{FB}$-19/pile 7)

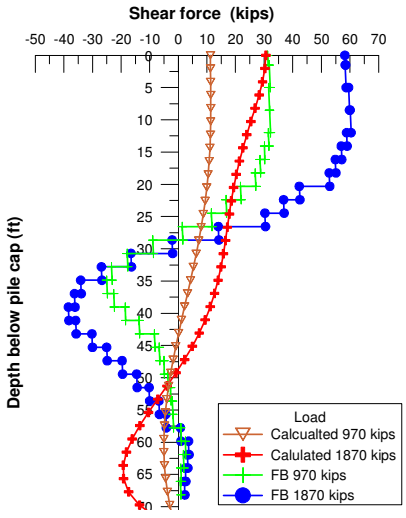

(d) 4th row pile$_{FB}$-20/pile 8

Figure 6.24: Comparison of predicted and calculated shear force of piles in rows

6.4 Analysis of a Single Vertical Pile

FB-MultiPier analyses were also performed on a single vertical pile and the results were compared with the static loads derived from the statnamic lateral load test applied to that pile. The soil input parameters used for the analyses are similar to the parameters used for battered pile group analysis. It was intended to perform analysis at the derived static loads of 34.5, 56.6, 59.7, 72.9 and 74.5 kips. However, the preliminary analysis performed by the FB-MultiPier at the given soil and pile input parameters showed that the analysis could be performed only up to static lateral load of 34 kips. At 56.6 kips and higher loads, the FB-MultiPier was not able to perform the analysis. This indicates that modeling a single vertical pile using the FB-MultiPier for the given soil conditions has failed at 56.6 kips. This, however, contradicts with the field performance of that vertical pile, which was able to resist up to 75 kips lateral load. It was noted that all these analysis were conducted out assuming non-linear material behavior of the pile. In the non-linear analysis, the FB-MultiPier uses default stress-strain curves which are integrated over the cross section of the piles. Thus, several re-analysis were then performed through FB-MultiPier using linear material behavior of pile. It was found that the analyses were successfully completed until the highest derived static load of 74.5 kips. Therefore, the lateral performance of a single vertical pile was analyzed in this study assuming both linear and non-linear material behavior of pile in order to study the profiles of lateral displacement, moment, shear force and soil lateral resistance force developed by FB-Multiper analysis. In addition, the LPILE analysis was also performed to evaluate the performance of the single vertical pile and to compare its results with the result of FB-MultiPier.

6.4.1 Profile of Lateral Displacement

The lateral displacement profiles of the single pile were determined with the FB-MultiPier analysis assuming both linear and non-linear behavior of pile material. The analysis assuming non-linear material behavior of pile was performed at the static lateral loads of 34.5, 40, 45, 48 and 50 kips. The resulting predicted displacement profiles are presented in Figure 6.25. The FB-MultiPier predicts the maximum lateral displacements at pile head of 3.78, 10.5, 19.0, and 25 in, at 34.5, 40, 45 and 48 kips, respectively. However, an extreme increment of lateral displacement is observed at the static load of 50 kips; the lateral displacement of pile increased to 55 in, indicating plastic deformation or failure of pile beyond a lateral load of 48 kips.

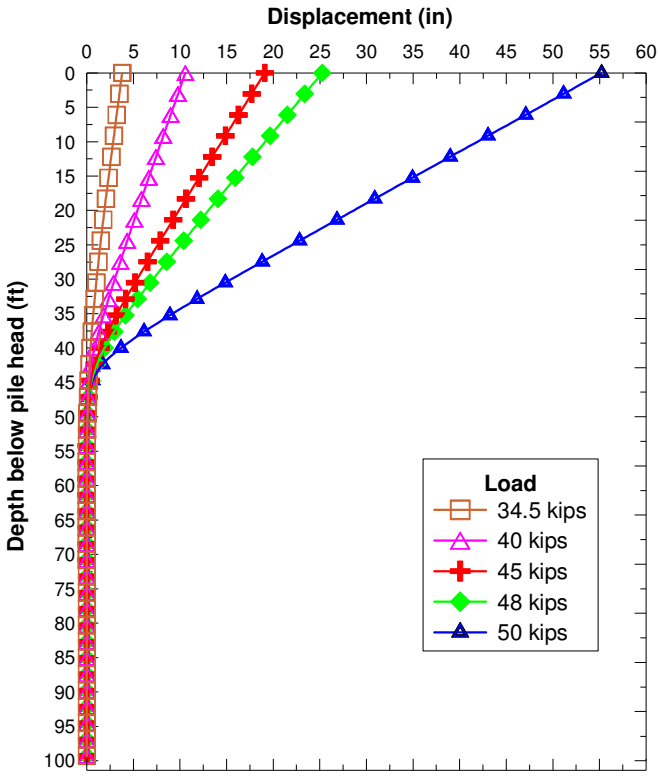

Figure 6.25: Predicted lateral displacement profile of a single vertical pile

The load-displacement curve corresponding to the maximum lateral displacement at pile head was drawn using the predicted displacement profile by FB-MultiPier at different static load increments, and also compared with the measured load-displacement curve from the statnamic test as shown in Figure 6.26. At the static lateral load of 34.5 kips, the predicted maximum lateral displacement at pile head is 3.78 in, whereas, the measured displacement at pile head was only 2.1 in (i.e., the predicted displacement is about 80% larger than the measured displacement). The FB-MultiPier predicts pile head displacement of 10.5 in at 40 kips load; while the measured lateral load was 10 in at 75.5 kips load, suggesting that the vertical pile installed in the field resisted larger lateral load than predicted by FB-MultiPier. This discrepancy may be due to assuming non-linear material behavior of pile material; assumption made in deriving static load form statnamic tests, or may be the soil strength is stronger than estimated from lab and in-situ tests.

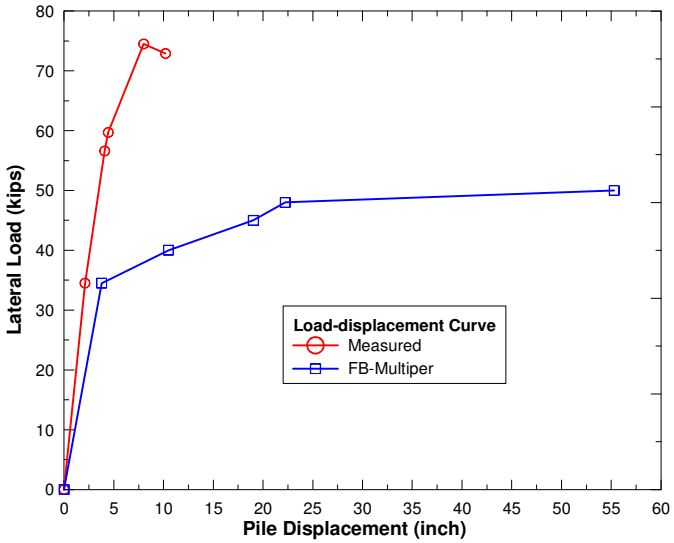

Figure 6.26: Comparison of load -displacement curves

On contrary, the pile head displacement determined by FB-MutltiPier analysis assuming linear material behavior of pile showed different result. The displacement profiles predicted by the FB-MultiPier analysis at the derived static loads of 34.5, 56.6, 59.7, 72.9 and 74.5 kips are presented in Figure 6.27. It is clear that the displacements predicted by the FB-MultiPier assuming linear material behavior are much smaller compared to those predicted from the non-linear analysis, and are closer to the measured displacement values as shown in Figure 6.28.

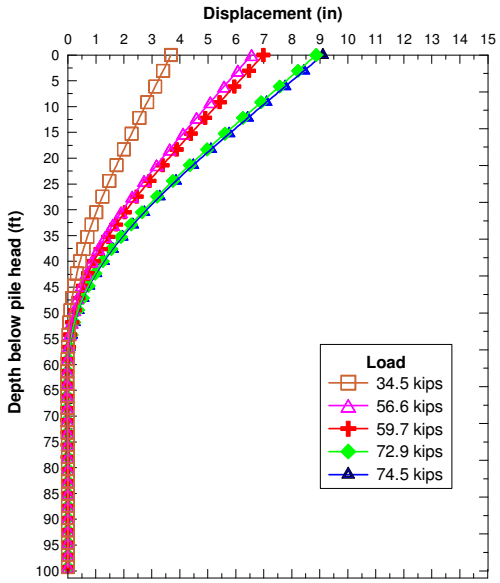

Figure 6.27: Predicted displacement profiles

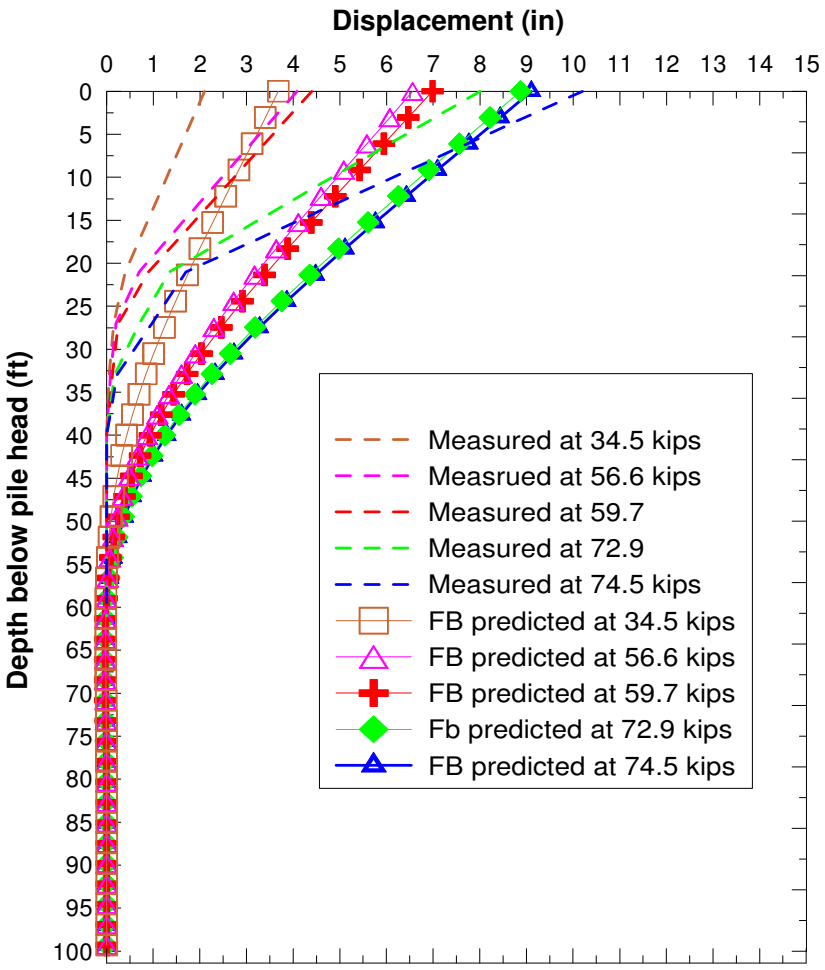

Figure 6.28: Comparison between measured and predicted displacement profiles using linear analysis by FB-Multipier

The LPILE software was also used to predict the lateral displacement profiles of a single vertical pile assuming linear and nonlinear behavior of pile material. Similar to FB-MultiPier analysis, the LPILE was also not able to complete the analysis assuming non-linear material behavior of the pile. However, it was possible to perform the analysis till a static lateral load of 50 kips by assuming a linear material behavior of the pile. The comparison between the displacements of pile head predicted at increasing static lateral load using FB-MultiPier and LPILE analysis with the measured values is given in Figure 6.29.

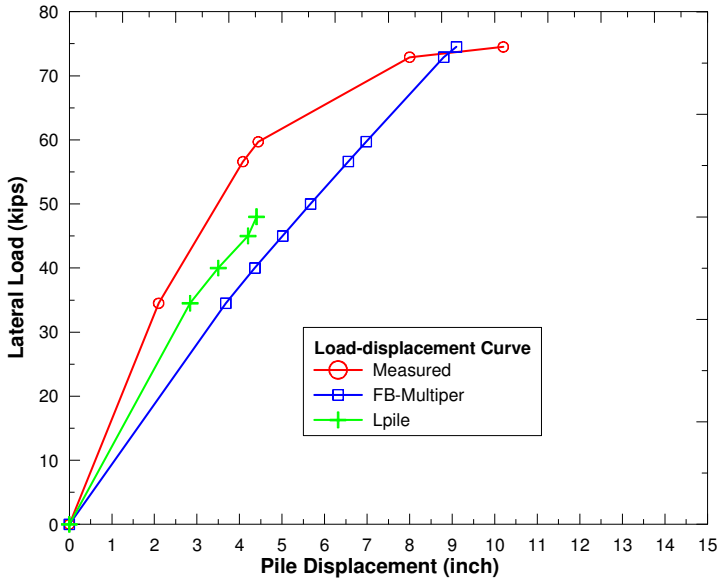

Figure 6.29: Comparison of displacement profiles predicted using linear analysis by FB-MultiPier and LPILE with measured profiles

Figure 6.30 shows that the displacements determined by the linear analyses through FB-MultiPier and LPILE show somewhat good agreement with the measured displacements. Since, the LPILE could not perform analysis beyond the 50 kips, the displacement predicted by LPILE at higher loads than 50 kips could not be compared with the measured values. However, the results of FB-MultiPier linear analysis clearly show that the predicted displacements do not vary too much with the measured displacements. Thus, it can be concluded here that the lateral deformation of a single vertical pile caused by the applied static lateral load may be within the linear range behavior of the pile.

6.4.2 Profile of Bending Moment

The moment profiles of the single vertical pile were determined by the FB-MultiPier analysis assuming both linear and non-linear material behavior of the pile. The moments predicted by the FB-MultiPier non-linear analyses at the static lateral loads of 34.5, 40, 45, 48, and 50 kips were determined and presented in Figure 6.30a. The FB-MultiPier predicts zero moment at the free end pile head, as expected, to the point of applying the load. The maximum predicted moments predicted by FB-MultiPier are 1050, 1240, 1400, 1482 and 1565 kips-ft at the applied static lateral load of 34.5, 40, 45, 48 and 50 kips, respectively. One can observe that the moment value

gradually increases with increasing the applied static load. Unlike the lateral displacement profile, no extreme moment value was observed at the applied lateral load of 50 kips.

The moments were also predicted by performing the FB-MultiPier and LPILE analyses assuming linear material behavior of the pile. The moment profiles predicted by the FB-MultiPier linear analysis at different static loads of 34.5, 56.6, 59.7, 72.9 and 74.5 kips are shown in Figure 6.30b. It can be noticed that the moment values were very close in both type of analysis. The curves of load versus maximum moments observed form the linear analysis using FB-MultiPier and LPILE are compared with the non-linear analysis of FB-Multipier as shown in Figure 6.31. The curve clearly shows that the predicted moments from the FB-MultiPier and LPILE are very close to each other.

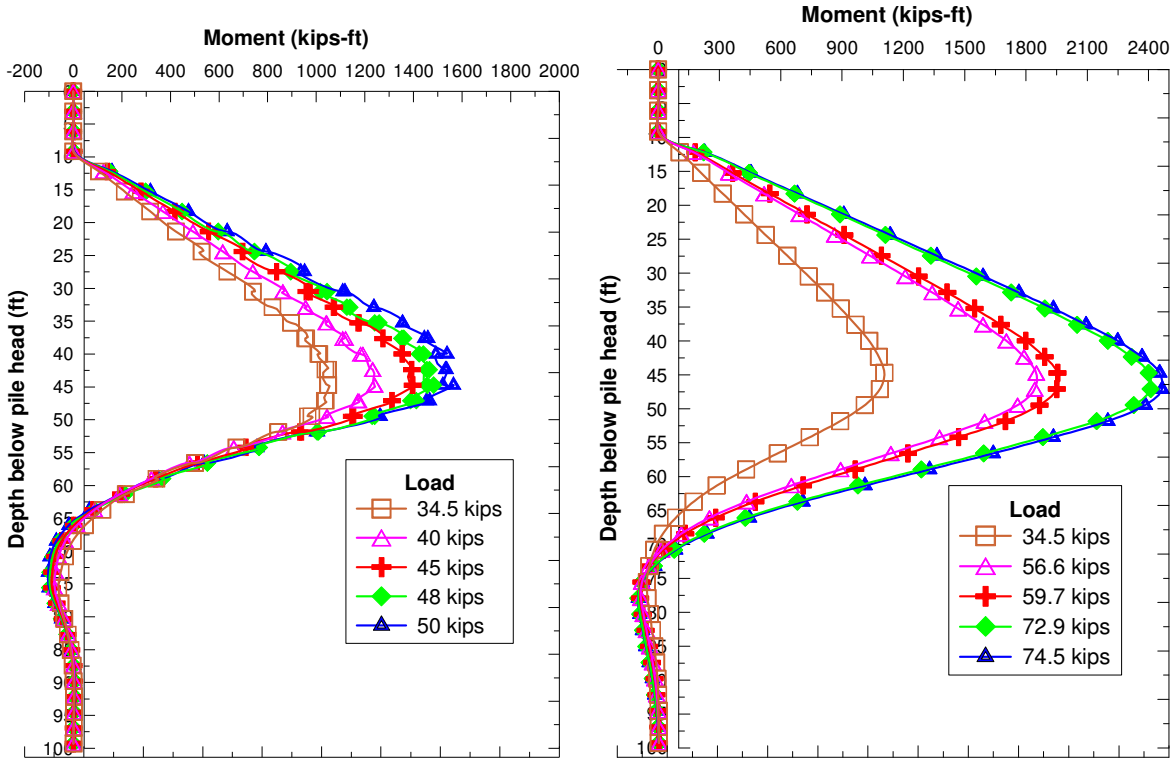

(a) Non-linear (b) Linear

Figure 6.30: Predicted moment profiles at different static loads

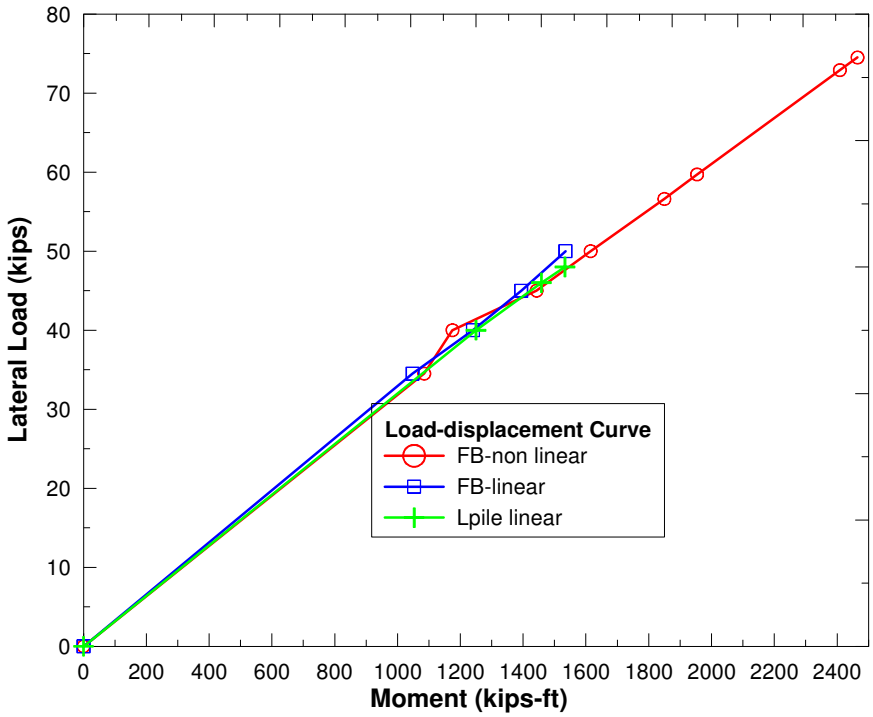

Figure 6.31: Comparison of maximum moments versus load

6.4.3 Profile of Shear Force

The profiles of shear force were also determined using the FB-MultiPier program. The profiles of shear force predicted by FB-MultiPier assuming both non-linear and linear material behavior of the pile are presented in Figures 6.32a and 6.32b, respectively. In both cases, the predicted value of shear force is zero at the pile head to the loading position. The FB-MultiPier predicts shear force approximately equals to the applied load at the loading position, and it remains constant until 40 ft depth. The predicted shear force then gradually reduced to zero at 45 ft depth. The maximum predicted negative shear force predicted corresponding to all applied lateral load is found at 55 ft depth below the pile head, and the value is almost double the value of applied lateral load.

6.4.4 Profile of Soil Lateral Resistance

Similarly, the profiles of soil lateral resistance were predicted by the FB-MultiPier considering both the linear and non-linear material behavior of pile and the results are presented in Figure 6.33. The soil resistance profiles predicted using the non-linear material behavior of pile at 34.5, 40, 45 , 48 and 50 kips are depicted in Figure 6.33a. The values of predicted maximum soil

resistance are 28, 31, 37, 39 and 40 kips corresponding to the static lateral loads of 34.5, 40, 45, 48 and 50 kips, respectively. Similarly, the values of maximum soil resistance predicted by the FB-MultiPier considering the linear material behavior of the pile are 28, 31, 39, 42, 47, 49, 56, 57 kips corresponding to applied lateral loads of 34.5, 40, 45, 50, 56.6, 57.9, 72.9 74.5 kips, respectively as shown in Figure 6.33b. It is observed that the lateral soil resistance values predicted form the FB-MultiPier analyses using both linear and non-linear material behavior of pile does not vary at all.

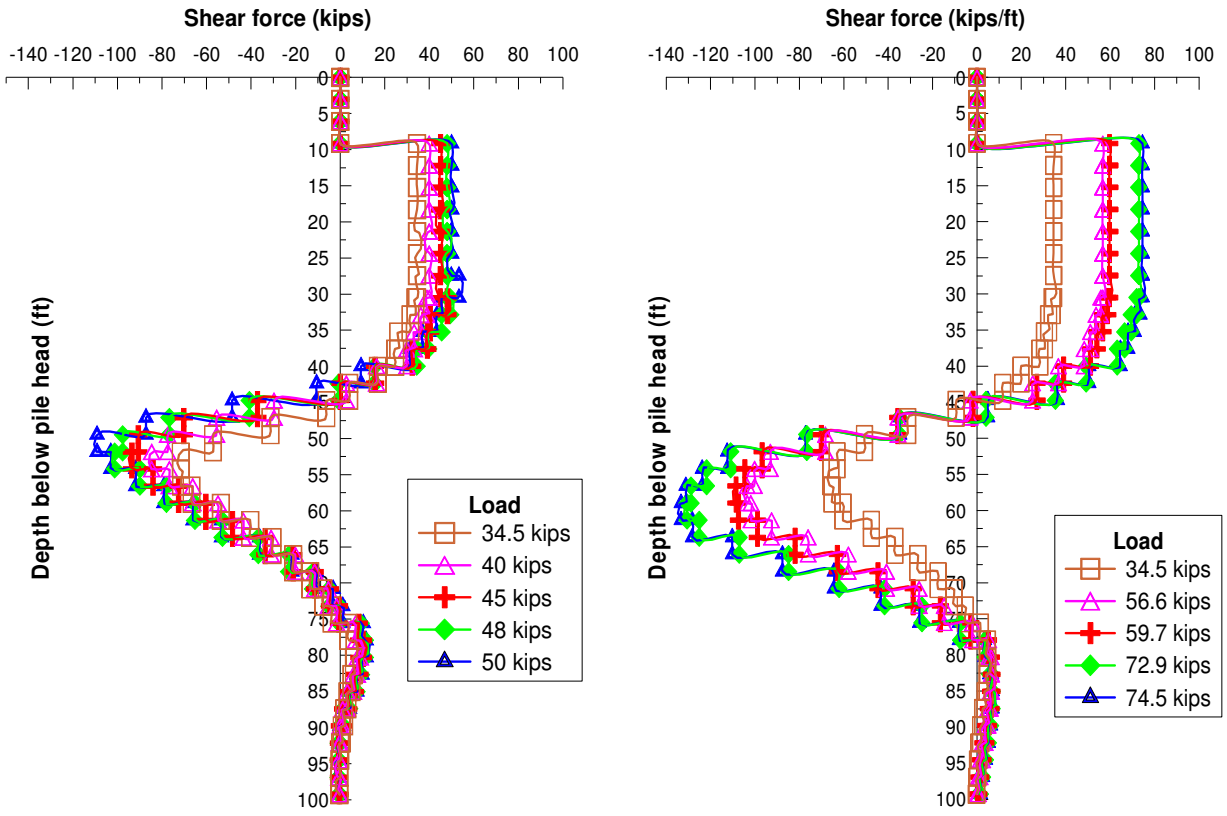

(a) Non-linear (b) Linear

Figure 6.32: Predicted profiles for shear force

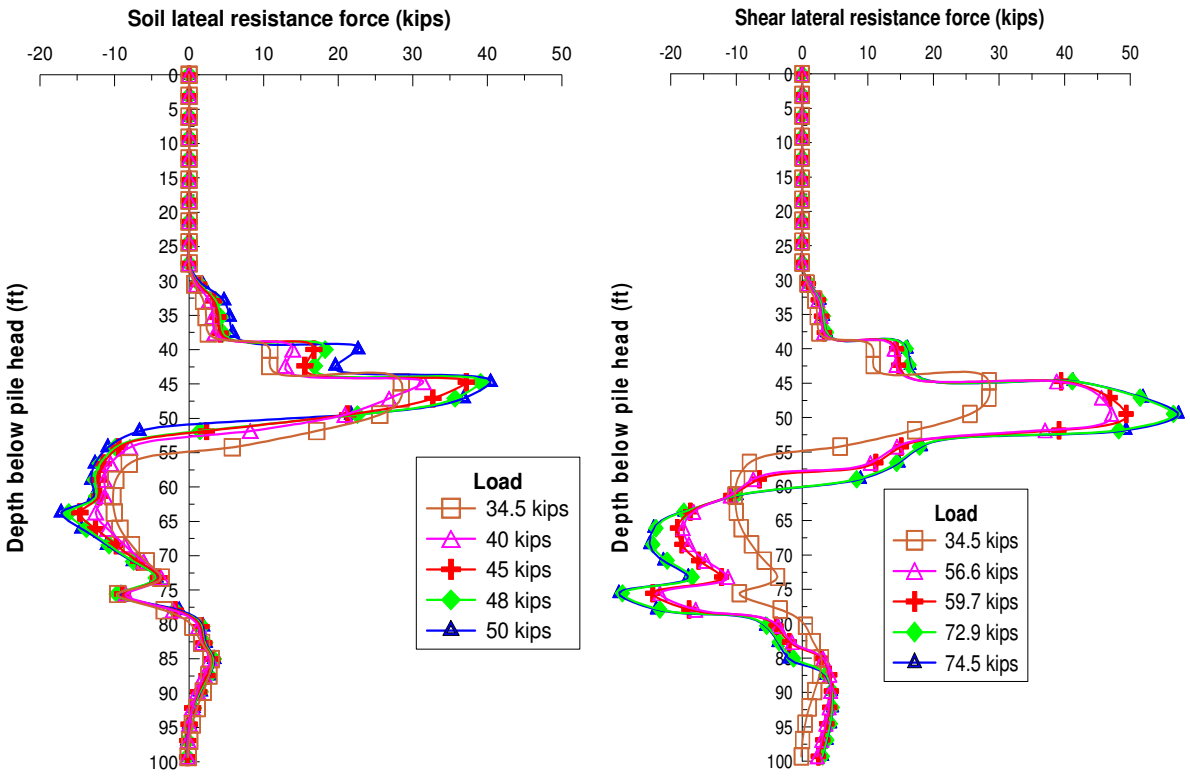

(a) Non-linear (b) Linear

Figure 6.33: Predicted lateral resistance profiles

CHPATER 7
SUMMARY AND CONLCUSIONS

7.1 Summary

In order to evaluate the lateral behavior of fixed headed battered pile group, a full-scale lateral load test was conducted by LTRC geotechnical research team at M19 eastbound Pier of the newly built I-10 Twin Span Bridge over Lake Ponchartrain, Louisiana. The M19 eastbound pier consist of 24 prestressed concrete battered (slope = 1:6) piles with pile spaced at 13 ft or 4.33B at pile cap level, where B is the pile width. The static lateral load test was conducted by pulling the M19 eastbound and the westbound piers toward each other using high strength steel tendons. The lateral responses of piles were measured using MEMS In-place inclinometers (IPI) and strain gauges that were installed in selected piles. The IPI readings of piles' lateral displacements measured during the lateral load test were interpreted using a high order polynomial fitting method. The lateral responses, which include the profiles of lateral displacement, moment, shear force, soil resistance and shear resistance force per unit length were derived. The p-y curves for different soil layers were then back-calculated from measured lateral displacement and derived soil resistance. Readings from strain gauges were used to calculate the transfer piles' axial loads and moment values from lateral loading. The moments obtained from strain gauge readings were compared with the IPI derived moments.

The M19 eastbound pier were also modeled and analyzed using the FB-MultiPier finite element program. Sensitivity analyses were first conducted to understand the effect of different soil and pile input parameters on the FB-MultiPier predicted results, which indicated that lateral deformation of M19 eastbound pier is highly sensitive to undrained shear strength (S_u) and young modulus of concrete (E_c). It also showed that the predicted result is not sensitive to strain at 50% stress (ε_{50}) and subgrade modulus (K_s). Preliminary analyses were first performed using S_{u_lab} estimated from unconsolidated undrained (UU) test as well as CPT (S_{u_CPT}) with different conditions. This analysis indicated that FB-MulitPier analysis using S_{u_CPT} (more trusted) and considering no group effect (based on preliminary analysis) produce closer displacement profiles compared with the measured one. Hence, FB-MultiPier analysis for the rest of study was

conducted using S_{u_CPT} and considering no group effect, and the predicted values were compared with measured results.

In addition, a statnamic lateral load testing was conducted on a free ended single vertical pile. The static loads were derived from the five load cycles of statnamic load testing. The displacement of pile caused by the static loads was compared with predicted displacement from the FB-MultiPier and LPILE programs.

7.2 Conclusions

7.2.1 Analysis of Battered Pile Group at M19 Eastbound Pier

Lateral Displacement Profiles

- Piles located in the back row (4th row) experienced lateral displacement larger than the other row piles at the same load; whereas piles in the front row (pile 11 of 1st row) had the least lateral displacements. In addition, the depth to the zero displacement in back row piles is deeper than the front row piles. Hence, the piles' lateral displacement and the depth to zero displacement vary depending upon the magnitude of loading and the row position of the pile.
- The piles located within the same row had almost similar displacement profiles.
- The FB-MultiPier predicted 30% to 50% larger displacements than the IPI measured displacements. In addition, the FB-MultiPier predicted the depth to zero lateral displacement at shallower depths than the measured depths.

Moment Profiles

- The moments in the piles increase when the applied lateral loads increase. The maximum positive moment at pile head does not differ substantially for all row piles. Somehow, the result indicated that the 1st row piles have a little larger moment at pile head as well as larger negative moments than the other piles.
- The moments developed at the ground level (12 ft below the pile cap level) in all piles are found to be 50% to 55% lower than that developed at the pile head.
- The FB-MulitPier predicted about 10% to 40% larger moments than the measured values from strain gauges. However, the maximum moments predicted at the ground level are

nearly 50% lower than the calculated moments for all loads. Since, the back-calculated moment from IPI measurements show a better agreement with strain gauge measured moments, it can be concluded that the moment form strain gauge and inclinometer follows similar profiles, whereas the FB-Multiplier predicts higher moments than the developed moments.

Axial Force

- The distribution of axial forces along the pile length was not uniform. Nearly, 5% to 12% of applied lateral load was transmitted to axial pile load at SG1 location. However, the percent of transmitted applied lateral load to axial pile loads decreases with pile depth as only 5% to 6% was transmitted at 5 ft below than SG1 location.
- The direction of axial force depends on the row position: the piles locating in the nearby row (4^{th} row and 3^{rd} row piles) from loading position developed tensile forces, whereas piles located at the farthest row (1^{st} row and 2^{nd} row) developed compressive forces.
- The FB-Multipier verified that the piles loaded near the loading zones developed tensile forces and those located farther from the loading zone developed compressive forces. The predicted axial forces using the FB-MultiPier are somehow smaller than the measured axial forces obtained from strain gauges. However, the predicted axial forces are within acceptable margin from the measured axial forces.
- The proper distribution of axial force along the length of each pile is not distinctly defined, since the predicted axial forces at SG1 (10-12 ft below pile head) and SG2 (5 ft below SG1) locations, which are 5 ft apart, are very close.

Soil Resistance Force per unit Length

- At the same displacement value, the 1^{st} row piles exhibit approximately 20% to 40% higher soil resistance derived (high order polynomial fitting method) than the 4^{th} row pile. However, the value of soil resistance corresponding to the same depth does not vary significantly; merely 7% to 8% variation of soil resistance at same depth is observed.

- The distributing range of soil resistance for the front row piles is smaller than the back row piles. The soil resistance distribution extends to 16B in back row piles; whereas the soil resistance distribution extends to 14B depth for leading row piles.
- The FB-MultiPier predicted maximum soil resistance forces are nearly four times larger than the IPI derived values. In addition, it predicted that the maximum soil resistances of all piles occurred at shallower depths than measured one.

Shear Force

- The FB-MultiPier predicted shear forces are much larger than the derived shear force. However, the locations of the first zero shear force predicted by FB-MultiPier are at shallower depths.

P-y Curves

- Pile 11 of the 1st row showed stiffer p-y curve than the other row piles at all depth intervals; whereas other row piles displayed similar p-y curves. This could be due to the presence of stiff soil around pile 11. Considering pile spacing of 4.3B which is increasing with depth between rows 2 and 3 and the similarity of back-calculated p-y curves for all row piles, it can be concluded that the group effect in pile foundation of M19 pier is negligible between rows 2, 3, and 4; while the negligible group effete between rows 1 and 2.
- The p-y curves were fully developed only at 5 ft and 10 ft depths below ground level. The p-y curves below 10 ft depth were not fully developed. The soil resistance increases with increasing depth. This might be due to increasing of the soil stiffness with increasing the depth.

It is thoroughly observed that the FB-MultiPier over-predicted the lateral behavior of battered pile group foundation. This behavior can be due to: 1) The soil input properties in FB-MultiPier program, which are based on in-situ tests that were conducted prior to pile driving. It is evident that pile driving can alter the properties of surrounding soil. The undraiend shear strength of soil layers can be increased due to the dissipation of excess pore water pressure (or consolidation)

over time. Thus, the pre-driving soil properties which were input in the FB-MultiPier may not represent the actual soil properties at M19 pier during the lateral load test. 2) The p-y curve method for analyzing the lateral response is based on several assumptions and consists several drawbacks such that soil is not treated as a continuum. In addition, the selected p-y curves were developed considering only the soil properties. However, as Ashour et al. (2000) explained, the p-y curves are influenced by the properties of surrounding soil, the properties of pile and head condition of the pile. 3) The profiles of moment, shear force and soil resistance are derived by differentiating the high order rotation profile once, twice and three times, respectively. Hence, there is possible accumulation of errors during each differentiation, so the derived profiles could be accompanied with errors.

7.2.2 Analysis of Single Pile

- The non-linear analysis of a single vertical pile by the FB-MultiPier and LPILE program indicated that the pile resisted much lower static lateral loads than field test measurement. The results of the field statnamic lateral load tests and the corresponding derived static lateral loads showed that the pile could resist up to a static load of 75 kips undergoing only 10 in displacement. However, the FB-MulitiPier, as well as, the LPILE analysis indicates that the pile failed at about 50 kips. This may be due to either the actual properties of soil surrounding the pile has higher strength than the estimated input values in these programs, or the static loads derived from the statnamic lateral load are higher than the actual applied static loads in the pile.

- It was also found that the displacements predicted by the FB-MultiPier using linear material behavior are smaller than the non-linear analysis and somehow closer to the measured displacements. Thus, it can be concluded that the lateral deformation of pile caused by the applied static lateral load on a single vertical pile may be in the linear range.

7.3 Recommendation

- The use of soil properties estimated form the CPT tests should be preferred when compared to laborarotry tests on sample obtained from boring for the design of pile

foundation using the FB-MulitPier program.

- The pre-driving soil properties which was input in FB-MultiPier may not represent post driving soil properties. Hence, it is recommended to consider the post-driving soil properties for FB-MultiPier input.

- Derivation of p-y curves from differentiation of high order polynomial fitting of rotation may be accompanied with accumulated errors. It is recommend considering other options in analyzing the lateral load test, such as finite element numerical analysis of lateral load test.

REFERENCES

Abu-Farsakh, M., Zhang, A., Tumay, M., Morvant, M. (2008). "Development of MS-Windows CPT Soil Classification Software". 87th *Transportation Research Board Annual Meeting*.

Awoshika, K. (1971). "Analysis of foundation with widely spaced piles". *Ph.D thesis*, University of Texas, Austin,Texas.

Ashour, M., Norris, G., and Pilling. P. (1998). "Lateral loading of a pile in layered soil using the strain wedge model". *Journal of Geotechnical Engineering*. Vol 124, No 4, pp: 303-315

Ashour, M., and Norris, G. (2000). "Modeling lateral soil-pile response based on soil-pile interaction. " *Journal of Geotechnical and Geoenvironmental Engineerin.* Vol 126, No 5, pp: 420-7428

Ashour, M., Norris, G., and Pilling. P. (2002) "Strain Wedge model Capability of analyzing behavior of laterally loaded isolated piles, drilled shafts and pile groups". *Journal of Bridge Engineering*, Vol 7, No 4, pp: 245-254

Broms, B. (1964a). "The lateral resistance of piles in cohesionless soils." *Journal of Soil Mechnaics foundation* , Vol 90, No 2, pp: 27-63

Broms, B. (1964b). "The lateral resistance of piles in cohesionless soils." *Journal of Soil Mechnaics foundation* , vol 90, No 3 pp: 123-156

Brown, D. A., Hidden, A. S., and Zhang, S. (1994). "Determination of p-y curves using inclinometer data." *Geotechnical Testing Journal*. Vol 17, pp : 150-158.

Brown, D. A., O'Neill, W. M., Hoit, M., McVay, M., EL Naggar, H. M., and Chakrobarty, S. (2001). "Static and dynamic lateral loading of pile groups." *Transportation Research Board*. NCHRP Report 461.

Brown, D. A., Reese, L. C., and O'Neill, W. M. (1987) "Cyclic lateral loading of a large-scale pile group." *Journal of Geotechnical and Geoenvironmental Engineering.* Vol. 114(11), pp: 1261–1276.

Brown, D.A., Morrison, C., and Reese,L.c (1998). "Lateral load behavior of piel group in sand." *Journal of Geotechncial Engineering*. Vol 114, No 11, pp: 1261-1276

Charels, W., Ng, W., Zhang, L., and Dora C. N. Nip. (2001) "Response of Laterally Loaded Large-Diameter Bored Pile Groups," *J. of Geotechnical and Geoenvironmental Engrg.* Vol. 127(8): 658–669.

Davisson, M.t. (1970). “Lateral load capacity of piles.” Hwy, Res. Rec. 333, Hwy. Res. Board, Washington, D.C., pp:104-112

Dunnavant, T.W., (1986). “Experimental and analytical investigation of the behavior of single piles in overconsolidated clay subjected to cyclic lateral loads.” *Ph.D. Dissertation*, University of Houston, TX.

Dou, H. and Bryne, P.M. (1996). “Dynamic Response of single pile and soil-pile interaction,” *Canadian geotechnical Journal*., vol. 33, pp:80-96

Feagin, L.B. (1937). “Lateral pile loading test,” Transactions, ASCE, vol 102, paper no 1959, pp:236-254

Feagin, L.B. (1953). “Lateral load tests on groups of battered and vertical piles. “ *Proceeding Symp. on lateral Load Tests on Piles*, ASTM, New York, pp: 12-20.

Francis, A.J. (1964). “Analysis of pile groups with flexural resistance”. *Journal of Soil Mechanics Foundation Division*, ASCE, Vol 90, No SM3, pp:1-32

Hansen, J. B (1961). “The ultimate resistance of rigid piles against transversal forces”. *Danish Geotechnical Insitiute*, Bulletin No. 12, Copenhagen, Denmark, PP 5-9

Huang, A., Hsueh, C., O’neill, M.W., Chern, S., and Chen, C (2001). “Effects of construction on laterally loaded pile groups.” *Journal of Geotechnical and Geo-environmental Engineering* , vol 127, No 5, PP: 385-397

Hetenyi, M. (1946). “Beams on elastic foundation”, University of Michigan Press, Michigan

Hoit, I. M., McVay, M., Hays, C., and Andrade,W. P (1995) “Nonlinear Pile Foundation Analysis Using Florida-Pier” *Journal of Bridge Engineering*. Vol.1, No.4 , pp: 135-142

Janoyan, D.K., Stewart, P. J., and Wallace, W.J (2001). “Analysis of p-y curves from lateral load test of large diameter drilled shaft in stiff clay.” *Porceeding, 6th Seismic Design Workshop*, Sacramneto,

Kim, J. B., and Brungraber, R. J. (1976), “Full scale lateral load tests of pile groups”. *Journal of the Geotechnical Engineering Division*, ASCE, Vol. 102, No. GT1, pp: 87-105

Kim, J. B., Brungraber, R. J., and Singh, L.P. (1979). “Pile cap sol interaction form full-scale lateral load tests.” *Journal of Geotechnical Engineering Division*., ASCE, Vol 105, No 5, PP: 643-653

King, G. J (1994) “The interpretation of data from test on laterally loaded piles.”*Proceedings of the International Conference*: Centrifuge 94, Singapore, pp: 485-490

Kramer, S., and Brown, D. A., Hidden, A, S., and Zhang, S. (1998) "Development of p-y curves for analysis of laterally loaded iiles in western Washington," *Final Report, Washington State Department of Transportation,* Report No WA-RD 153.

Kubo, K. (1965). "Experimental study of the behavior of laterally loaded piles. *Proceeding, 6th Internatinal conferencee on soil Mechanics and Foundation Engineering*, Montreal, QC.

Liao, C. J., and Lin, S. S. (2003). "An analytical model for deflection of laterally loaded piles." *Journal of Marine Science and Technology.,* Vol 11 (3), pp :149-154

Lin, S. S., Liao, J. C., Chen, T. J., Chen, L. (2005). "Lateral performance of piles evaluated via inclinometer data." *Computer and Geotechnics*., Vol. 32: 411-421.

Lin, S. S., and Liao, J. C . (2006). "Lateral Response evaluation of single piles using inclinometer data". *Journal of Geotechnical and Geo-environmental Engineering.,* Vol 132, pp: 1566-1573.

Lu, S.S (1981). "Design load of bored pile laterally loaded." *Proceeding, 10th International conference on Soil mechanics and Foundation Engineering.,* Balkema,Rotterdam. The Netherlands, vol. 2, 767-770

Manoliu, l., Botesa, E., and Constaninescu, A. (1997). "Behavior of pile foundations submitted to lateral loads. *International Proceedings, 9th Conference*, ICSMFE: 437-440, tokyo

Mezazigh, S. and levacher, D., (1998). " laterally loaded piles in Sand: slope effect on p-y reaction curves." *Canadian Geotechnical Journla.,* Vol. 35, No3, pp. 433-441

Matlock, H., and reese, L.C. (1961). "Generalized solution for laterally loaded piles. " *Journal of Soil Mechanics and Foundation*, Div., ASCE, vol 86, No 5, pp: 673-694

Matlock, H. (1970). "Correlations for Design of laterally loaded piles in soft clay". *2nd Offshore Technology Conference*, Houston Texas.

Matlock, H., and Ripperger, E. A. (1956). "Procedures and instrumentation for tests on a laterally loaded pile". *Proceedings, 8th Texas Conference on soil Mechanics and Foundation Engineering*, Austin Texas.

Matlock, H., Ingram, W.B., Kelley, A. E., and Bogard, D. (1980). "Field tests of the lateral load behavior of pile groups in soft clay." *Proceedings, 12th Annual Offshore Technology Conference. Houston, Texas.*

Mcclleland, B., and Focht, J. A. (1958). "Soil modulus for laterally loaded piles. " Trans. ASCE., vol 123, pp:1049-1063

McVay, C. M., Wasman, J. S., Consolazio, R. G., Bullock, J. P., Cowan, G. D., and Bollmann, T. H. (2009). "Dynamic Soil–Structure Interaction of Bridge Substructure Subject to Vessel Impact." *Journal of Bridge Engineering.* 14 (1) pp: 7-16

McVay, C. M., Shang, I. Te., and Casper, Robert. (1996). "Centrifuge Testing of Fixed-Head Laterally Loaded Battered and Plumb Pile". *ASTM geotechnical testing journal.*, Vol 19, pp:41-50

McVay, M., Zhang, L., Molnit, t., and Lai, P. (1998). " Centrifuge testing of large laterally loaded pile groups in sands." *Journal of Geotechnical and Geo-environmental Engineering.*, Vol 124, No 10, Pp: 1016-1026

Mokwa, R.L., and Duncan, J. M (2000). "Investigation of the resistance of pile caps and integral abutments to lateral loading." *Research Report Submitted to the Virginia Transportation Research Council*, Report NO. VTRC 00-CR4, Charlottesville, VA

Mokwa, R. L., and Duncan, J. M (2001). "laterally loaded pile group effects and p-y multipliers." *ASCE special publication No 113, Foundation and Ground Improvement*, pp:729-742

Murthy, V. N. S. (1964). "Behavior of battered piles embedded insand subjected to lateral loads." *Proceedings , Symp on Bearing Capacity of piles CBRI*, Roorkee, India, 142-153

Nip, N, C, D., and Ng, W, W. C., (2005) "Back analysis of laterally bored piles." *Geotechnical Engineering* 158 Issue GE2: 63-73.

Norris, G. M. (1986). "Theoretically based BEF laterally loaded pile analysis." *Proceedings, 3rd International Conference on Numerical Methods in Offshore Piling*, TECHNIP, Ed., Paris, pp:361-386

O'neill, M. W. and Dunnavant, T. W. (1984). "A study of effect of scale, velocity, and cyclic degradability on laterally loaded single piles in overconsolidated clay". *Report No. UHCE 84-7, Dept. of Civil Engineering*, University of Houston, Texas.

Pinot, P., McVay. M., Hoit. M., and Lai. P. (1997). "Centrifuge testing of plumb and battered pile groups in sand." *Transportation Research Record 1569, pp 8-16.*

Poulos, G.H., and Madhav, R. (1971). "Analysis of the Movements of Battered Piles" *Proceeding Conference on Geo-mechanics*, Vol 1, PP:268-275

Poulos, H.G. (1971). "Behavior of laterally loaded piles;II-Pile groups." Journal of Soil Mechanics and Foundaiton, vol 97, No 5, PP: 733-751

Prakash, S., and Kumar, S. (1996). "Nonlinera Lateral Pile Deflection Prediction in Sands". *Journal of Geotechnical Engineering*, Vol. 122, No 2, Pp 130-138

Prakash, S., and Subramanyam, G. (1965). "Behavior of battered piles under lateral loads." Journal of Indian National Society of Soil Mechanis and Foundaiotn Engineering, New Delhi, vol 4, Pp 177-196

Prakash, S., and Sharma, H.D. (1990). "Analysis and design of piel foundations under lateral loads." Pile foundation in engineering practice. John Wiley and Sons, Inc, New York, N.Y., pp: 322-472

Rajashree, S. S, and Sitharam G.T. (2001). "Nonlinear finite-element modeling of batter piles under lateral load." *Journal of Geotechnical and Geoenvironmental Engineering., vol* 127 (7), pp: 604-612.

Reese, L.C. (1958). "Discussion of Soil modulus for laterally loaded pile analysis." *Proceeding, third International Conference on Numerical Methods in offshore Piling*, Edicitons Tecnhip, Paris, France, pp: 361-386

Reese, L. C., Cox, W.R., and Koop, F.D., (1974). "Analysis fo laterally loaded piles in sand." *Proceedings of 6th Offshore Technology conference*, Houston TX.

Reese, L.C. and Welch, R.C. (1975). "Lateral Loadings of Deep Foundations in Stiff Clay." *Journal of Geotechnical Engineering, Div*, ASCE, vol 101, No 7, pp: 633-649

Ranjan, G., Ramasamy, G., and Tyagi, R. P (1980). "Latearl response of battered piles and pile bents in clay." *Indian Geotechnical Journal*, New Delhi, vol 10,No 2, pp: 135-1742

Reese, L.C., Wang, S.T., Arrellaga, J.A., and Hendrix, J. (1997). LPILE Plus 3.0 for windows, Ensoft, Inc., Austin, Texas.

Rollins, M. K., Peterson, T. K., and Weaver, J. T. (1998). "Lateral load behavior of full scale pile group in clay." *J. of Geotechnical and Geo-environmental Engineering.* Vol. 124 (6), pp: 468-478.

Rollins, K., Olsen, R., Egbert, J., Olsen, K., Jensen, D., and Garrett, B. (2003), "Response, analysis and design of pile groups subjected to static and dynamic lateral loads," *Utah Department of Transportation Research and Development Division*, Report No. UT-03.03.

Rollins, M. K., Lane, D. J., and Gerber, M. T. (2005). "Measured and computed lateral response of a pile group in sand. *Journal of Geotechnical and Geoenvironmental Engineering.,* Vol 121, pp: 103-114.

Ruesta, F., and Townsend, C. F., (1998). "Evaluation of laterally loaded pile group at Roosevelt Bridge." *Journal of Geotechnical and Geoenvironmental Engineering.* 123 (12): 1153-1161.

Salgado, R. (2008). The engineering of foundations. *The McGraw-Hill Companies, Inc*.

Sheikhbahaei, A., and Vafaeian. M (2009). "Dynamic study of batter pile groups under seismic excitations through finite element method*., World Academy of Science, Engineering and Technology,* pp:51-57.

Shinobora, T., and Kubo, K. (1961). "Experimental study on the lateral resistance of piles

Smith, T. and Slyh, R. (1986). "Side Friction Mobilization Rates for Laterally Loaded Piles from the Pressuremeter," *The Pressuremeter and Its Marine Applications:Second Intl. Symposium*, ASTM STP 950, pp: 478-491.

Snyder, J. L. (2004). "Fill-scale lateral-load tests of a 3x5 pile group in soft clays and silts," *Thesis (M.S.)*, Brigham Young University, Department of Civil and Environmental Engineering.

Terzaghi, K. (1955). "Evaluation of coeffeceints of subgrade reaction". Geotechnique, vol 5, pp: 297-326

Tschebotarioff, G.P. (1952). " The resistance to lateral loading of single piles and pile groups. " *ASCE speical publication*, No 154, ASTM, West Conshohocken, pp: 38-48

Walsh, J. M. (2005). "Full-scale lateral load test of a 3 x 5 pile group in sand". *Thesis, Master of Science in Civil Engineering*, Brigham Young University

Whelan, J,M., and JanoyanD, K.(2005) "Mobilization of Component Interface Stresses Between Soil and Pile Under Lateral Loading," GSP 132, Advances in Deep Foundations PP 1-10

Wilson, D. (1998). "Soil-Pile-Superstructure interaction in liquefying sand and soft clay." *Ph.d.Dissertation*, University of California at Davis.

Yang, K., and Liang, R. (2006) "Methods for deriving p-y curves from instrumented lateral load tests." *Geotechnical Testing Journal*, Vol. 30: 1-8.

Zhang, L., McVay, M.C., Han, J. H.,Lai, P. W. (1999a) Centrifuge modeling of laterally loaded single battered piles in sand. *Candian Geotechnical Journa., voll* 36(6): 561-575

Zhang., L., McVAy, M.C., Han, J.H., Lai,P.W. (1999b) Numerical Analysis of laterlly loaded 3 X 3 to 7 X 3 pile groups in sands. *Journal of Geotechnical and Geoenvironmental Engineering*, ASCE, 125(11):936-946 .

Zhang. L., McVAy., and Han, M. C. (2001). Response of Laterally Loaded 4x4 battered pile group . *Geotechnical Engineering Ho and Li* .

Zhang, L. M., McVAy, C .M., Han, J. S., Lai,.W. P., and Gardner, R (2002). "Effects of dead loads on the lateral response of battered pile groups". *Canadian Geotechnical Journal.,* vol 39, pp: 561-575.

Zhang, Z.,and Tumay, M. (1999). "Statistical to fuzzy approach toward CPT soil classification," *J. of Geotechnical and Geoenvironmental Engrg.*125 (3): 179-186.

VITA

Binay Pathak was born in Kathmandu, Nepal. He finished his school level education from S.I.T.A Academy, Kathmandu, Nepal and 10+2 in science from Siddhartha Vanasthali Institute, Kathmandu, Nepal. He attended National Institute of Technology, Rourkela, India, from 2000 to 2004, under student exchange scholarship program for Bachelor of Technology degree in Civil Engineering. After finishing Bachelor of Engineering degree, he was employed at Engineering Section/Department of Education, Kathmandu, Nepal, as a district engineer. He joined Louisiana State University, Baton Rouge, in the fall semester of 2008. He is anticipated to fulfill his requirements for the master's degree in civil engineering in May 2011.